Department of Physics and Astronomy

Heidelberg University

Master's thesis

in Physics

submitted by

Jan Nicolas Meibohm

born in Berlin

2015

Matter in Asymptotically Safe Quantum Gravity

This Master's thesis has been carried out by Jan Nicolas Meibohm

at the

Institut für Theoretische Physik

Universität Heidelberg under the supervision of

Prof. Jan Martin Pawlowski

Materie in Asymptotisch Sicherer Quantengravitation:

In dieser Arbeit wird der Einfluss von Materiefeldern auf asymptotisch sichere Quantengravitation untersucht. Dafür verwenden wir die Methoden der funktionalen Renormierungsgruppe auf Basis der Vertexentwicklung einer verallgemeinerten Einstein–Hilbert Wirkung.
Im ersten Teil entwickeln wir das Konzept der Lokalität der Gravitonen-n-Punkt-Funktion. Mit der verwendeten Approximation bestätigen wir den nicht-Gausschen Fixpunkt für reine Gravitation. Auf Grundlage dessen, untersuchen wir den Einfluss einer beliebingen Anzahl von nicht-wechselwirkenden Materiefeldern (Fermionen und Skalare) auf den nicht-Gausschen Fixpunkt. Wir beobachten ein generisches Verhalten des Fixpunktes unter dem Einfluss der unterschiedlichen Materiespezies. In unserer Analyse schwächen Fermionenfelder die Newtonkopplung am Fixpunkt, Skalare verstärken die sie.
Danach richten wir unser Augenmerk auf den Einfluss asymptotisch sicherer Quantengravitation auf wechselwirkende Materiesysteme. Wir interpretieren diese als Spielzeugmodelle einzelner Sektoren des Standardmodells der Teilchenphysik. Dafür untersuchen wir zunächst die Konsistenz unseres Ansatzes mit leichten Fermionen verglichen mit der Plankskala. Wir zeigen, dass eine beliebige Anzahl leichter Fermionen mit asymptoisch sicherer Gravitation vereinbar ist. Im Anschluss betrachten wir das Ultravioletlaufen der Yukawa-Kopplung im Rahmen unserer Theorie. Wir zeigen, dass unter den Einfluss von asymptisch sicherer Gravitation das Laufen der Yukawa-Theorie in einen Landau-Pol verhindert wird.

Matter in Asymptotically Safe Quantum Gravity:

In this work, we study the influence of matter on the asymptotic safety scenario of quantum gravity. We use a functional renormalisation group approach and employ the vertex expansion of a generalised Einstein–Hilbert action.
First, we develop the concept of locality of the flow for the graviton n-point functions. In the following, we confirm the non-Gaussian fixed point of the pure gravity system and investigate the impact of gravity-matter interactions on the existence and the properties of this fixed point. We find that the fixed point persists under the inclusion of an arbitrary number of matter fields. Furthermore, a generic behavior of the fixed point under the influence of the different matter species, namely, fermions and scalars is observed. In this picture, fermions weaken Newton's coupling at the fixed point. On the other hand, scalar fields enhance it.
Subsequently, we highlight two particular aspects of interacting matter in asymptotically safe quantum gravity. We interpret these systems as toy models for certain sectors of the Standard Model of Particle Physics. First, we confirm the consistency of light fermions with the asymptotic safety scenario for an arbitrary number of fermion fields. Subsequently, we consider the ultraviolet running towards a Landau pole in systems with Yukawa interactions. We find that the Landau pole is avoided due to the interaction with gravity in the UV limit.

Contents

1 Introduction

Is there a unified theory of quantum physics and gravity? This question is one of the most fundamental puzzles in modern theoretical physics. Both quantum physics and gravity are described separately by very successful, but also very different theories, namely, quantum field theory and general relativity. The main difference between the two theories is based on their mathematical structure. Observables in quantum field theories are described by operators on Hilbert spaces. The underlying spacetime is intrinsically flat. The dynamics of gravity in the framework of general relativity on the other hand, is based on a spacetime metric which is a dynamical function of the matter content and of the metric itself. Thus, spacetime in general relativity is not only curved but is also a dynamical quantum field in its own right, which should obey a description in terms of a quantum operator. As a consequence, the usual formulation of gravity as a quantum field theory fails. In the path integral formalism these technical issues are not that obvious. However, they manifest themselves in the fact that gravity is perturbatively non-renormalisable as a quantum field theory [1]. The deep mathematical differences between the theories make a unification very difficult from a technical point of view.

Another, maybe even more profound problem, lies in the fact that the two theories describe the physics in very different regimes. Quantum fields theories govern the behaviour of systems at very small length scales. Thus, they allow to accurately predict the interaction of molecules in liquids as well as the scattering of the smallest constituents of matter in particle colliders. On the other hand, general relativity is valid on large length scales. It describes with high precision the physics from the collision angle of balls on a pool table to the dynamics of the solar system. The first question is why there is very little overlap between the two regimes. In other words, why the electromagnetic, weak and strong interactions that govern the physics in quantum systems do not play a measurable role on the scales of the solar system and why gravity, on the other hand, is negligible in the collision of elementary particles. The reason is threefold. First, the weak and strong interactions are very short-ranged. Second, the electromagnetic force, which is long-ranged, appears with positive and negative charges which are equally distributed in the universe. Therefore, its impacts cancel out on large length scales. Third, the gravitational interaction is long-ranged and only has one charge. Hence, it cannot be shielded and is the relevant force at large scales. Since its coupling is about 10^{40} times smaller than that of the other forces, it is negligible on small scales. This results in the existence of two regimes, namely small and large length scales, whose physics is described by mathematically very different theories.

One may pose the question if there actually is - in this seemingly consistent picture

- the need for a unified theory of quantum gravity, apart from the desire to have a complete theory, or the pure beauty of the description.

From a physics point of view the answer is far from obvious. However, we know that the above description is incomplete if we go to much shorter length scales than those governed by usual quantum field theories like quantum electrodynamics or the Standard Model of Particle Physics. In the following we motivate why physics on these extremely short length scales are expected to be very different from the regimes that are described by the presented theories. In order to make these scales experimentally accessible, processes at extremely high energies have to considered. Very high energies, however, are expected to curve spacetime within the theory of general relativity. As soon as these gravitational effects are strong enough to become relevant e.g. in particle collisions, a unified theory of quantum gravity is needed.

Unfortunately, experimental data from these regimes is very rare and the experimental guidance for a theory of quantum gravity is therefore rather weak. The reason is that the energies, at which gravity is expected to play a role is the Planck scale Λ_{Planck} which is of the order of

$$\Lambda_{\text{Planck}} \approx 10^{19}\,\text{GeV}\,. \tag{1.1}$$

Thus, it is certainly not attainable with particle colliders in the foreseeable future which nowadays provide collision energies of up to $\sim 10^7\,\text{TeV}$. However, quantum gravity effects are expected to have played a role in the early universe. These effects could now manifests themselves on cosmological scales, for instance in the anisotropy of the cosmic microwave background [2].

The already discussed technical issues have been a puzzle for more than one generation of theoretical physicists. In order to get a handle on the mathematical description different, roads have been pursued. The two approaches that have received most attention in the past are String Theory and Loop Quantum Gravity. A more conservative approach that has made much progress recently is the Asymptotic Safety Scenario. Proposed by Weinberg in 1976 [3], it conjectures that instead of quantising gravity perturbatively, a quantum field theory of gravity could be formulated in a non-perturbative way. In this light, quantum gravity is an interacting theory in the deep ultraviolet. However, the gravitational coupling does not diverge as the cutoff is sent to infinity, but assumes a non-zero, but finite value. In this case, the coupling is said to approach a non-trivial (non-Gaussian) fixed point of the renormalisation group flow. In order for the theory to remain predictive, the non-Gaussian fixed point must have a finite number of tunable parameters. A theory for which this is true is called asymptotically safe in analogy to asymptotic freedom in Yang-Mills theories, where the gauge coupling goes to zero (the Gaussian fixed point) as the cutoff is removed [4, 5]. The first analyses of asymptotic safety in quantum gravity were made by means of ϵ-expansions around its critical dimension in $2+\epsilon$ dimensions [6, 7]. Since it is questionable if the results of the ϵ-expansion can be applied to $d = 4$ spacetime dimensions, the asymptotic safety scenario did not receive much attention at that time. This changed with the introduction of the

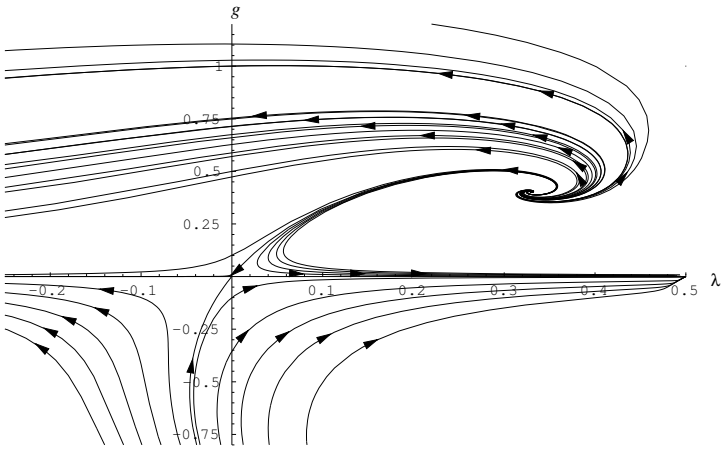

Figure 1.1: Phase diagram of quantum gravity in the Einstein-Hilbert truncation. The stream lines point towards the infrared. There exists a non-Gaussian fixed point of the renormalisation group flow of quantum gravity. Figure taken from [14].

renormalisation group [8] and its modern formulation, the functional renormalisation group (FRG) [9–11]. The FRG is a non-perturbative tool for finding solutions to the path integral in quantum field theories. It leads to a formulation of the dimensionless couplings in terms of flow equations. In this framework, gravity can be investigated non-perturbatively and the existence of non-Gaussian fixed points of the renormalisation group flow can be studied. A first FRG study of asymptotic safety in quantum gravity was conducted by Reuter in 1998 [12]. For a small truncation of the system, the so-called Einstein-Hilbert truncation, he could derive flow equations which were later shown to admit precisely the non-Gaussian fixed point conjectured by Weinberg [13]. Figure 1.1 depicts the phase diagram for the Einstein-Hilbert truncation as derived by Reuter. The Einstein–Hilbert truncation comprises two flowing couplings, namely, the dimensionless Newton coupling g and the dimensionless cosmological constant λ. Later studies have established the non-Gaussian fixed point for pure gravity by using larger truncations with higher order invariant operators [15–17]. An encouraging agreement in all of these studies is that the non-Gaussian fixed point has a maximum of only three attractive directions. This means that the corresponding theories are completely fixed by tuning a maximum of three parameter. However, all of these studies involved only the quantisation of the metric.

In order to have a more realistic description of the field content of the universe and thus, of a unification of all forces, matter fields have to be included. The first matter studies of asymptotic safety have led to the conclusion that in fact matter has a crucial impact of the non-Gaussian fixed point [18–21]. In the most recent analysis, it was shown that the inclusion of matter fields can even lead to a vanishing of the fixed point, which was used for the formulation of matter-bounds on the asymptotic safety scenario of quantum gravity [20]. The strong impact of matter fields on the

UV behaviour of gauge theories is known from Yang-Mills theories where asymptotic freedom is destroyed when a critical number of fermion fields is exceeded [4, 5].

In order to achieve a realistic description of the Standard Model of Particle Physics coupled to gravity the inclusion of matter-matter interactions is necessary. First analyses in this direction have been carried out recently [22, 23].

In this work, we discuss the impact of matter on the asymptotic safety scenario of quantum gravity. We employ the FRG to make a detailed analysis of the consequences of matter-gravity interactions on the non-Gaussian fixed point of quantum gravity. The approach is based on a vertex expansion of the effective average action. We obtain the flow for the couplings from the flow of the n-point functions together with suitable projection procedures. The truncation we use was established and applied in [24–28]. For the pure-gravity setup we confirm the non-Gaussian fixed point that we discussed above.

This work is aimed at making a step towards a unified description of the Standard Model of Particle Physics and quantum gravity. To that end, we consider asymptotically safe quantum gravity under the influence of interacting and non-interacting matter fields. First, we study the influence of fermions and scalars on the non-Gaussian fixed point. Analogous to the case in Yang-Mills theories we examine whether matter fields can destroy asymptotic safety. We find that the fixed point persists under the inclusion of arbitrary numbers of fermion and scalar fields. The fixed point exhibits a very different generic behaviour under the influence of the different species of matter fields. Thus, we find that fermions shield gravity in the UV whereas scalar enhance it in contrast to what was found in [20, 21].

Furthermore, we discuss important aspects of a unification of gravity with Standard Model in detail for two toy models with interacting matter. We raise the question whether gravity-induced chiral symmetry breaking at Planck scale energies arises in theories of with 4-fermion interactions [22]. This study is seen as a consistency check for the compatibility of fermion models with asymptotic safety. We find that chiral symmetry breaking at the Planck scale is avoided due to a general mechanism. Afterwards we discuss the influence of asymptotic safety on the UV behavior of Yukawa theories. The UV-running towards a Landau pole is conjectured to be prevented by unified theories of matter and gravity [29, 30]. In our study, the Yukawa interaction becomes perturbatively relevant in the ultraviolet and the running towards a Landau pole is in fact avoided.

The present work is organised as follows: There are four parts, which are divided into different chapters. Part I is concerned with general quantum field theory tools as well as the FRG, which are needed for the discussion of the asymptotic safety scenario (Chapter 2 and 3). Part II discusses the introduction of non-interacting matter into the theory of quantum gravity. More precisely in Chapter 4 the truncation and its construction are explained in detail. The flow of the n-point functions is considered in Chapter 5. Subsequently, we discuss the general property of locality of the flow in momentum space for the n-point functions in the pure gravity setup (Chapter 6), before investigating the different truncations of the combined gravity-matter theory (Chapter 7). In Part III we consider chiral symmetry breaking in

systems with 4-Fermi interactions (Chapter 8) and the avoidance of the Landau pole in Yukawa systems (Chapter 9). In the end, general conclusions are drawn and possible further analyses are discussed. The appendix (Part IV) contains the notation and conventions, as well as some technicalities.

Part I

Fundamentals

2 Functional Renormalisation Group

In quantum field theories it is of great importance to understand how macroscopic physics arises from microscopic interactions. A quantum field theory (QFT) is usually defined, at some (high energy) reference scale at which the relevant degrees of freedom and the corresponding couplings are known. The question is how these couplings change when quantum fluctuations come into play. In practice, the high energy fluctuations need to be integrated out down to some scale in order to obtain an effective QFT which is valid at that respective scale. For example, in quantum chromodynamics (QCD) the microscopic degrees of freedom i.e. the quarks and gluons are weakly coupled at high energies. When going to lower energies the relevant degrees of freedom change from quarks to mesons and hadrons. The coupling, weak at first, becomes stronger and stronger as high momentum quantum fluctuations are integrated out.

$$\begin{array}{ccc} \text{micro} & \overset{fluctuations}{\longrightarrow} & \text{macro} \\ \text{weak coupling} & \longrightarrow & \text{strong coupling} \end{array}$$

In turn, any description that relies on perturbation theory will fail at a certain energy scale. This means that to make the transition from micro to macro for systems like QCD we need a method that is non-perturbative. For gravity this picture is different. Almost all observations of gravity are made at relatively low energies where gravity is weak compared to all other forces. The Planck scale, Λ_{Planck}, at which we expect gravitational interactions to become relevant is of the order of 10^{19} GeV. For the asymptotic safety scenario, we are interested in the high-energy limit of a theory which we know only at low energies. This is an important subtlety that we elaborate in section 3.3 where we discuss the asymptotic safety scenario in detail. Fortunately, the FRG serves the purpose of 'integrating down' as e.g. in QCD as well as 'integrating up' in field fluctuations in quantum gravity.

In the following section, a short introduction to the FRG approach to quantum field theory is be given. The FRG and the flow equation for the effective average action provide tools that allow to describe strongly coupled systems at arbitrary energy scales. The FRG combines Wilson's approach of integrating out momentum shells with the computational advantages of functional differential methods. Together with easy-to-apply systematic approximation schemes the FRG approach is a powerful technique to solve the path integral in quantum field theory at arbitrary energy scales.

2.1 Functional methods in QFT

In quantum field theory all physics information is stored in the n-point correlation functions $G_Z^{(n)}$. In the following, we consider a general field φ which depends on a multi-index $\mathbf{a}$. Multi-indices and conventions in general are discussed in more detail in Appendix A. The n-point correlators are given by

$$G_Z^{\mathbf{a_1},\ldots,\mathbf{a_n}} =< \varphi^{\mathbf{a}} \ldots \varphi^{\mathbf{a_n}} >= \int \varphi^{\mathbf{a_1}} \ldots \varphi^{\mathbf{a_n}} e^{-S[\varphi]} \mathcal{D}\varphi_\Lambda \,. \tag{2.1}$$

The integral measure $\mathcal{D}\varphi_\Lambda$ is assumed to be suitably UV-regularised by a UV-cutoff Λ, such that the path integral is well defined. The $G_Z^{(n)}$ are generated by the generating functional $Z[J]$ which is often called partition function depending on the external source J. The partition function reads

$$Z[J] = \int e^{-S[\varphi]+\varphi^{\mathbf{a}} J_{\mathbf{a}}} \mathcal{D}\varphi_\Lambda \,. \tag{2.2}$$

The term generating functional comes from the fact that the $G_Z^{(n)}$ are the expansion coefficients of $Z[J]$ for an expansion in terms of the source J:

$$Z[J] = \sum_{n=0}^{\infty} \frac{1}{n!} G_Z^{\mathbf{a_1}\ldots\mathbf{a_n}} J_{\mathbf{a_1}} \ldots J_{\mathbf{a_n}} \tag{2.3}$$

The importance of n-point functions in quantum field theory is be understood by considering the following example: Two particles that are described the quantum field φ scatter off each other producing $n-2$ particles of the same species. We have

$$\begin{array}{ccc} \text{particle} + \text{particle} & \longrightarrow & n-2 \text{ particles}\,, \\ \circ + \circ & \longrightarrow & \underbrace{\circ\,\circ\ldots\circ}_{n-2} \end{array} \quad .$$

All physical information about this process is contained in the n-point correlation function $G_Z^{(n)}$. The information about all observable is provided by the n-point functions which is why their importance in quantum field theories can hardly be overestimated.

2.1.1 Generating functionals

It is often impractical to perform calculations with the n-point functions $G_Z^{(n)}$. One reason for this is that they carry redundant information. They contain disconnected parts and parts which are not one particle irreducible (1PI). The connected and the 1PI components are the building blocks for n-point correlation functions, as all $G_Z^{(n)}$ can be constructed from them.

Therefore, it is consider functionals that are generators for these building blocks. We define the Schwinger functional $W[J]$ which generates the connected components

$G^{(n)}$ of the n-point correlators. We call them connected Green's functions of our theory. We have

$$W[J] = \ln Z[J] \,. \tag{2.4}$$

The effective action $\Gamma[\phi]$, is constructed from the Schwinger functional $W[J]$ via a Legendre transform. It reads

$$\Gamma[\phi] = \sup_J \left(\phi^{\mathbf{a}} J_{\mathbf{a}} - W[J] \right) , \tag{2.5}$$

where $\sup_J$ denotes the supremum under the variation of the source $J_{\mathbf{a}}$. The flow of the effective action Γ is the starting point for our analysis of quantum gravity, as it has proven most convenient for this purpose. In the following, we will briefly discuss some important properties of Γ.

Properties of the effective action

1. It can shown to be the generating functional for 1PI components $G^{(n)}_{\text{1PI}}$ of the n-point functions [31]. The 1PI components are represented by graphs which cannot be split into two separate parts by cutting one line.

2. The effective action is a convex functional. Furthermore, (2.5) its definition as a Legendre transform implies

$$\frac{\delta \Gamma[\phi]}{\delta \phi_{\mathbf{a}}} = \Gamma^{\mathbf{a}|}[\phi] \;\; = \gamma^{\mathbf{a}}{}_{\mathbf{b}} J^{\mathbf{b}}(\phi) \,, \tag{2.6a}$$

$$\frac{\delta W[J]}{\delta J^{\mathbf{a}}} = W_{\mathbf{a}|}[J] = \phi_{\mathbf{a}}(J) \,, \tag{2.6b}$$

   where we introduce the $|$-notation for field or source variations from the left.

3. The second variation of $\Gamma[\phi]$ is the inverse of the second variation of $W[J]$ according to

$$W_{\mathbf{ac}|}\Gamma^{\mathbf{cb}|} = \gamma^{\mathbf{b}}{}_{\mathbf{a}} = (-1)^{\mathbf{ab}} \delta^{\mathbf{b}}_{\mathbf{a}} \,. \tag{2.6c}$$

4. The background field equation relates Γ to the classical action S.

$$e^{-\Gamma[\phi]} = \int e^{-S[\phi+\varphi] + \varphi^{\mathbf{a}} \Gamma_{\mathbf{a}|}} \mathcal{D}\varphi_\Lambda \tag{2.7}$$

Equation (2.7) relates the classical action S that captures the microscopic interactions at energies of the cutoff scale Λ to the full quantum potential Γ. The path integral $\int \mathcal{D}\varphi_\Lambda$ can be seen as the sum over all quantum fluctuations up to the cutoff scale. In particular, equation (2.7) suggests that the fluctuations of the field φ are integrated out all at once. This is one of the reasons why solving this equation is so

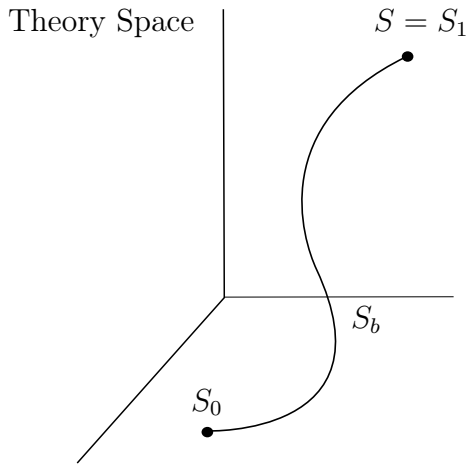

Figure 2.1: Graphical representation of the rescaled action S_b as a trajectory in theory space.

difficult. Therefore, it is computationally disadvantageous to use (2.7) to compute the full quantum effective action Γ from the classical action S. A groundbreaking idea, which is due to Wilson [8] is to parametrise all fluctuations modes contained in $\int \mathcal{D}\varphi_\Lambda$ by an initially arbitrary parameter b. As an example we set $0 \leq b \leq 1$. Now, we perform the integration only for infinitessimal steps of b. In most cases, the parameter b corresponds to a momentum or energy scale, i.e., $b \to \tilde{b} = b\Lambda$. Loosely speaking, we first order the field modes according to the parameter b. Then we integrate out infinitessimal small integral shells corresponding to small steps of b, starting at the cutoff scale Λ. In our example we set $b = 1$ at the cutoff and $b = 0$ if all modes are integrated out. An immediate observation which follows from this idea is that after performing one integration step, the classical action S in the path integral becomes an effective action S_b. Note that due to our definitions $S_1 = S$. By lowering b to $0 < b < 1$, we successively integrate out the ordered modes. Thereby, S_b acquires extra terms which in general include all possible functionals of the respective fields that are compatible with the symmetries of the classical action. Due to its inventor S_b is often called Wilsonian effective action.

In principle, by successively integrating out infinitely small integral shells we can calculate the flow of S_b. The Wilsonian effective action S_b defines a trajectory in the space of all functionals compatible with the symmetry of the classical action. Figure 2.1 depicts the trajectory S_b through theory space. It starts at the classical action S_1 and ends at S_0 where all modes are integrated out. The flow of S_b is finite and the full quantum theory can be reconstructed from the flow by integration.

In sum, we have introduced functional methods in quantum field theories which will proove indespensible in this work. We have discussed the difficulties of making calculations with the functional objects on the level of the path integral. An alternative approach, namely the shell-wise integration of the path integral was discussed. In the following, we will introduce an alternative way of implementing the successive integration of field modes which offers numerous computational advantages, namely,

the FRG.

2.2 Flow equation for the effective average action

In the previous section we argued that the Wilsonian effective action, S_b, defines a trajectory in theory space, starting at the classical action. In the same spirit, we now construct an interpolating functional Γ_k between the classical action S and the full quantum effective action Γ parametrised by one continuous parameter k. We call Γ_k the effective average action. Instead of performing the path integral in small steps ordered by the parameter b as before, we construct a one-parameter family of quantum field theories parametrised by the momentum scale k which has the properties

$$\Gamma_k \xrightarrow{k\to\Lambda} S\,, \tag{2.8a}$$

$$\Gamma_k \xrightarrow{k\to 0} \Gamma\,. \tag{2.8b}$$

Constructing Γ_k

We start at the level of the partition function (2.2) and add a k-dependent infrared regulator term ΔS_k to the classical action. In order to obtain a 1-loop structure for the flow equation the infrared regulator is chosen quadratic in the fields φ. In this case, ΔS_k can be thought of as a k-dependent mass term. We write

$$S[\varphi] \to S_k[\varphi] = S[\varphi] + \Delta S_k\,, \tag{2.9}$$

$$\Delta S_k = \frac{1}{2} R_{k,\mathbf{ab}} \varphi^{\mathbf{a}} \varphi^{\mathbf{b}}\,. \tag{2.10}$$

ΔS_k suppresses fluctuations with momenta lower than scale k. Thus, it acts like a mass only for that fraction of modes. The modes with $p \gg k$ are not suppressed by ΔS_k. In order to meet the requirements for the effective average action, (2.8), the regulator R_k as a function of the momentum p needs to fulfill the following conditions [32]:

$$\lim_{\frac{p^2}{k^2}\to 0} R_k(p^2) > 0\,, \qquad \text{(IR-regularisation)} \tag{2.11a}$$

$$\lim_{\frac{k^2}{p^2}\to 0} R_k(p^2) = 0\,, \qquad \left(\lim_{k\to 0} \Gamma_k = \Gamma\right) \tag{2.11b}$$

$$\lim_{k^2\to\Lambda^2} R_k(p^2) = \infty\,. \qquad \left(\lim_{k\to\Lambda} \Gamma_k = S\right) \tag{2.11c}$$

The relation (2.11c) is necessary if we demand an interpolating functional between S and Γ. It contains a few more subtleties, which we will discuss when we apply the formalism developed here to the case of gravity in section 2.3.

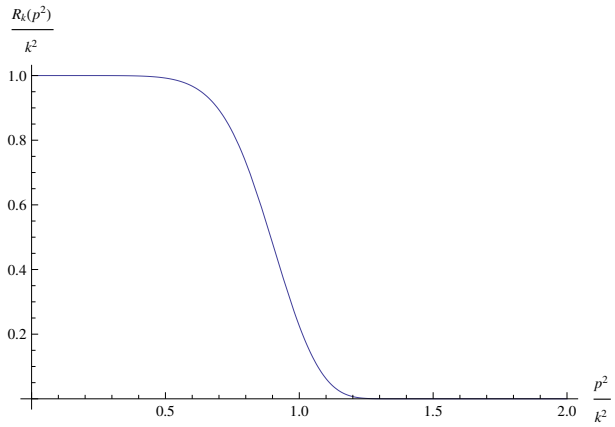

Figure 2.2: A typical, so called exponential regulator. It scales with k^2 for small p^2 and decays quickly for $p^2 > k^2$.

In Figure 2.2 a typical regulator is shown. Obviously, it fulfills the requirements (2.11).

The scale dependent action $S_k[\varphi]$ leads to a scale dependent partition function $Z_k[J]$ via the defining equation (2.2). Now, exactly in the same way as in section 2.1.1 we derive the k-dependent Schwinger functional $W_k[J]$ by taking the logarithm of $Z_k[J]$. The effective average action $\Gamma_k[\phi]$ is defined via a modified Legendre transform according to

$$\Gamma_k[\varphi] = \sup_J \left(J_k^{\mathbf{a}}\phi_{\mathbf{a}} - W_k[J]\right) - \Delta S_k[\phi]\,. \tag{2.12}$$

Indeed, the functional Γ_k fulfills the requirements (2.8):

1. Since ΔS_k vanishes when k goes to zero (equation (2.11b)), Γ_k will go to the full Γ in this limit, i.e. (2.8b) is satisfied.

2. Following equation (2.11c) the regulator $R_k(p^2)$ tends to infinity in the limit $k \to \infty$. Consider the background field equation for Γ_k which is given by equation (2.7) in the presence of a regulator term. In the limit $k \to \Lambda$, $\exp(-\Delta S_k[\varphi])$ becomes a delta functional peaked at $\varphi = 0$. This leads to the limit $\Gamma_\Lambda[\phi] = S[\phi]$ (c.f. equation (2.8a)) [33].

The definition (2.12) has further implications. Since we are dealing with k-dependent quantities and we are using a modified Legendre transform, the properties of the effective average action are slightly modified compared to the k-independent effective action Γ. We now have

$$(\Gamma_k + \Delta S_k)^{\mathbf{a}|}[\phi] = \gamma^{\mathbf{a}}{}_{\mathbf{b}}\, J^{\mathbf{b}}(\phi)\,, \tag{2.13a}$$

$$W_{\mathbf{a}|}[J] = \phi_{\mathbf{a}}(J)\,, \tag{2.13b}$$

and furthermore,

$$W_{k,\mathbf{ac}|}(\Gamma_k + \Delta S_k)^{\mathbf{cb}|} = \gamma^{\mathbf{b}}{}_{\mathbf{a}}$$
$$G_{k,\mathbf{ac}}(\Gamma_k + \Delta S_k)^{\mathbf{cb}|} = \gamma^{\mathbf{b}}{}_{\mathbf{a}} = (-1)^{\mathbf{ab}}\delta^{\mathbf{b}}_{\mathbf{a}}\,, \tag{2.13c}$$

where we write the second field variation of W_k as the k-dependent connected Green's function G_k. These relations are similar to the ones derived for Γ in section 2.1.1. In fact, we easily obtain the equations (2.13) from (2.6) by making the substitution

$$\Gamma[\phi] \to \Gamma_k[\phi] + \Delta S_k[\phi]\,.$$

We understand this by noting that the modified Legendre transform in (2.12) for Γ_k is the usual Legendre transform for the sum $\Gamma_k[\phi] + \Delta S_k[\phi]$.

Thus, we have constructed an interpolating functional between the classical action and the full quantum effective action. The problem of dealing with the path integral which integrates out all momentum shells at once, however, remains.

2.2.1 Exact flow equation for Γ_k

Instead of dealing with the effective average action Γ_k itself it turns out favourable to consider the change of Γ_k under an infinitesimal variation of k, namely, the flow of Γ_k. This quantity is always finite, just as the flow of the Wilsonian effective action. To derive an equation for the flow of Γ_k it is convenient to introduce a dimensionless 'renormalisation group time' $t = \ln(\frac{k}{\Lambda})$. Derivatives with respect to t are given by $\frac{\partial}{\partial t} = k\frac{\partial}{\partial k}$. We take the derivative of (2.12) with respect to t and use (2.13a). Rearranging terms and using (2.13) we arrive at the exact flow equation for the effective average action in its various guises [10, 11, 32–34]

$$\dot{\Gamma}_k = \frac{1}{2} G_{k,\mathbf{ab}} \dot{R}_k^{\mathbf{ab}}\,, \tag{2.14a}$$
$$\dot{\Gamma}_k = \frac{1}{2}(-1)^{\mathbf{ab}} \left[(\Gamma_k^{(2)} + R_k)^{-1}_{\mathbf{ab}} \dot{R}_k^{\mathbf{ab}}\right]\,, \tag{2.14b}$$
$$\dot{\Gamma}_k = \frac{1}{2}\,\mathrm{Str}\left[(\Gamma_k^{(2)} + R_k)^{-1}\dot{R}_k\right]\,, \tag{2.14c}$$

were we denote derivatives with respect to t with a dot, Str denotes the super trace. This equation was first derived by Wetterich in 1993 [10]. We use all three formulations (2.14a), (2.14b) and (2.14c) in the rest of the present work. Formulation (2.14b) is particularly convenient to trace back the appearence of the minus sign for fermionic fields.

Properties of the exact flow equation

1. Equation (2.14) is an exact relation. Since we have not made any approximations (2.14) could just as well be used as a definition for the quantum field

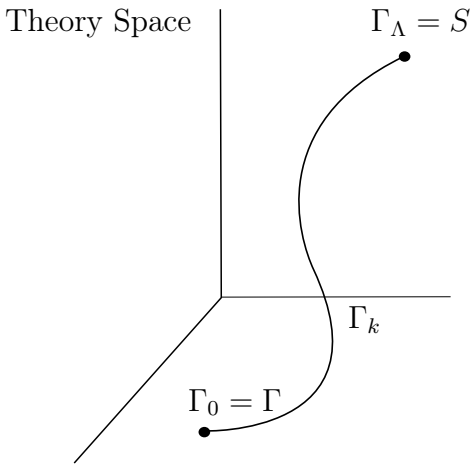

Figure 2.3: Graphical representation of the effective average action Γ_k as a trajectory in theory space. Γ_k starts at $k = \Lambda$ where it is identifed with the classical action and ends at the full quantum effective action at $k = 0$.

theory. It is also a 1-loop equation. The one loop structure of the equation becomes obvious if (2.14) is written in terms of a diagram with fully dressed propagators and vertices according to

$$\dot{\Gamma}_k = \frac{1}{2}$$  , (2.15)

where we introduced the symbols

(2.16)

2. Since the right hand side of the flow equation contains $\Gamma_k^{(2)}$, (2.14) is a functional differential equation. Because $\Gamma_k^{(2)}$ enters the right hand side nonlinearly, it is also a nonlinear. Its solution is interpreted as a trajectory through theory space with fixed starting point ($\Gamma_\Lambda = S$) and fixed end point ($\Gamma_0 = \Gamma$). Figure 2.3 depicts this idea schematically. Although we got rid of the path integral that we had in the background field equation (2.7), this equivalent, nonlinear functional differential equation is still not solvable in general. However, as we will see in section 3.4 it is comparably easy to make systematic non-perturbative approximations for which we find solutions.

3. On the right hand side of (2.14) R_k and its t-derivative $\dot{R}_k$ enter. R_k plays the role of an IR-regulator as discussed above. $\dot{R}_k$ additionally acts as a UV-regulator and thereby renders the flow finite. In Figure 2.4 a typical exponential regulator and its derivative with respect to t are shown. The fact that $\dot{R}_k$ is sharply peaked around $p^2 = k^2$ suggests that mainly momentum modes around k enter the flow of Γ_k. We interpret this as the implementation of the Wilsonian idea of integrating out momentum shells.

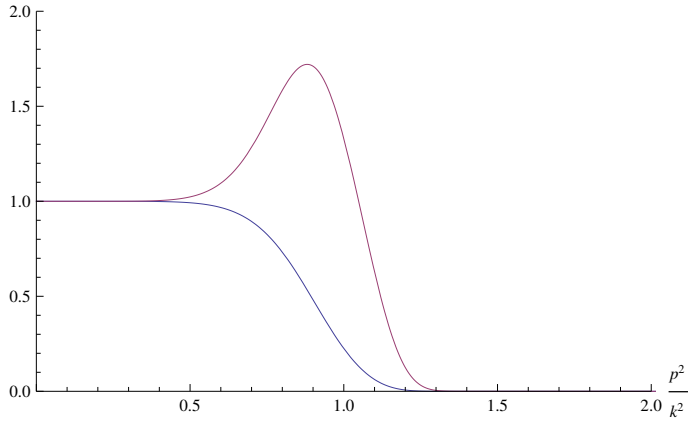

Figure 2.4: A typical exponential regulator R_k (blue curve) and the associated derivative $\dot{R}_k$ (red curve) with respect to the RG-time t. $\dot{R}_k$ is divided by two so that the functions match at $p^2 = 0$.

4. It is simple to recover perturbation theory from (2.14). To this end, we consider the case of one scalar field, for which Str $\to$ Tr and expand Γ_k to one-loop order, reinstalling $\hbar$ we have

$$\Gamma_k = S + \hbar {\Gamma_k}^{1-loop}. \tag{2.17}$$

We substite (2.17) into the flow equation (2.14) and consider lowest order in $\hbar$ on both sides. This arrive at

$$\begin{aligned} \dot{\Gamma}_k^{1-loop} &= \frac{1}{2}\frac{\mathrm{d}}{\mathrm{dt}} \operatorname{Tr} \ln\left(S^{(2)} + R_k\right) , \\ \Rightarrow \Gamma_k^{1-loop} &= \frac{1}{2} \operatorname{Tr} \ln\left(S^{(2)} + R_k\right) - \frac{1}{2} \operatorname{Tr} \ln\left(S^{(2)} + R_\Lambda\right) + S , \\ \Rightarrow \Gamma_0^{1-loop} &= \frac{1}{2} \operatorname{Tr} \ln\left(S^{(2)}\right) - \frac{1}{2} \operatorname{Tr} \ln\left(S^{(2)} + R_\Lambda\right) + S . \end{aligned} \tag{2.18}$$

The first term in (2.18) is the usual one loop expression for the effective action. The second and third term are constant and the second term is infinite (since R_Λ is infinite). We interpret this term as perturbative regularisation term that leads to a finite expression on the left hand side of (2.18). We arrive at the renormalised one-loop effective action, which is known from standard perturbative renormalisation [31, 35].

The flow equation for the effective average action (2.14) is the starting point for our analysis of quantum gravity. As we have argued, it is a non-perturbative evolution equation for the functional Γ_k through an infinite dimensional theory space. The flow equation (2.14) is an exact relation for the flow of Γ_k which has a wide range of applications in particle physics, condensed matter theory and statistical physics [32–34].

2.3 The FRG in Quantum Gravity

All we have done so far holds for general quantum field theories and arbitrary fields $\phi_{\mathbf{a}}$. In this work, we work with a superfield Φ which we define as the collection of all fluctuating fields in our theory. We have

$$\Phi_{\mathbf{a}} = (g, \bar{c}, c, \bar{\psi}, \psi, \phi)\,, \tag{2.19}$$

where we suppress all field indices on the right hand side for convenience. Let us first discuss the field content in more detail.

Path Integral for Gravity

With $g_{\mathbf{a}}$ we denote the metric, which is a fluctuating spin-2 field in our formulation. Thus, reinstalling all indices in coordinate space $g_{\mathbf{a}}$ is given by

$$g_{\mathbf{a}} = g_{\mu\nu}(x)\,. \tag{2.20}$$

Classical gravity is governed by the Einstein-Hilbert action. In d-spacetime dimensions it reads

$$S_{\mathrm{EH}}[g_{\mathbf{a}}] = \frac{1}{16\pi G_N}\int (2\Lambda - R)\,\sqrt{g}d^dx\,, \tag{2.21}$$

where Λ denotes the cosmological constant and R is the curvature scalar which is quadratic in first spacetime derivatives and linear in second spacetime derivates of $g_{\mathbf{a}}$. $\sqrt{g}$ denotes the square root of the determinant of $g_{\mathbf{a}}$. More information is found in Appendix A.1. Newton's coupling G_N has mass dimension

$$[G_N] = 2 - d\,. \tag{2.22}$$

In $d = 4$ dimensions quantum gravity is therefore a perturbatively non-renormalisable quantum field theory according to the BPHZ theorem [36–38]. Thus, renormalisability can only be achieved non-perturbatively.

The action (2.21) is invariant under general coordinate transformations also called diffeomorphisms. The symmetries of (2.21) are discussed in more detail in section 4.1. If we turn to a path integral description we want to make sense of the sum over all metrics. We write

$$Z = \int e^{-S_{\mathrm{EH}}[g_{\mathbf{a}}]}\mathcal{D}g_{\mathbf{a}\Lambda}\,. \tag{2.23}$$

In this formulation, however, the path integral not only sums over different metrics but also over the same metric in different parametrisations. Therefore, the formulation in (2.24) suffers from overcounting of gauge-equivalent configurations. This is prevented by fixing the gauge which is a common procedure in the path integral

formulation of gauge theories [31]. We add a gauge fixing action $S_{\rm gf}$ and a ghost action $S_{\rm gh}$ according to

$$S_{\rm EH}[g_{\mathbf{a}}] \to S_{\rm EH}[g_{\mathbf{a}}] + S_{\rm gf}[g_{\mathbf{a}}, \bar{c}_{\mathbf{b}}, c_{\mathbf{c}}] + S_{\rm gh}[g_{\mathbf{a}}, \bar{c}_{\mathbf{b}}, c_{\mathbf{c}}]\,. \tag{2.24}$$

We discuss the terms $S_{\rm gf}$ and $S_{\rm gh}$ in more detail in section 4.2. The fields $\bar{c}$ remove the gauge redundancy from the path integral, thereby preventing overcounting of gauge-equivalent field configurations of $g_{\mu\nu}$. They are Grassmann-valued spin-1 fields and, therefore, obey anticommutation relations. We interpret them as negative degrees of freedom. Their full set of indices is given by

$$(\bar{c}_{\mathbf{a}}, c_{\mathbf{b}}) = (\bar{c}_{\mu}(x_1), c_{\nu}(x_2))\,. \tag{2.25}$$

The gauge-fixed path integral of quantum gravity now reads

$$Z = \int e^{S_{\rm EH}[g_{\mathbf{a}}]+S_{\rm gf}[g_{\mathbf{a}},\bar{c}_{\mathbf{b}},c_{\mathbf{c}}]+S_{\rm gh}[g_{\mathbf{a}},\bar{c}_{\mathbf{b}},c_{\mathbf{c}}]}\mathcal{D}g_{\mathbf{a}\Lambda}\mathcal{D}\bar{c}_{\mathbf{b}\Lambda}\mathcal{D}\bar{c}^{\mathbf{b}}{}_{\Lambda}\,. \tag{2.26}$$

The fields $(g, \bar{c}, c)$ are required for a quantum field theory of pure gravity. The metric field $g_{\mu\nu}$ appears as the square root of the determinant $\sqrt{g}$ in all action integrals to account for diffeomorphism invariance of the classical action. This leads to interactions of arbitrary order of gravity with all fields.

Matter Fields

In order to include matter, we will furthermore consider arbitrary numbers of complex Grassmann-valued spin-1/2 and a real spin-0 fields, $(\bar{\psi}, \psi)$ and ϕ, respectively. Expanding the multi-indices we have

$$(\bar{\psi}_{\mathbf{a}}, \psi_{\mathbf{b}}) = (\bar{\psi}_{a,A}(x_1), \psi_{b,B}(x_2))\,, \tag{2.27}$$

$$\phi_{\mathbf{a}} = \phi_c(x_1)\,, \tag{2.28}$$

where a and b denote flavour indices for the fermions, the index c is a colour index. The captial letters A and B denote spinor indices for Dirac spinors, $A, B \in \{1, \ldots, 4\}$. Flavour and coulour indices take the values $a, b \in \{1, \ldots, N_f\}$ and $c \in \{1, \ldots, N_s\}$, respectively.

Flow Equation

Considering the whole field content the flow equation (2.14) has to be evaluated for the superfield Φ. Expanding its indices, we bring (2.14) for $\Gamma_k[\Phi]$ into the form

$$\begin{aligned}\dot{\Gamma}_k[\Phi] = \frac{1}{2}\,\mathrm{Tr}\left[(\Gamma_k^{(2)} + R_k)^{-1}\dot{R}_k\right]_{gg} - \mathrm{Tr}\left[(\Gamma_k^{(2)} + R_k)^{-1}\dot{R}_k\right]_{\bar{c}c} \\ - \mathrm{Tr}\left[(\Gamma_k^{(2)} + R_k)^{-1}\dot{R}_k\right]_{\bar{\psi}\psi} + \frac{1}{2}\,\mathrm{Tr}\left[(\Gamma_k^{(2)} + R_k)^{-1}\dot{R}_k\right]_{\phi\phi}\end{aligned} \tag{2.29}$$

Here, the traces still have to be performed with respect to the remaining indices of the respective constituent fields of Φ. In particular, the trace over the continuous variable x (or alternatively, p) is given by an integral.

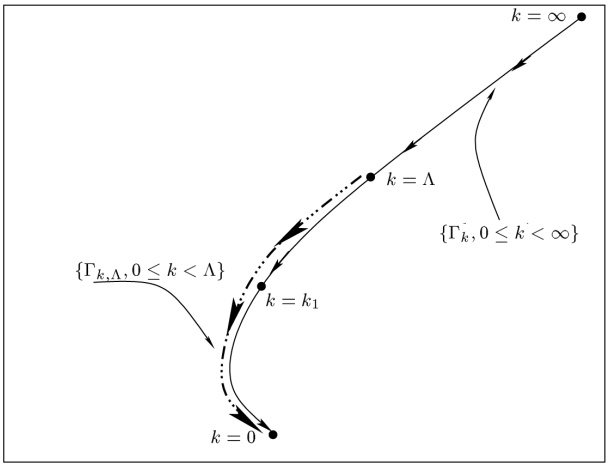

Figure 2.5: Schematic representation of the flow of the functional Γ_k from the UV ($k = \infty$) to the IR ($k = 0$). The cutoff scale Λ at which the effective action is defined fixes the incomplete trajectory. It serves as initial condition for the study the UV and the determination of the complete trajectoy. Taken from [39].

2.3.1 'Flowing Up' towards the UV

In the previous section we considered the flow equation (2.14) which was defined for a quantum field theory with a microscopic description incorporated in the classical action S_Λ. We assumed that there exists a regularized and thus well-defined path integral description with a UV-cutoff at scale Λ. In this picture, the flow equation (2.14) is viable in order to study the physics for $k < \Lambda$ and describes the 'flowing down' towards the infrared. In the Wilsonian picture, this is interpreted as integrating out high momentum shells. By definition, this is only possible for $k < \Lambda$. In order to study the asymptotic safety scenario quantum gravity we intend to do the direct opposite. In our picture the classical gauge fixed Einstein–Hilbert action (2.21) is an effective quantum field theory which is valid at low energies compared to the Planck scale [40]. We start with this effective theory defined at cutoff scale Λ and use it as an initial condition for a study of the ultraviolet limit $k \gg \Lambda$ [39, 41, 42]. This is possible since, the flow $\dot{\Gamma}_k$, which we obtain for the UV-regularized functional $\Gamma_{k,\Lambda}$ from the flow equation (2.14), does not depend on Λ any more. This allows to send Λ to infinity and thus study Γ_k also for $k \gg \Lambda$. In Figure 2.5 depicts the explained situation schematically. The 'classical action' only serves as an initial condition for the study of the UV-behavior of theory and has lost its interpretation as a microscopical action. The microscopic interactions at the Planck scale are governed by the 'bare action' Γ_∞ which is a prediction rather than an input of asymptotic safety.

An important ingredient for this to be possible is the locality of the flow of Γ_k in momentum space. Since the flow $\dot{\Gamma}_k$ decays rapidly for field momenta $p \gg k$ it, does not 'feel' the cutoff for $k < \Lambda$ which is why Λ does not appear explicitly in

the flow. The locality in momentum space appears in the trace of the flow, due to the UV-regulating term $\dot{R}_k$ [39]. The locality of the flow in momentum space is therefore of great importance in order to be able to 'flow up' towards higher scales than the cutoff initially allows. Otherwise, the physics at high energy scales would spuriously depend of the physics at the low energy cutoff scale.

The locality for $\dot{\Gamma}_k$ is closely connected to the locality of the flow of the n-point functions. Thus, in order to study the UV behavior of a theory where only an effective classical action at lower energies is known, we also demand this kind of locality for the flow the n-point functions of the theory. In the present work, we show locality in momentum space for the graviton n-point functions up to $n = 3$ in chapter 6.

Since the flow equation Γ_k loses its explicit dependence on the cutoff scale Λ, we omit this dependence in the following. However, we keep in mind that the classical action defines the initial condition for the flow towards the UV. Therefore, it fixed the trajectory which defines the asymptotically safe theory.

In this section, we discussed the subtlety of 'flowing up' the FRG towards the UV. It is the direct opposite of what is done in most other applications of the FRG. Studying the UV behaviour of a theory with the flow equation even beyond its cutoff scale is possible because of the locality of the flow in momentum space. The classical action enters this picture as an initial condition for Γ_k.

3 RG flows in theory space

In the section 2.2 we have interpreted Γ_k as a trajectory of a functional through the space of all functionals, which we call theory space. We make this idea more specific in the following chapter. We mainly follow [42].

3.1 Theory Space

The effective average action Γ_k is a functional of the fields Φ which depends on one real scaling parameter k. We interpret it as a parametrized curve in theory space. Generally, theory space is the space of all functionals $\mathcal{F} : \Phi \to A[\Phi]$ that have the same symmetries as the classical action [42]. For gravity, the symmetry is the invariance under diffeomorphisms. We assume there exists a complete set of basis functionals $\{\mathcal{E}_\alpha[\Phi]\}$ of theory space, in which we expand Γ_k according to

$$\Gamma_k[\Phi, \bar{w}_\alpha] = \sum_{\alpha=1}^{\infty} \bar{w}_\alpha(k)\mathcal{E}_\alpha[\Phi]\,, \tag{3.1}$$

where the $(\bar{w}_\alpha)$ are generalized couplings. The flow equation (2.14) defines a vector field $\bar{\boldsymbol{\beta}}$ on theory space. The components $(\bar{\beta}_\alpha)$ are the β-functions of the respective couplings $\bar{w}_\alpha$. Integral curves along the vector field $\bar{\boldsymbol{\beta}}$ are given by the trajectories of Γ_k. They define the quantum field theory completely for a chosen initial condition. We obtain $\bar{\boldsymbol{\beta}}$ by inserting (3.1) into the flow equation (2.14). We have

$$\partial_t\Gamma_k[\Phi, \bar{w}_\alpha] = \sum_{\alpha=1}^{\infty} \partial_t\left(\bar{w}_\alpha\mathcal{E}_\alpha[\Phi]\right) = \frac{1}{2}\sum_{\alpha=1}^{\infty}(-1)^{\mathbf{ab}}(\bar{w}_\alpha\mathcal{E}_{\alpha,\mathbf{ab}|}[\Phi] + R_{k,\mathbf{ab}})^{-1}\dot{R}_k^{\mathbf{ab}}\,. \tag{3.2}$$

The traces on the right hand side are also functionals in theory space. Thus, we obtain the components $\bar{\beta}_\alpha = \partial_t\bar{w}_\alpha$ by expanding the right hand side of (3.2) in terms of the basis functionals $\mathcal{E}_\alpha$, and comparing the coefficients. Generally, the $\bar{\beta}_\alpha$ take the form

$$\partial_t\bar{w}_\alpha(k) = \bar{\beta}_{\alpha,k}(\bar{w}_1, \bar{w}_2, \ldots)\,. \tag{3.3}$$

Hence, each $\bar{\beta}_\alpha$, in general depends on all other couplings $\bar{w}_n$ with $n \in \mathbb{N}$. This suggests that we will not be able to integrate the whole system of β-functions exactly. This is what we expect, since a solution to (3.3) means finding a solution for the full quantum system, which is impossible in most cases.

Often it is useful to express the dimensional couplings $\bar{w}_\alpha$ in terms of their dimensionless counter parts w_α. They are given by

$$w_\alpha = k^{-d_\alpha}\bar{w}_\alpha\,, \tag{3.4}$$

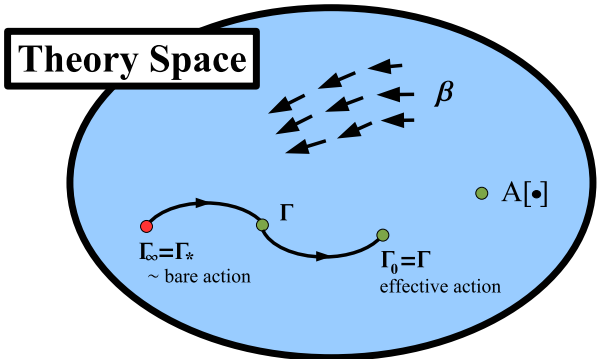

Figure 3.1: A schematic drawing of theory space. Each point is a functional $A[\cdot]$. RG-trajectories are Γ_k are integral curves of the vector field β. Figure taken from [42]

where d_α is the canonical mass dimension of the coupling $\bar{w}_\alpha$. The β-functions for the dimensionless couplings are given by

$$\partial_t w_\alpha = -d_\alpha w_\alpha + k^{-d_\alpha} \bar{\beta}_{\alpha,k}(\bar{w}_1, \bar{w}_2, \ldots) = \beta(w_1, w_2, \ldots)\,. \tag{3.5}$$

By making the couplings dimensionless, their respective β-functions loose their explicit k-dependence. We understand this by considering the scaling property of Γ_k, namely

$$\Gamma_k[\Phi, \bar{w}_\alpha] = \Gamma_{bk}[b^{d_\Phi}\Phi, b^{d_\alpha}\bar{w}_\alpha]\,, \tag{3.6}$$

where b is a positive real and positive scaling parameter [41]. The quantities d_Φ and d_α are the canonical mass dimensions of the field content Φ and that of the dimensionful couplings $\bar{w}_\alpha$, respectively. For the choice $b = k^{-1}$, we obtain a trajectory $\hat{\Gamma}$ which does not depend on k explicitly, but only via the dimensionless couplings (w_α). We have

$$\hat{\Gamma}[k^{-d_\Phi}\Phi; w_\alpha] := \Gamma_1[k^{-d_\Phi}\Phi; k^{-d_\alpha}\bar{w}_\alpha] = \Gamma_k[\Phi; \bar{w}_\alpha]\,. \tag{3.7}$$

A rescaling with $b = k^{-1}$ leads to a vector field $\boldsymbol{\beta}$ on theory space which is independent of the 'RG-time' $t = \ln k$. The geometric interpretation of Γ_k gives rise to an interpretation of the concept of renormalisation in general, in terms of geometric quantities. In Figure 3.1 theory space is depicted schematically. In this picture, the shaded area represents points in theory space, where all (w_α) are well defined. At the border, they become divergent, and thus, an expansion of Γ_k in terms of the chosen basis is not possible. In this light, we define the task of renormalisation as finding a global trajectory which entirely lies inside the shaded area. Hence, a meaningful but still effective quantum field theory has a parametrization with well defined couplings (w_α) for $k \in [0, k_\Lambda]$. If some of the couplings diverge at the finite scale k_Λ, we interpret this as the onset of 'new physics' at this scale which is not covered by the effective description. If we find a trajectory Γ_k with well defined couplings

(w_α) for $k \in [0, \infty]$, we obtain a self-consistent description of the physics which is valid at arbitrary momentum scales. We call such a theory fundamental [41]. In the geometrical picture, we interpret the shaded area in Figure 3.1 as a coordinate patch on an infinite dimensional manifold. At the border the coordinates become singular and we have to change the coordinate basis, and thus, the set of basis functionals $\{\mathcal{E}_\alpha\}$, in order to be able to study Γ_k in that region. A divergence of the (w_α) is prevented, if they approach a fixed point of the renormalisation group flow within the region where the quantum field theory is well defined. This is satisfied if the (β_α) become zero for all α. Another possibility is, that the couplings approach a limit cycle [43]. In those cases the trajectory Γ_k stays in a located region of theory space for an infinite period of RG-time.

To conclude, we have taken the geometrical interpretation of the RG-flow further, to the definition of vector fields on theory space. In this picture, quantum field theories are entirely defined by the integral curves of these vector fields with initial conditions defined by the classical action. We identified the vector field $\boldsymbol{\beta}$ with the β-functions of the couplings. We have seen that fixed points of the RG-flow are closely related to the concept of renormalisability, which is why we discuss them in more detail in the next section.

3.2 Fixed points of the RG-flow

A fixed point of the RG-flow is reached, if the β-functions become zero for all couplings (w_α). As shown in (3.5), we can write the β_α as a sum of the canonical scaling part, which comes from the mass dimension of the coupling and a non-classical part which is due to quantum fluctuations governed by the flow equation. Consequently the two parts of (3.5) read

$$\beta_\alpha = \underbrace{-d_\alpha w_\alpha}_{\text{canonical scaling}} + \underbrace{k^{-d_\alpha}\bar{\beta}_\alpha(w_1, w_2, \ldots)}_{\text{quantum fluctuations}} . \tag{3.8}$$

Thus, in order to approach a fixed point which we denote as (w^*_α), the quantum fluctuations must cancel the canonical scaling terms in the β-functions. There are two possibilities where such a fixed point can be located.

Categories of Fixed Points

1. All couplings are zero at the fixed point,

$$w^*_\alpha = 0 \qquad \text{for all } \alpha\,, \tag{3.9}$$

   then we refer to (w^*_α) as a Gaussian fixed point.

2. For at least one α the corresponding coupling w_α is non-equal to zero. We have

$$w^*_\alpha \neq 0 \qquad \text{for at least one } \alpha\,. \tag{3.10}$$

In this case, we call (w_α^*) a non-Gaussian fixed point (NGFP).

A Gaussian fixed point in the ultraviolet is for instance realized in Yang-Mills theories. There, the coupling tends to zero as $k \to \infty$. The theory becomes free at high energies, a phenomenon, which is referred to as asymptotic freedom [4, 5]. Theories for which the couplings approach a Gaussian fixed point for $k \to \infty$ are those which are perturbatively renormalisable in the usual sense. Examples for theories with a non-Gaussian fixed point are interacting fermionic models of the Gross-Neveu-Type [44], interacting scalar theories like the sine-gordon model [45] and quantum gravity.

3.2.1 Stability of Fixed Points

The most important property of a given fixed point (w_α^*) is its stability, i.e., whether it attracts or repels nearby RG-trajectories. We call fixed point (w_α^*) attractive, if all trajectories in its vicinity are driven towards the fixed point. A fixed point which is attractive for $k \to 0$ is called an infrared (IR) attractive. On the other hand, we denote an attractive fixed point for $k \to \infty$ as ultraviolet (UV) attractive. In order to study the behavior of trajectories close to a fixed point we consider the linear approximation of the flow (β_α) around (w_α^*). The linearized flow is given by the Jacobi matrix $\underline{\mathbf{B}} = (B_{ij}) = \partial_j \beta_i(w^*)$ according to

$$\partial_t w_\alpha(k) = \sum_{j=1}^{\infty} B_{\alpha j}(w_j - w_j^*)\,. \tag{3.11}$$

This is now a linear differential equation in contrast to the full flow considered before. We can solve equation (3.11) in a general fashion. Its solution is given by

$$w_\alpha(k) = w_\alpha^* + \sum_{j=1}^{\infty} C_j V_\alpha^j \left(\frac{k}{k_0}\right)^{\theta_j}\,. \tag{3.12}$$

Here, $\mathbf{V^i}$ are right eigenvectors of $\underline{\mathbf{B}}$ with eigenvalues θ_i, which we call the critical exponents of the fixed point. We have

$$(\underline{\mathbf{B}} \cdot \mathbf{V^i})_\alpha = \theta_i V_\alpha^i\,. \tag{3.13}$$

Note that on the right hand side the index i is not summed over. The matrix $\underline{\mathbf{B}}$ is not necessarily symmetric such that the critical exponents θ_i are complex in general. The scale k_0 is a fixed reference scale and the C_j are constants of integration, which we have to fix by the initial conditions for the trajectory Γ_k. In the vicinity of a fixed point (w_α^*), Γ_k is always attracted by the fixed point for $k \to \infty$ $(k \to 0)$, if the real parts of all eigenvalues are smaller than zero (larger than zero). We express this statement as

$$\Re(\theta_j) \begin{cases} > 0 & \text{for all } j \qquad \text{(fully UV attractive)} \\ < 0 & \text{for all } j \qquad \text{(fully IR attractive)} \end{cases}\,. \tag{3.14}$$

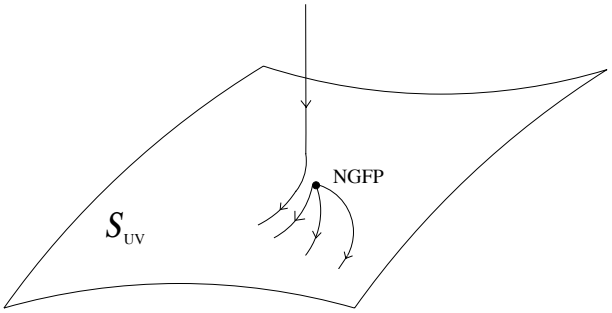

Figure 3.2: Schematic depiction of a UV-critical hyper surface $\mathcal{S}$ of a NGFP. Trajectories that start on $\mathcal{S}$ remain on $\mathcal{S}$ and diverge otherwise. The flow, represented by arrows, is pointing towards the IR in the picture. Figure taken from [42].

We call couplings that correspond to attractive (repulsive) critical exponents relevant (irrelevant). Couplings that correspond to vanishing critical exponents are called marginal. For fixed points which are not fully attractive, nearby trajectories still have the potential to approach them. In order for this to be possible, the coefficients C_j that correspond to critical exponents θ_j must be zero.

With this in mind, we develop the concept of the UV or IR critical hyper surface of a fixed point (w^*_α). The UV- or IR-critical hyper surface $\mathcal{S}_{\mathrm{UV/IR}}$ is defined as the union of all points that are pulled into (w^*_α) for $k \to \infty$ or $k \to 0$, respectively. Trajectories that start on $\mathcal{S}$ will stay on $\mathcal{S}$ and flow towards the fixed point. Those Γ_k that do not start on $\mathcal{S}$ however, will flow away from the fixed point and possibly towards infinity. Figure 3.2 schematically shows the trajectories of a UV-critical hyper surface corresponding to a non-Gaussian fixed point. Note that the arrows correspond to the flow in the IR-direction. The dimensionality of the critical hyper surface $\dim(\mathcal{S})$ is given by the number of attractive directions of the fixed point. Consequently, $\dim(\mathcal{S})$ is the number of coefficients C_j which can be tuned arbitrary, in order to reach the fixed point. All C_j that correspond to repulsive directions must be set to zero. Hence, if we require that a given fixed point is approached by a theory defined by the trajectory Γ_k, we interpret $\dim(\mathcal{S})$ as the number of input parameters that are needed to fix Γ_k. Thus, all other constants are fixed to be zero by that requirement. A valid initial point for Γ_k is for instance the classical action S_Λ which provides a description of the physics at that particular scale Λ. Hence, the constants we want to fix are related to the couplings that we can determine by experiments at that scale. The concept of fixed points of the renormalisation group flow that we introduced in this section is of great importance for the formulation of the asymptotic safety scenario.

3.3 Asymptotic Safety

In the following, we use the formalism discussed in the previous section in order to define the notion of a perturbatively non-renormalisable but yet fundamental and predictive quantum field theory. Quantum gravity formulated as a quantum field theory of the metric is perturbatively non-renormalisable [46]. In the language of RG-flows this means that the Gaussian fixed point for quantum gravity is UV unstable. However, quantum gravity could exhibit a UV attractive non-Gaussian fixed point instead. The corresponding theory is predictive, if we can completely fix the RG-trajectory Γ_k by a finite number of measurements. To that end, the non-Gaussian fixed point should have a finite dimensional UV-critical hyper surface. Thus, in order to define gravity as a fundamental quantum field theory of the metric, we require:

1. There exists a NGFP of the RG-flow of Γ_k for quantum gravity. We have
$$w^*_{\text{gravity},\alpha} \neq 0 \qquad \text{for at least one } \alpha\,. \tag{3.15}$$
2. The NGFP has a finite dimensional UV-critical hyper surface. Accordingly, we write
$$\dim \mathcal{S}_{\text{UV}} < \infty\,. \tag{3.16}$$

We use the combination of these two requirements for the definition of a fundamental and predictive quantum field theory of gravity. This set of conditions is called asymptotic safety scenario and was formulated by Weinberg in 1978 [3]. We use the classical action for gravity at some low energy as an initial condition for the flow equation (2.14). The procedure of 'flowing up' the renormalisation group towards the UV was discussed in detail in section . We can think of the bare action of the one that appears in the path integral with infinite cutoff. We obtain the bare action as the UV limit of Γ_k if it approaches a non-Gaussian for $k \to \infty$ [39]. Hence, the bare action action in the path integral is initially unknown and therefore, a prediction rather that an input of the theory [41].

3.4 Truncated RG-flows

It is impossible to solve the flow equation (2.14) exactly in general. Therefore, it is of great importance to apply efficient approximation methods. The architecture of the flow equations as functional differential equation is an ideal starting point for systematic non-perturbative approximation schemes. In general, we approximate the RG-flow by truncating the infinite dimensional theory space to a finite, N-dimensional subspace. We denote the trajectory Γ_k in truncated theory space as $\tilde{\Gamma}_k$ according to
$$\tilde{\Gamma}_k[\Phi, \bar{w}_\alpha] = \sum_{\alpha=1}^{N} \bar{w}_\alpha(k)\mathcal{E}_\alpha[\Phi]\,. \tag{3.17}$$

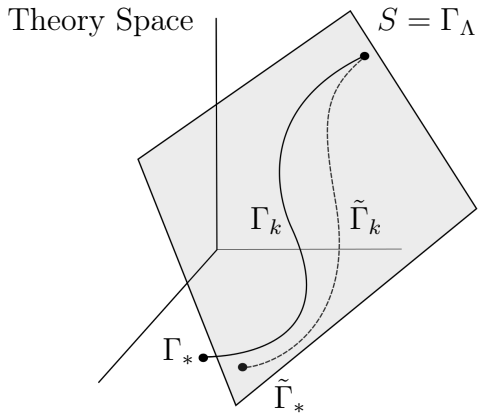

Figure 3.3: The full trajectory Γ_k is projected to a finite dimensional subspace (shaded plane). The projected and the exact trajectories $\tilde{\Gamma}_k$ and Γ_k approach different fixed points $\tilde{\Gamma}_*$ and Γ_* for $k \to \infty$, respectively. The truncation is typically chosen such that the classical action S lies within the truncated theory space.

The flow equation (2.14) now governs the flow of the dimensionless couplings $(w_\alpha)_{1\leq\alpha\leq N}$. Along the same lines as in section 3.1 we derive the corresponding β-functions according to

$$\partial_t w_\alpha = \beta(w_1, w_2, \ldots) \qquad \alpha \in \{1, \ldots, N\}\,. \tag{3.18}$$

As equation (3.18) suggests, the truncated system is in general not closed, since the right hand side depends on all couplings (w_α) of the full trajectory Γ_k. Typically, we close the system by making the identifications

$$0 = w_{N+1} = w_{N+2} = \ldots\,, \tag{3.19a}$$

or

$$w_N = w_{N+1} = w_{N+2} = \ldots\,. \tag{3.19b}$$

Systematic choices of the finite set of basis vectors $(\mathcal{E}_\alpha)_{1\leq\alpha\leq N}$ often entail only a finite number of identifications. In the next section we discuss some of the most commonly used truncation for quantum gravity.

In the geometrical picture, we think of the truncation procedure as a projection of the full trajectory Γ_k to some finite dimensional surface lying in theory space. Figure 3.3 depicts this idea graphically. For the asymptotic safety scenario, the classical action S_Λ is known at comparably low energies and we are interested in fixed point value of Γ_k at $k = \infty$, Γ_*. Since the flow produces in general all functional terms that are compatible with the symmetry of S_Λ, the endpoints of the exact trajectory Γ_k and that of the projected one $\tilde{\Gamma}_k$ need not agree in general. In turn, their fixed point values $\tilde{\Gamma}_*$ and Γ_*, are different in most cases. We chose the truncation such that the truncated system has qualitatively the same properties (e.g. fixed points

of the flow) as the full quantum system. This is usually a non-trivial task. Since the flow equation is non-perturbative, there is no (small) parameter which controls the accuracy of the approximation. Often the only possibility to validate the results is by investigating the impact of an extension of the truncation. In case additional basis functionals $\{\mathcal{E}_{N+1}, \mathcal{E}_{N+2}, \ldots\}$ do not have a relevant impact on the results, we consider the results reliable. As another possibility we vary the regulator which is be discussed in section 3.4.2.

3.4.1 Systematic Approximation Schemes

The choice of truncation in the presented picture amounts to choosing the finite basis $(\mathcal{E}_\alpha)_{1\leq\alpha\leq N}$. There are different common choices for systematic bases. In the following, we introduce the two which are used most often. Namely, the vertex expansion and the derivative expansion.

Vertex Expanison

In a vertex expansion the effective action is parametrized by a power series in the field Φ according to

$$\tilde{\Gamma}_k = \sum_{\alpha=0}^{N} \frac{1}{\alpha!} \Gamma_k^{(\mathbf{a_1}\ldots\mathbf{a}_\alpha)}\Big|_{\Phi=0} \Phi_{\mathbf{a_1}} \ldots \Phi_{\mathbf{a_n}} \,. \tag{3.20}$$

We denote by $\Gamma_k^{(\mathbf{a_1}\ldots\mathbf{a}_\alpha)}$ the n^{th} variation of the effective action with respect to the fields Φ, evaluated at vanishing fields. We have

$$\bar{w}_\alpha \mathcal{E}_\alpha[\Phi] = \frac{1}{\alpha!} \Gamma_k^{(\mathbf{a_1}\ldots\mathbf{a}_\alpha)}\Big|_{\Phi=0} \Phi_{\mathbf{a_1}} \ldots \Phi_{\mathbf{a_n}} \,. \tag{3.21}$$

However, the full quantum effective action is of course unknown. The approximation amounts to making an ansatz for ${\Gamma_k}^{(\mathbf{a_1}\ldots\mathbf{a}_\alpha)}$. In this work we use as an ansatz a certain tensor structure $\mathrm{T}_\alpha^{\mathbf{a_1}\ldots\mathbf{a}_\alpha}$, which we construct from the classical action. We extract the dimensionful couplings $(\bar{w}_\alpha)$ from T_α with help of an appropriately chosen projection procedure. We represent the projection by the operator Π and we write

$$\Pi \circ {\Gamma_k}^{(\mathbf{a_1}\ldots\mathbf{a}_\alpha)} = \Pi \circ \mathrm{T}_\alpha^{\mathbf{a_1}\ldots\mathbf{a}_\alpha} = \bar{w}_\alpha(k) \tag{3.22}$$

In our setup the object $\mathrm{T}_\alpha^{\mathbf{a_1}\ldots\mathbf{a}_\alpha}$ depends on derivatives and thus on the field momenta, as well as on spacetime indices. In order to extract the flow of the couplings $(w_\alpha)_{1\leq\alpha\leq N}$ we expand the right hand side of (3.2) in the vertices. This is done by taking the α^{th} functional derivative of (2.14) with respect to Φ. In doing so, we obtain flow equations for the n-point functions that we evaluate at vanishing fields $\Phi = 0$ according to

$$\partial_t \Gamma_k^{(\mathbf{a_1}\ldots\mathbf{a}_\alpha)}\Big|_{\Phi=0} = (-1)^{\mathbf{ab}} \frac{\delta^\alpha}{\delta\Phi_{\mathbf{a_1}}\ldots\delta\Phi_{\mathbf{a}_\alpha}} \left[(\tilde{\Gamma}_k^{(2)} + R_k)^{-1}_{\mathbf{ab}} \partial_t R_k^{\mathbf{ab}}\right]\Big|_{\Phi=0} . \tag{3.23}$$

We applying Π to both sides of equation (3.23) and use (3.22). Thereby, we arrive at a flow equation for the coupling $\bar{w}_\alpha$ given by

$$\partial_t \bar{w}_\alpha(k) = (-1)^{\mathbf{ab}} \Pi \circ \left[(\tilde{\Gamma}_k^{(2)} + R_k)^{-1}_{\mathbf{ab}} \partial_t R_k^{\mathbf{ab}} \right]^{\mathbf{a_1 \ldots a_\alpha}|} \Big|_{\Phi=0} , \tag{3.24}$$

where employ the short-hand notation for field variation introduced in Appendix A. The right hand side of the flow equation (2.14) contains a second variation of the effective action. Therefore, we have field variations up to order $\alpha + 2$ on the right hand side of (3.24). Consequently, the right hand side of (3.24) depends on the couplings $\{\bar{w}_2, \ldots, \bar{w}_{\alpha+2}\}$. In the same spirit, the flows of $\bar{w}_{N-1}$ and $\bar{w}_N$ depend on the couplings up to w_{N+1} and w_{N+2}, respectively. Therefore, the flow is not closed. However, closing is be achieved by making the identification

$$\bar{w}_N = \bar{w}_{N+1} = \bar{w}_{N+2} \, . \tag{3.25}$$

Thus, by making a vertex expansion for the projected flow $\tilde{\Gamma}_k$, we get the flow equations for the dimensionful couplings $(\bar{w}_\alpha)$. These are connected to the flow for the dimensionless couplings in a simple way through (3.5). Furthermore, we make only a finite number of identifications of couplings (cf. equation (3.25)). In the present work, exactly this kind of truncation is used. It will be explained in much more detail and on a less abstract level in the next chapter. For completeness, we will briefly go through the important concept of a derivative expansion which is most commonly used in quantum gravity [12, 17, 41, 42].

Derivative Expansion

The derivative expansion is a parametrisation of Γ_k in powers of invariants $(\mathcal{O}_i)_{1 \leq i \leq n}$ under the respective symmetries of the theory. They are classified by their highest power in the spacetime derivative. In the case of gravity, the operators $\mathcal{O}_j$ are invariants under diffeomorphisms. In Table 3.1 diffeomorphism invariant operators with different highest powers in derivatives are given. For the very simple example of a real scalar field with $\mathbb{Z}_2$-symmetry in flat spacetime, a derivative expansion for $\tilde{\Gamma}_k$ takes the form

$$\tilde{\Gamma}_k = \int V_k[\phi] + \frac{1}{2} Z_k[\phi] \, (\partial \phi)^2 + \mathcal{O}(\partial^2) d^4x \, , \tag{3.26}$$

where V_k denotes the effective potential and Z_k is the wavefunction renormalisation [32]. In the general case, we write the derivative expansion as

$$\tilde{\Gamma}_k[\Phi] = \sum_{\alpha=1}^{N} \bar{w}_\alpha \mathcal{O}_\alpha[\Phi, \partial] \tag{3.27}$$

Just as in case of the derivative expansion, we expand the trace on the right hand side of the flow equation (2.14) in terms of the invariants $\mathcal{O}_\alpha$ according to

$$\mathrm{Str} \left[(\tilde{\Gamma}_k^{(2)} + R_k)^{-1} \partial_t R_k \right] = \sum_{\kappa=1}^{\infty} \bar{v}_\kappa \mathcal{O}_\kappa[\Phi, \partial] \, . \tag{3.28}$$

number of derivatives $\leq$	operators
0	1
2	R
4	R^2,$R^{\mu\nu}R_{\mu\nu}$,$R^{\mu\nu\rho\sigma}R_{\mu\nu\rho\sigma}$,$C^{\mu\nu\rho\sigma}C_{\mu\nu\rho\sigma}$
...	...

Table 3.1: Diffeomorphism invariant operators ordered by their maximum power of spacetime derivatives. R, $R^{\mu\nu}$, $R^{\mu\nu\rho\sigma}$ and $C^{\mu\nu\rho\sigma}$ are the Ricci scalar, the Ricci tensor, the Riemann curvature tensor and the Weyl tensor, respectively.

In order to extract the couplings from this equation we evaluate this equation for certain choices of field. For the metric $g_{\mathbf{a}}$ a typical choice are maximally symmetric geometries. Then we employ heat kernel techniques in order to evaluate the integrals [41, 42]. This gives an expansion of the right hand side of (2.14) in terms of the Ricci scalar R, which is compared with the left hand side to get the flows for the respective couplings.

3.4.2 Regulator dependence of the flow

An important input to the flow equation is the regulator R_k. As we discussed in section 2.2 it is left arbitrary, up to the requirements (2.11). The trajectory Γ_k in theory space depends on the chosen regulator R_k. However, starting point and endpoint of Γ_k are fixed by definition. This ceases to be true for the truncated system. The UV fixed point Γ_* of Γ_k does in general not lie within the truncation subspace. Furthermore, the UV fixed of the truncated effective average action $\tilde{\Gamma}_k$, $\tilde{\Gamma}_*$, depends also on the choice of regulator. All results obtained in a truncated system therefore depend on the choice of regulator. This makes it difficult to decide whether properties of the truncated flow are actual properties of the system or if they are merely artifacts of the truncation. To avoid regulator related artifacts we are in principle obliged to make regulator studies where we consider the stability of the results under the change of regulator. This stability is also used as an indicator for the quality of a truncation. Since for the complete system the starting and endpoints of the flow are fixed, we expect the endpoint of the truncated flow to change only slightly under the change of regulator for a good truncation [33]. In most cases this requirement is fulfilled. The choice from a class of optimized regulators allows to improve behavior of the RG-flow and in some cases even leads to analytic flow equations for the couplings [47].

Part II

Gravity and Non-Interacting Matter

4 Quantum Gravity with Matter

In this section, we make the analysis of quantum gravity with matter more specific. In particular, we discuss the used truncation for the effective average action. We further explain how the background field formalism for gravitons and the spin base invariant formalism for fermions enter our formulation. In the following section, we expand the multi-indices used up to this point. Hence, as discussed in section 2.3 we write the superfield Φ as

$$\Phi_{\mathbf{a}} = (g, \bar{c}, c, \bar{\psi}, \psi, \phi)\,. \tag{2.19}$$

For notational convenience, we suppress the spacetime coordinates and spinor indices. Hence, we write the constituent fields of Φ as

$$g_{\mathbf{a}} = g_{\mu\nu}\,, \quad (\bar{c}_{\mathbf{a}}, c_{\mathbf{b}}) = (\bar{c}_{\mu}, c_{\nu})\,, \quad (\bar{\psi}_{\mathbf{a}}, \psi_{\mathbf{b}}) = (\bar{\psi}_{a}, \psi_{b})\,, \quad \phi_{\mathbf{a}} = \phi_{a}\,.$$

For the parametrization of the trajectory $\tilde{\Gamma}_k$ through truncated theory space we use a truncated effective average action $\tilde{\Gamma}_k$ in terms of a vertex expansion of Γ_k. To construct the vertices $\Gamma_k^{(n)}$ we use the classical action with suitable IR-regulator terms, $S_{\text{class,k}}$ that are discussed in the sequel. Note, that this action is not classical in the conventional sense, since it contains a ghost sector which is only relevant for the quantisation of gauge degrees of freedom. Therefore, what we regard as classical here is the Einstein–Hilbert action known from General Relativity together with suitable ghosts in order to avoid gauge redundancy in the path integral. Furthermore, we add minimally coupled kinetic terms for fermion and scalar fields to account for the field content of our theory of gravity and non-interacting matter. The classical action, including k-dependent IR-regulators is then given by

$$S_{\text{class},k} = S_{\text{grav},k} + S_{\text{ferm},k} + S_{\text{scal},k}\,. \tag{4.1}$$

The vertex expansion we are considering here extends up to order $N = 3$ (cf. equation (3.20)) in the fields. Hence, we have

$$\tilde{\Gamma}_k[\Phi] = \sum_{\alpha=0}^{3} \frac{1}{\alpha!} \Gamma_{\alpha}^{(\boldsymbol{a_1}\ldots\boldsymbol{a_\alpha})} \Phi_{\boldsymbol{a_1}} \ldots \Phi_{\boldsymbol{a_\alpha}}\,. \tag{4.2}$$

The vertices $\Gamma_k^{(n)}$ in the expansion are given by field variations of $S_{\text{class},k}$

$$\Gamma_{\alpha}^{(\boldsymbol{a_1}\ldots\boldsymbol{a_\alpha})} = S_{\text{class},k}^{\boldsymbol{a_1}\ldots\boldsymbol{a_\alpha}|}[\Phi]\Big|_{\Phi=0}\,. \tag{4.3}$$

The truncated effective average action is discussed in more detail in section 4.3. The IR-regularised classical action $S_{\text{class,k}}$ studied in larger extent in the following.

4.1 Diffeomorphism Symmetry and Background Field Formalism

Physical quantities like the effective action and, thus, the effective average action Γ_k for $k \to 0$ are used to compute observables like scattering amplitudes. These quantities should be diffeomorphism invariant. In our formulation, the effective average action is given in terms of a vertex expansion. Thus, for $k \to 0$, we require the vertices to be diffeomorphism invariant in order to retain a diffeomorphism invariant effective action. Therefore, we first have to find a way to define a diffeomorphism invariant classical action which, on the other hand, fixes the gauge. To this end, we employ the background field formalism [32, 48, 49]. It allows for the construction of a gauge-invariant action for arbitrary gauge fields. Within this formalism, a background field is introduced with respect to which the considered dynamical gauge field fluctuates. In fact, in the case of gravity, it is mandatory to introduce a background field for yet another reason: In order to have a notion of the 'size' of momentum modes of the metric $g_{\mu\nu}$, we need a background metric $\bar{g}_{\mu\nu}$, with respect to which the this momentum is measured. As was pointed out in section (2.2) the ordering of modes is required for the IR regulator R_k. Concretely, the momentum modes of $g_{\mu\nu}$ are ordered by the size of the eigenvalues of the respective background covariant Laplacian $\underline{\Delta}$. Hence, the background field $\bar{g}_{\mu\nu}$ is a crucial ingredient for the IR-regularisation in quantum gravity. In this section, we want to discuss the implications of the background field formalism for the symmetries of the effective average action.

The general strategy for the construction of a diffeomorphism invariant effective action in the limit $k \to 0$ using the background field method is the following [32]:

1. Introduce a background field $\bar{g}_{\mu\nu}$ accompanied by a symmetry transformation $\bar{\mathcal{G}}$ given by background diffeomorphisms. This results in an effective average action which depends on the background metric $\Gamma_k[g;\bar{g}]$. Loosely speaking $\bar{g}_{\mu\nu}$ appears as external source which is not summed over in a path integral representation.

2. Construct an effective average action $\Gamma_k[g;\bar{g}]$ that is invariant under combined background diffeomorphism and background diffeomorphim transformations $\mathcal{G} + \bar{\mathcal{G}}$. However, it is not invariant under the full diffeomorphism transformations $\mathcal{G}$ alone, due to gauge fixing of the action.

3. For $k \to 0$ it is possible to identify

$$\bar{g}_{\mu\nu} = g_{\mu\nu}, \tag{4.4}$$

which results in an effective action $\Gamma_k[g]$ which is invariant under the full diffeomorphism transformations.

Let us make this construction more precise. The gravity part of the classical action (4.1) comprises four terms,

$$S_{\mathrm{grav},k} = S_{\mathrm{EH}} + S_{\mathrm{gh}} + S_{\mathrm{gf}} + \Delta S_{\mathrm{grav},k}\,, \tag{4.5}$$

where S_{EH} is the usual Einstein–Hilbert action known from classical gravity, S_{gh} and S_{gf} are the ghost action and the gauge fixing terms, respectively. Furthermore, $\Delta S_{\mathrm{grav},k}$ is the graviton regulator term. The terms in (4.5) are discussed in more detail in section 4.2. For now, we only consider general symmetry properties of $S_{\mathrm{grav},k}$ and discuss the relation to the background field formalism. Clearly, the standard Einstein-Hilbert action S_{EH} is invariant under diffeomorphism transformations given by

$$g_{\mu\nu} \to g_{\mu\nu} + \delta_\epsilon g_{\mu\nu} \tag{4.6}$$

$$\delta_\epsilon g_{\mu\nu} = \mathcal{L}_\epsilon g_{\mu\nu}\,, \tag{4.7}$$

where ϵ_μ is an arbitrary variation vector field and $\mathcal{L}$ denotes the Lie-derivative. In this simple case, the expression $\mathcal{L}_\epsilon g_{\mu\nu}$ reads

$$\mathcal{L}_\epsilon g_{\mu\nu} = \epsilon_\sigma \partial^\sigma g_{\mu\nu} + 2 g_{\sigma(\mu}\partial_{\nu)}\epsilon^\sigma\,. \tag{4.8}$$

The infinitesimal diffeomorphism (4.7) is associated to the generator $\mathcal{G}$ given by

$$\mathcal{G} = \mathcal{L}_\epsilon g_{\mu\nu} \frac{\delta}{\delta g_{\mu\nu}} \tag{4.9}$$

In order to define the notion of a background, the full metric $g_{\mu\nu}$ is now split linearly into background and fluctuation fields according to

$$g_{\mu\nu} = \bar{g}_{\mu\nu} + h_{\mu\nu}. \tag{4.10}$$

For the linear split treat $\bar{g}_{\mu\nu}$ as a background field. Thus we gauge fix $\bar{g}_{\mu\nu}$ such that it is invariant under the action of $\mathcal{G}$:

$$\delta_\epsilon h_{\mu\nu} = \mathcal{L}_\epsilon g_{\mu\nu} \tag{4.11a}$$

$$\delta_\epsilon \bar{g}_{\mu\nu} = 0. \tag{4.11b}$$

This fixes the generator $\mathcal{G}$ to be

$$\mathcal{G} = \mathcal{L}_\epsilon g_{\mu\nu} \frac{\delta}{\delta h_{\mu\nu}}. \tag{4.12}$$

The Einstein–Hilbert action is invariant under the action of $\mathcal{G}$. Hence, the fluctuating field $h_{\mu\nu}$ inherits the gauge dependence of the metric $g_{\mu\nu}$.

On the other hand, the introduction of the linear split (4.10) allows for the definition of a transformation of the background field under which the action is invariant. We write

$$\delta_\epsilon h_{\mu\nu} = -\mathcal{L}_\epsilon \bar{g}_{\mu\nu} \tag{4.13a}$$

$$\delta_\epsilon \bar{g}_{\mu\nu} = \mathcal{L}_\epsilon \bar{g}_{\mu\nu}\,, \tag{4.13b}$$

which can be represented by the generator

$$\bar{\mathcal{G}} = -\mathcal{L}_\epsilon \bar{g}_{\mu\nu} \frac{\delta}{\delta h_{\mu\nu}} + \mathcal{L}_\epsilon \bar{g}_{\mu\nu} \frac{\delta}{\delta \bar{g}_{\mu\nu}} \,. \tag{4.14}$$

Obviously, metric $g_{\mu\nu}$ in (4.10) is invariant under (4.13). Now we introduce a gauge fixing term $S_{\rm gf}$ in the action. In particular, we chose a certain type of 'background gauge' . A gauge fixing term for a theory otherwise invariant under (4.11) explicitly breaks this invariance. However, the gauge fixing is chosen such that the action with the gauge fixing term included is in fact invariant under the combined 'background gauge transformations' given by

$$\delta_\epsilon h_{\mu\nu} = \mathcal{L}_\epsilon h_{\mu\nu} \tag{4.15a}$$

$$\delta_\epsilon \bar{g}_{\mu\nu} = \mathcal{L}_\epsilon \bar{g}_{\mu\nu} \,. \tag{4.15b}$$

Apparently, (4.15) is just the combined transformation of (4.11) and (4.13), thus represented by the generator $\mathcal{G} + \bar{\mathcal{G}}$. The metric $g_{\mu\nu}$ in (4.10) transforms as (4.7) under both (4.11) and (4.15). Since the effective average action inherits the symmetries of the classical action, the untruncated Γ_k is also diffeomorphism invariant at least in the limit of vanishing regulator, $k \to 0$. Note again that the success of this method requires the choice of a gauge from the class of 'background gauges'. We stress that according to (4.15), the background and fluctuating fields $\bar{g}_{\mu\nu}$ and $h_{\mu\nu}$ are treated on almost equal footing. Thus, the field $\bar{g}_{\mu\nu}$ has a kinetic term and is therefore not just an auxiliary field. It is in principle possible to make both fields fully dynamical. This is done in the so-called bi-metric approaches to quantum gravity [50]. In our approach, however, we leave $\bar{g}_{\mu\nu}$ as an external input. In particular, we choose $\bar{g}_{\mu\nu} = \delta_{\mu\nu}$ as the expansion point for the vertices which has manifold computational advantages.

We are left with a simple three-step procedure which allows for the construction of a diffeomorphism invariant and gauge-fixed action $S_{{\rm grav},k}$. Since this invariance is transferred to the effective action Γ, we expect that is also holds for the effective action Γ. For $k > 0$ the diffeomophism invariance is broken by the regulator term. The price we have to pay is a spurious dependence of the action on the arbitrary background metric $\bar{g}$.

4.2 Classical Action

Let us now turn to the classical action $S_{{\rm class},k}$ that captures the physics of gravity and matter at some low energy scale. We separately discuss the parts of the decomposition of $S_{{\rm class},k}$ according to (4.1).These parts are the gravity-ghost sector $S_{{\rm grav},k}$, the fermion sector $S_{{\rm ferm},k}$ and scalar sector $S_{{\rm scal},k}$.

$$S_{{\rm class},k} = S_{{\rm grav},k} + S_{{\rm ferm},k} + S_{{\rm scal},k} \,. \tag{4.1}$$

4.2.1 Gravity-Ghost Sector

In this section, we follow the notation used in [42]. As we already know from equation (4.5) the graviton-ghost action decomposes into four parts. Having discussed the background field method in the previous section we can make the dependencies on the respective fields more specific. We have

$$S_{\text{grav},k} = S_{\text{EH}}[\bar{g}+h] + S_{\text{gf}}[h;\bar{g}] + S_{\text{gh}}[h,\bar{c},c;\bar{g}] + \Delta S_{\text{grav},k}[h,\bar{c},c;\bar{g}]\,. \tag{4.16}$$

The first term denotes the classical Einstein-Hilbert action in Euclidean space given by

$$S_{\text{EH}}[\bar{g}+h] = \frac{1}{16\pi}\int (2\Lambda - R)\,\sqrt{g}d^4x \tag{2.21}$$

The second term in (4.16), S_{gf}, is the gauge fixing-term

$$S_{gf}[h;\bar{g}] = \frac{1}{32\pi\alpha}\int \bar{g}^{\mu\nu}F_\mu F_\nu\sqrt{\bar{g}}d^4x \tag{4.17}$$

with the gauge-fixing condition F_μ. S_{gh} is the action for the ghosts $\bar{c}_\mu$ and c_μ which arises due to the Faddeev-Popov determinant:

$$S_{gh}[h,\bar{c},c;\bar{g}] = -\frac{1}{16\pi G_N}\int \bar{c}_\mu\bar{g}^{\mu\nu}\frac{\partial F_\nu}{\partial h_{\alpha\beta}}\mathcal{L}_c(\bar{g}_{\alpha\beta}+h_{\alpha\beta})\sqrt{\bar{g}}d^4x \tag{4.18}$$

The gauge fixing condition F_μ can be chosen at will. Throughout this work, we choose a De-Donder-type gauge condition with

$$F_\mu = \bar{D}^\nu h_{\mu\nu} - \frac{1+\beta}{4}\bar{D}_\mu h^\nu{}_\nu\,, \tag{4.19}$$

which is linear in the fluctuation field $h_{\mu\nu}$. A linear gauge fixing is advantageous since it introduces only linear interactions between gravitons and the ghosts. Thus, the ghost system computationally tractable for linear gauges. Furthermore, the gauge choice (4.19) is of the background gauge type and hence obeys invariance under (4.15). The parameter β in (4.19) is arbitrary. In case of $\beta = 1$ and using a flat background $\bar{g}_{\mu\nu} = \delta_{\mu\nu}$, (4.19) reduces to the usual harmonic gauge. For $F_\mu = 0$ it reads

$$\partial^\nu h_{\nu\mu} = \frac{1}{2}\partial_\mu h\,. \tag{4.20}$$

For the choice of gauge (4.19), the ghost action (4.18) takes the form

$$S_{gh}[h,\bar{c},c;\bar{g}] = -\frac{1}{16\pi}\int \bar{c}_\mu\mathcal{M}[g,\bar{g}]^\mu{}_\nu c^\nu\sqrt{\bar{g}}d^4x\,. \tag{4.21}$$

The Fadeev-Popov operator $\mathcal{M}$ for the gauge fixing condition (4.19) is given by

$$\mathcal{M}[g,\bar{g}]^\mu{}_\nu = \bar{D}^\rho\bar{g}^{\mu\sigma}g_{\sigma\nu}D_\rho + \bar{D}^\rho g_{\rho\nu}D^\mu - \frac{(1-\beta)}{4}\bar{D}^\mu\bar{g}^{\rho\sigma}g_{\rho\nu}D_\sigma\,. \tag{4.22}$$

We shall see later that the ghost propagator simplifies considerably upon the choice $\beta = 1$, i.e., harmonic gauge. In this case, the last term in equation 4.22 vanishes.

The IR regulator term ΔS_k is given by

$$\Delta S_k = \frac{1}{16\pi G_N} \int h_{\mu\nu} R_k^h[\bar{g}]^{\mu\nu\rho\sigma} h_{\rho\sigma} \sqrt{\bar{g}} d^4x + \int \bar{c}_\mu R_k^c[\bar{g}]^{\mu\nu} c^\nu \sqrt{\bar{g}} d^4x \tag{4.23}$$

where R_h and R_c are the graviton and ghost regulators, respectively. As discussed in section 4.1, it is crucial that the regulator terms depend only on the background metric $\bar{g}$ in order to have a precise notion of high and low field modes. The choice of regulators is specified in section 4.3.2.

4.2.2 Interlude: Spin-base Invariant Formalism

For the inclusion of fermionic matter into our system we use the spin-base invariant formalism. It alows forthe consistent formulation of fermions in curved space-time. The standard approach for formulating fermion fields in curved spacetime is by introducing a vielbein e_μ^a (also called tetrad), which is related to the metric means of

$$g_{\mu\nu} = e_\mu^a e_\nu^b \delta_{ab}. \tag{4.24}$$

The vector fields e can be regarded as comoving coordinate vector fields. They are linear maps from the tangent space of the (possible curved) manifold of spacetime to flat Euclidean space. In approaches, fermions are considered inherently flat-spacetime quantities that require the introduction of a vielbein to be formulated consistently in a curved space. One may go even further and consider the vielbein e instead of the metric g as fundamental degrees of freedom of quantum gravity [51]. This, however, would require the path integral to contain the vielbein as fluctuating quantity. This is often avoided by making a certain gauge choice which relates the vielbein to the metric in a simple way and then reexpressing the path integral in terms of metric fluctuations [52]. However, neither the ghost-terms from the $SO(4)$ gauge freedom which needs to be fixed nor the Jacobian from the transformation to metric fluctuations in the path integral are well understood. One way to circumvent these uncertainties is to avoid the use of a vielbein at all. This is achieved by making the γ-matrices dynamical spacetime quantities in their own right without the necessity of a vielbein [53–56].

For the construction of spacetime dependent γ-matrices we use the Clifford-algebra given by

$$\{\gamma^\mu, \gamma^\mu\} = 2g^{\mu\nu}\mathbb{1}\,. \tag{4.25}$$

This relation is invariant under arbitrary spin-base transformations $\mathcal{S} \in \mathrm{SL}(4,\mathbb{C})$ of the γ-matrices. These transformations act nontrivially on the gammas and the

spinors $(\bar{\psi}, \psi)$ according to

$$\gamma^\mu \to \mathcal{S}\gamma^\mu\mathcal{S}^{-1} \tag{4.26a}$$
$$\psi \to \mathcal{S}\psi \tag{4.26b}$$
$$\bar{\psi} \to \bar{\psi}\mathcal{S}^{-1}\,. \tag{4.26c}$$

In curved spacetime, Dirac conjugation is performed with help of the spin metric $\mathfrak{h}$ which itself transforms non-trivially under spin-base transformations $\mathcal{S}$ according to

$$\bar{\psi} = \psi^\dagger\mathfrak{h}\,, \tag{4.27}$$
$$\mathfrak{h} \to (\mathcal{S}^\dagger)^{-1}\mathfrak{h}\mathcal{S}^{-1}\,, \tag{4.28}$$
$$\det\mathfrak{h} = 1\,. \tag{4.29}$$

Note that $\mathfrak{h}$ is equal to γ_0 in flat space, but in general this is not true. Now, one can construct a covariant derivative ∇_μ which conserves spin-base invariance. This procedure is explained in much detail in [53, 54] for the case of four dimensions. A generalization to higher spacetime dimensions can be found in [55]. The covariant derivative is constructed by demanding certain properties of ∇_μ, which are summarized in the following.

Properties of the Spin-Base Covariant Derivative

1. The covariant derivative ∇_μ is linear.

2. It obeys a Leibnitz (product) rule.

3. It transforms covariantly under Dirac conjugation, i.e.

$$\nabla_\mu\bar{\psi} = \overline{\nabla_\mu\psi}\,, \qquad\qquad \nabla_\mu\psi^\dagger = (\nabla_\mu\psi)^\dagger\,. \tag{4.30}$$

4. For objects that transform as scalars under spin-base transformations, ∇_μ reduces to the usual spacetime covariant derivative D_μ.

5. The fermion action introduced below is always real.

From these requirements we can derive the general form of ∇_μ acting on a spinor. We find

$$\nabla_\mu\psi = \partial_\mu\psi + \Gamma_\mu\psi\,, \tag{4.31}$$
$$\nabla_\mu\bar{\psi} = \partial_\mu\bar{\psi} - \bar{\psi}\Gamma_\mu\,. \tag{4.32}$$

Here Γ_μ is the traceless, torsion free[1] spin connection. It transforms non-covariantly under spin-base transformations

$$\Gamma_\mu \to \mathcal{S}\Gamma_\mu\mathcal{S}^{-1} - (\partial_\mu\mathcal{S})\mathcal{S}^{-1} \tag{4.33}$$

$$\mathrm{Tr}\,\Gamma_\mu = 0 \tag{4.34}$$

Furthermore, the requirements made above imply that the covariant derivatives of the γ matrices and the spin-metric $\mathfrak{h}$ are given by

$$\nabla_\mu\gamma^\nu = D_\mu\gamma^\nu + [\Gamma_\mu, \gamma^\nu] = 0\,, \qquad \nabla_\nu\mathfrak{h} = \partial_\mu - \mathfrak{h}\Gamma_\mu - \Gamma^\dagger = 0\,. \tag{4.35}$$

The main features of the spin-base invariant formalism and, in particular, the main properties of the spin metric $\mathfrak{h}$ and the spin-connection Γ_μ are in fact all we need for the spacetime and spin-base covariant formulation of fermions in quantum gravity. There is no need to introduce a vielbein at any point. When constructing the gravity-fermion vertices the given properties for $\mathfrak{h}$ and Γ_μ will prove relevant for the derivation of the variations with respect to the fluctuating graviton field $h_{\mu\nu}$. More details on this can be found in Appendix A.1.

4.2.3 Fermions

The spin-base invariant formalism enters as a crucial ingredient into the formulation of the fermionic action. Apart from these technicalities, and regarding the field content, the fermionc action is much simpler than that of the gravity-ghost system, since there is no gauge redundancy for fermions. The fermionic action S_{ferm} reads

$$S_{\mathrm{ferm},k} = \int \left\{\bar{\psi}^i \left(\not{\nabla} + m\right)\psi^i\right\}\sqrt{g}d^4x + \Delta S_{\mathrm{ferm},k}\,, \tag{4.36}$$

where the $(\bar{\psi}^i, \psi^j)$ are Dirac fermions carrying a flavour index $i \in \{1, \ldots, N_f\}$, which is summed over. Furthermore, $\not{\nabla}$ is the covariant Dirac operator

$$\not{\nabla} = \gamma_\mu\left(D^\mu + \Gamma^\mu\right)\,, \tag{4.37}$$

which contains the spin connection Γ^μ and space-time dependent gamma matrices $\gamma_\mu(x)$. Following the spin-base invariance formalism introduced in section 4.2.2, the vielbein is avoided and the $\gamma_\mu(x)$ are the relevant dynamical quantities. The fermion regulator term $\Delta S_{\mathrm{ferm},k}$ is given by

$$\Delta S_{\mathrm{ferm},k}[\bar{g}] = \int \bar{\psi}^i R_{\mathrm{ferm},k}(\not{\nabla})\psi^i\sqrt{\bar{g}}d^4x\,, \tag{4.38}$$

where $R_{\mathrm{ferm,k}}$ is the fermion regulator. Again, the specific choice of the regulator function is discussed further in section 4.3.2.

[1] In general, the spin connection also contains a trace part and is not torsion free. However, we assume for now that we can gauge away these parts by a suitable choice of spin-base transformation

4.2.4 Scalars

As the last part of the classical action we discuss the scalar sector to complete our system. It is given by

$$S_{\mathrm{scal},k}[\bar{g}+h] = \int \left(\partial^\mu \phi^i \partial_\mu \phi^i + \phi^i m_s^2 \phi^i\right) \sqrt{g} d^4x + \Delta S_{\mathrm{scal},k}[\bar{g}]\,, \tag{4.39}$$

where $i \in \{1, \ldots, N_f\}$ denotes a colour index that is summed over and $\Delta S_{\mathrm{scal},k}$ is the scalar regulator term given by

$$\Delta S_{\mathrm{scal},k}[\bar{g}] = \int \phi^i R_{\mathrm{ferm},k}(\underline{\Delta}) \phi^i \sqrt{\bar{g}} d^4x\,. \tag{4.40}$$

We have now collected all the parts of the classical action $S_{\mathrm{class},k}$. As discussed briefly in the beginning of this chapter, the truncated effective average action is constructed from $S_{\mathrm{class},k}$. Therefore, it is an important ingredient for the truncation.

We have shown that we can make the gauge-fixed action diffeomorphism invariant in the limit of vanishing regulator $k \to 0$. To this end, we introduced the background field formalism which also provides for an elegant way to include a mode regularisation into the gravity-ghost action. The fermionic action relies on the spin-base invariance formalism which avoids the vielbein and, therefore, gets rid of several tetrad-associated drawbacks.

4.3 Effective Average Action

In this section, we discuss the main aspects of the truncation for the effective average action Γ_k that is used in the present work. Generally, the truncation scheme employed here is a vertex expansion in the fluctuating field Φ.

4.3.1 Truncation

In terms of the superfield Φ, the truncation for the graviton-ghost system is driven up to third order in the fluctuation fields. It reads

$$\Gamma_k = \Gamma_k^{(0)} + \Gamma_k^{(\boldsymbol{a})}\Phi_{\boldsymbol{a}} + \frac{1}{2}\Gamma_k^{(\boldsymbol{ab})}\Phi_{\mathbf{a}}\Phi_{\mathbf{b}} + \frac{1}{6}\Gamma_k^{(\boldsymbol{abc})}\Phi_{\mathbf{a}}\Phi_{\mathbf{b}}\Phi_{\mathbf{c}}\,. \tag{4.2}$$

The vertices $\Gamma_k^{(n)}$ are given by the variation of the classical action with respect to the superfield Φ according to

$$\Gamma_\alpha^{(\boldsymbol{a_1}\ldots\boldsymbol{a_\alpha})} = S_{\mathrm{class},k}^{\boldsymbol{a_1}\ldots\boldsymbol{a_\alpha}|}[\Phi]\Big|_{\Phi=0}\,. \tag{4.3}$$

Rescaling of Fields

We can rescale all dynamical fields in the path integral by an arbitrary function via

$$\Phi_{\boldsymbol{a}} \to f(\boldsymbol{a})\Phi_{\boldsymbol{a}} \tag{4.41}$$

Rescalings of the type (4.41) only alter the path integral by a constant which does not affect measurable quantities. Hence, we can use this kind of rescaling in order to make calculations simpler. First of all, it will prove convenient to rescale all fields by means of their wave function renormalisation via

$$\Phi_{\boldsymbol{a}} \to \hat{\Phi}_{\mathbf{a}} = \frac{1}{\sqrt{Z_{\boldsymbol{a}}}}\Phi_{\boldsymbol{a}} \tag{4.42}$$

For computational reasons, it is desirable to have a graviton 2-point function which is independent of Newtons coupling G_N. in this way, it is possible to extract the graviton anomalous dimension and the flow of G_N independently from the 2- and 3-point function, respectively. We have seen that the classical Einstein-Hilbert action (2.21) is proportional to G_N^{-1}. However, the matter parts $S_{\text{ferm},k}$ and $S_{\text{scal},k}$ are not. By relabeling Φ according to

$$\Phi_a \to \Phi_a = \left(h, \bar{c}, c, \sqrt{G_N}\bar{\psi}, \sqrt{G_N}\psi, \sqrt{G_N}\phi\right) , \tag{4.43}$$

the complete classical action $S_{\text{class},k}$ becomes proportional to G_N^{-1}. Thus, G_N^{-1} can be factored out of $S_{\text{class},k}$ according to

$$S_{\text{class},k}[\Phi] = G_N^{-1} S_{\text{class},k}[\check{\Phi}, G_N = 1] . \tag{4.44}$$

Now, we perform a rescaling of Φ given by

$$\Phi_a \to \hat{\Phi}_a = \left(\frac{1}{\sqrt{Z_h G_N}}h, \frac{1}{\sqrt{Z_c G_N}}\bar{c}, \frac{1}{\sqrt{Z_c G_N}}c, \frac{1}{\sqrt{Z_\psi}}\bar{\psi}, \frac{1}{\sqrt{Z_\psi}}\psi, \frac{1}{\sqrt{Z_\phi}}\phi\right) \tag{4.45}$$

In terms of the rescaled fields, we can now formulate our truncated effective average action as

$$\Gamma_k = \Gamma_k^{(0)} + \Gamma_k^{\boldsymbol{a}}\hat{\Phi}_{\boldsymbol{a}} + \frac{1}{2}\Gamma_k^{\boldsymbol{ab}}\hat{\Phi}_{\mathbf{a}}\hat{\Phi}_{\mathbf{b}} + \frac{1}{6}\Gamma_k^{\boldsymbol{abc}}\hat{\Phi}_{\mathbf{a}}\hat{\Phi}_{\mathbf{b}}\hat{\Phi}_{\mathbf{c}} , \tag{4.46}$$

where the $\Gamma_k^{(n)}$ now assume the particularly simple form

$$\Gamma_k^{(\boldsymbol{a_1 \ldots a_n})} = \left(\prod_{i=1}^{n}\sqrt{Z_{\mathbf{a_i}}}\right)\left(G_N^{(n)}\right)^{\frac{1}{2}(n-2)}\mathcal{T}_k^{\boldsymbol{a_1 \ldots a_n}}(p_1, \ldots, p_n) , \tag{4.47}$$

and the $\mathcal{T}$ read

$$\mathcal{T}_k^{\mathbf{a_1 \ldots a_n}} = S_{\text{EH}}^{\mathbf{a_1 \ldots a_n}|}[\Phi, G_N = 1, \Lambda = \Lambda_k^{(n)}]\Big|_{\Phi=0, \bar{g}=\delta} . \tag{4.48}$$

Note that we have associated separate running Newton's couplings $G_N^{(n)}$ and separate running 'cosmological constants' $\Lambda_k^{(n)}$ to each vertex $\Gamma_k^{(n)}$. This truncation has also been employed in [24, 26, 28, 57].

Let us make some remarks here in order to better understand the formulae (4.46) to (4.48).

1. The terms $\sim {\Gamma_k}^{(0)}$ and $\sim {\Gamma_k}^{(1)}$ in equation (4.46) are not be considered further in this work. That is because the term $\sim \Gamma_k^{(0)}$ is non-dynamical, since it does not depend on the fields. It is seen as a vacuum energy contribution which does not contribute to the flow of higher correlation functions. The term $\sim \Gamma_k^{(1)}$, on the other hand, is dynamical. Yet, it decouples from the flow as well due to the structure of the flow equation (2.14). This statement is elaborated further when we discuss the hierarchy of flow equations for the couplings. More information on the flow of the term $\sim {\Gamma_k}^{(1)}$ can also be found in [27].

2. As equation (4.48) suggests, the vertices are expanded in a flat Euclidean background, thus, $\bar{g}_{\mu\nu} = \delta_{\mu\nu}$ in the remaining work. In fact, the possibility of expanding about a flat background and still being able to extract the flow of the relevant quantities from the flow is one of the important advantages of the present vertex expansion [25].

3. As a first approximation, we may assume all wave function renormalisations Z_a to be independent of momentum. For pure gravity, there is evidence that the wave function renormalisation has only a weak momentum dependence [27]. However, the results in section 7.3.2 suggest, that the flow equations for the n-point function in fact exhibit a non-negligible momentum dependence. Hence, the approximation of momentum independent $Z_{\mathbf{a}}$ will eventually be dropped.

4. The vertices ${\Gamma_k}^{(n)}$ given in (4.47) are chosen such that the 2-point function is independent of G_N. This is a crucial point since it allows to distinguish between the flows of Z_Φ and G_N. This is a great advantage since does not require to identify $\dot{Z}_h/Z_h = \dot{G}/G$. The latter identification is necessary in many other approaches [12, 20].

5. The flow of G_N can be extracted from the flow of the 3-point function. In general, one would have to consider separate momentum dependent couplings $G_N^{(i)}(p_1, \ldots, p_i)$ for each vertex. However, as part of our approximation we use $G_N^{(i)}(p_1, \ldots, p_i) = G_N$, thus, identifying all order's Newton's constants and neglecting their momentum dependencies. This can be justified physically by the observation that gravity interacts with all matter identically. Furthermore, the important concept of locality of the flow of the n-point functions in momentum space does only hold if the couplings $G_N^{(i)}$ are identical in the UV limit. This property is discussed in chapter 6. Modified Slavnov-Taylor identities for gravity could provide for a mathematical justification for this identification [32]. However, a formal treatment is beyond the scope of this work.

In the previous section, we have discussed the used truncation in detail. The vertex construction used within the present work allows for the separate extraction of the graviton anomalous dimension and Newton's coupling from the graviton 2-point function. The graviton 3-point function provides for the flow of Newton's coupling G_N. The flow of the non-interacting matter quantities and that of the ghosts only involves the flow of wave function renormalisations and that of the masses which are all extracted from their respective 2-point functions. This line of reasoning is made more precise in the next chapter.

4.3.2 Choice of Regulator

The choice of regulators is a significant part of the truncation. In the setup presented in this work, all regulators $R_{\Phi,k}$ are given by the 2-point function of the respective field Φ evaluated at vanishing mass, multiplied with a dimensionless shape function r_k. Therefore, they regularise the background covariant Laplacian $\underline{\Delta}$. We have

$$R_k^{\Phi}(\underline{\Delta}) = {\Gamma_k}^{(\Phi\Phi)}(\underline{\Delta})\Big|_{m_\Phi=0} r_k(\underline{\Delta})\,. \tag{4.49}$$

Here, all regulators are functions of the background-covariant Laplacian $\underline{\Delta}$. In particular, the regulator terms are not affected by variations of the dynamical metric h. Furthermore, the regulators $R_{\Phi,k}$ are proportional to the wave function renormalisation of the respective field Φ via the 2-point functions ${\Gamma_k}^{(2)}$. This can be seen from (4.47) in the case $n = 2$. The proportionality of the regulators $R_{\Phi,k}$ to the $Z_{\Phi,k}$ is technically favorable. Indeed, the $Z_{\Phi,k}$ do not appear in the flow equations, but only in form of the quotients

$$\frac{\dot{Z}_{\Phi,k}}{Z_{\Phi,k}}$$

These quantities are defined as the anomalous dimensions of the respective fluctuating fields via

$$\eta_{\Phi,k} = -\frac{\dot{Z}_{\Phi,k}}{Z_{\Phi,k}}\,. \tag{4.50}$$

Hence, the regulator R_k^{Φ} being proportional to the wave function renormalisation Z_Φ allows to formulate the flow as a function of the anomalous dimensions η_Φ only. This can be understood by noting that the only scale dependence of the object

$${\Gamma_k}^{(\Phi\Phi)}(\underline{\Delta})\Big|_{m_\Phi=0}$$

is given by wave function renormalisations that are mutliplied to the 2-vertex according to (4.47). Factoring out the Z_Φ-dependence we can write

$$R_k^{\Phi} = Z_\Phi K_\Phi(\underline{\Delta}) r_k(\underline{\Delta})\,, \tag{4.51}$$

where K is the k-independent kinetic term of the field Φ. Consequently, the flow of R_k^Φ can be written as

$$\dot{R}_k^\Phi = Z_\Phi \left(\dot{r}_k(\underline{\Delta}) - \eta_\Phi r_k(\underline{\Delta})\right) K_\Phi(\underline{\Delta}) \,, \tag{4.52}$$

which leads to the diagrammatic representation

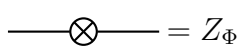

$$= Z_\Phi \left(\dot{r}_k(\underline{\Delta}) - \eta_\Phi r_k(\underline{\Delta})\right) K_\Phi(\underline{\Delta}) \,. \tag{4.53}$$

This term appears directly in the flow equation. Therefore, it is part of all n-point flows as well. We have to note that this choice of composite regulator can only be justified if the anomalous dimensions do not become too large. This observation leads us to an importand upper bound for the second term in equation (4.52) and thus, for the anomalous dimension η_Φ.

Upper Bound for η_Φ

The upper bound can be derived easily from equation (4.52) by factoring out r_k:

$$\dot{R}_k^\Phi = Z_\Phi K_\Phi(\underline{\Delta}) r_k(\underline{\Delta}) \left(\frac{\dot{r}_k(\underline{\Delta})}{r_k(\underline{\Delta})} - \eta_{\Phi,k}\right) \tag{4.54}$$

The scale derivative of the regulators $\dot{R}_k^\Phi$ must not become negative. A negative $\dot{R}_k^\Phi$ would mean that for increasing k, R_k^Φ would suppress modes which are at lower scale than those suppressed before. Thus, one loses control of the regulator if the inequality

$$\frac{\dot{r}_k(\underline{\Delta})}{r_k(\underline{\Delta})} > \eta_{\Phi,k} \tag{4.55}$$

is not satisfied. Apparently condition (4.55) depends on the choice of shape function $r_k(\underline{\Delta})$. We now discuss this inequality for the particular shape function used in our setup.

Shape Functions

Within the used truncation, all quantities can be extracted with respect to a flat background metric $\bar{g}_{\mu\nu} = \delta_{\mu\nu}$. This allows to present the shape functions in momentum space. In this work, we use Litim's cutoff which reads

$$r_k(p^2) = \left(\frac{k^n}{|p|^n} - 1\right) \theta(k^2 - p^2) \,, \tag{4.56}$$

where $n = 2$ or $n = 1$ for bosons and fermions, respectively. For this type of cutoff, the inequality (4.55) can be written in terms of $\kappa = \frac{k}{|p|}$:

$$\frac{\dot{r}_k(\kappa)}{r_k(\kappa)} = \frac{n\kappa^n \theta(\kappa^2 - 1)}{(\kappa^n - 1)\,\theta(\kappa^2 - 1)} \tag{4.57}$$

In the limit $\kappa \to \infty$, and thus $p \to 0$ or $k \to \infty$, (4.57) takes the form

$$\lim_{\kappa\to\infty} \frac{\dot{r}_k(\kappa)}{r_k(\kappa)} = n \qquad \text{(Litim's cutoff)}\,. \tag{4.58}$$

One can easily verify that the derivative of $\frac{\dot{r}_k(\kappa)}{r_k(\kappa)}$ with respect to κ is negative for $1 < \kappa < \infty$ such that (4.58) is in fact a lower limit. Hence, we demand

$$\eta_{\Phi,k} < \begin{cases} 2 & \text{if } \Phi \text{ bosonic} \\ 1 & \text{if } \Phi \text{ fermionic} \end{cases} \qquad \text{(Litim's cutoff)}\,. \tag{4.59}$$

In sum, we have seen that the construction of the vertices and the choice of regulators allow for flow equations in terms of the anomalous dimensions, which do not depend explicitly on the wave function renormalisations. However, the dependence of the regulator on the wave function renormalisations leads to upper bounds for the corresponding anomalous dimensions.

5 Flow of the 1-PI n-point functions

As we have seen when discussion the vertex expansion in section 3.4.1, the flow equation (2.14), provides the flow of the 1-PI n-point functions. This allows to extract the flows for the respective dimensionful couplings which we denote by $\bar{w}_n$. In the following section we discuss how the flow of the n-point functions is calculated. Furthermore, we develop a diagrammatic representation for the flow of the n-point functions up to $n = 3$. To this end, we develop functional flows for these quantities by taking variations of the flow equation (2.14)

$$\dot{\Gamma}_k[\Phi] = \frac{1}{2} G_{k,\mathbf{ab}} \dot{R}_k^{\mathbf{ab}} \,, \tag{2.14}$$

with respect to the superfield Φ_a. First, we consider the variation of the Green's function. Taking a field variation of (2.13) we get

$$0 = (G_{\mathbf{ac}}(\Gamma_k^{(2)} + R_k)^{\mathbf{cb}|})_{\mathbf{d}|} = G_{\mathbf{d}|\mathbf{ac}}(\Gamma_k^{(2)} + R_k)^{\mathbf{cb}} + (-1)^{ad}(-1)^{cd} G_{\mathbf{ac}} \Gamma_k^{\mathbf{ncb}|} \gamma_{\mathbf{dn}} \,, \tag{5.1}$$

$$G_{\mathbf{d}|\mathbf{ac}} \gamma^{\mathbf{c}}{}_{\mathbf{e}} = -(-1)^{ad}(-1)^{cd} G_{\mathbf{ac}} \Gamma_k^{\mathbf{ncb}|} G_{\mathbf{be}} \gamma_{\mathbf{dn}} \,, \tag{5.2}$$

$$G_{\mathbf{d}|\mathbf{am}} = -(-1)^{ad} G_{\mathbf{ac}} \Gamma_k^{\mathbf{cnb}|} G_{\mathbf{be}} \gamma_{\mathbf{dn}} \gamma^{\mathbf{e}}{}_{\mathbf{m}} \,, \tag{5.3}$$

where we dropped the scale index k for the Green's functions for convenience. Hence, Green's functions reproduce themselves upon taking variations with respect to the fields. This allows to interpret the flow equation for the n-point vertices in terms of one-loop diagrams. Using relation (5.1), we find the second variation of the Green's function

$$\begin{aligned} G_{\mathbf{nd}|\mathbf{am}} = (-1)^{ad}(-1)^{an} \gamma_{\mathbf{dq}} \gamma_{\mathbf{np}} \gamma^{\mathbf{e}}{}_{\mathbf{m}} \Big(& -G_{\mathbf{ac}} \Gamma_k^{\mathbf{cpqb}|} G_{\mathbf{be}} + \\ & + G_{\mathbf{ai}} \Gamma_k^{\mathbf{ipj}|} G_{\mathbf{jr}} \gamma^{\mathbf{r}}{}_{\mathbf{c}} \Gamma_k^{\mathbf{cqb}|} G_{\mathbf{be}} + \\ & + (-1)^{nd} G_{\mathbf{ai}} \Gamma_k^{\mathbf{iqj}|} G_{\mathbf{jc}} \Gamma_k^{\mathbf{cpb}|} G_{\mathbf{br}} \gamma^{\mathbf{r}}{}_{\mathbf{e}} \Big) \,. \end{aligned} \tag{5.4}$$

Having this at hand, we can take the second variation of the flow equation with respect to Φ

$$\begin{aligned} \dot{\Gamma}_{\mathbf{nd}|}[\Phi] = \frac{1}{2} G_{\mathbf{nd}|\mathbf{am}} \dot{R}^{\mathbf{am}} = \frac{1}{2}(-1)^{ad}(-1)^{an} \gamma_{\mathbf{dq}} \gamma_{\mathbf{np}} \gamma^{\mathbf{e}}{}_{\mathbf{m}} \Big(& -G_{\mathbf{ac}} \Gamma_k^{\mathbf{cpqb}|} G_{\mathbf{be}} + \\ & + G_{\mathbf{ai}} \Gamma_k^{\mathbf{ipj}|} G_{\mathbf{jr}} \gamma^{\mathbf{r}}{}_{\mathbf{c}} \Gamma_k^{\mathbf{cqb}|} G_{\mathbf{be}} + \\ & + (-1)^{nd} G_{\mathbf{ai}} \Gamma_k^{\mathbf{iqj}|} G_{\mathbf{jc}} \Gamma_k^{\mathbf{cpb}|} G_{\mathbf{br}} \gamma^{\mathbf{r}}{}_{\mathbf{e}} \Big) \dot{R}_k^{\mathbf{am}} \,. \end{aligned} \tag{5.5}$$

In order to obtain the flow equation of the 2-point function in the used expansion of the effective action (4.46), we have to evaluate (5.5) at vanishing fields $\Phi = 0$. In a diagrammatic representation of (5.5) we write an n-point function as a vertex with n legs:

$$\Gamma_k^{\mathbf{a_1 a_2 \ldots a_n}|}\Big|_{\Phi=0} = \quad \mathbf{a_1} \quad \mathbf{a_2} \quad \mathbf{a_n} \tag{5.6}$$

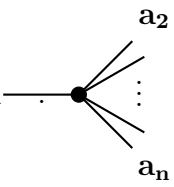

Representation in Momentum Space

In most cases, it is convenient to consider all quantities in momentum space. Since we are in fact evaluating all vertices with respect to a flat background metric, Fourier transformations are applicable. The classical action $S_{\text{class},k}$ which is used for the construction of the vertices contains an integral over position space. Hence, when constructing an arbitrary n-point function, the n^{th} variation of $S_{\text{class},k}$ introduces n δ-functions one of which is annihilated by the action integral. Thus, we end up with

$$\Gamma_k^{(\mathbf{a_1 \ldots a_n})}(x_1, \ldots, x_n) \sim \delta(x_1 - x_2)\delta(x_1 - x_3) \ldots \delta(x_1 - x_n)\,. \tag{5.7}$$

Fourier transforming with respect to $(x_1, \ldots, x_n)$ gives the n-point function as a function of the field momenta $(p_1, \ldots, p_n)$. The remaining $n - 1$ δ-functions (5.7) annihilate all Fourier (position space) integrals except for one. The remaining integral can be performed resulting in a δ-function in momentum space which accounts for momentum dependence at the vertex. We have

$$\Gamma_k^{(\mathbf{a_1 \ldots a_n})}(p_1, \ldots, p_n) \sim \delta\left(\sum_{i=1}^{n} p_i\right)\,. \tag{5.8}$$

Hence, all vertices remain with one δ-function in momentum space. Its arguments is given by the sum of all field momenta at the vertex. In the following,we omit the obligatory δ-function in the expression and only display the analytic parts of $\Gamma_k^{(n)}$ for notational convenience. Momentum conservation still allows to remove one of the vertex momenta from the equation, since the sum of all momenta must always be zero.

Diagrammatic Representation

In the beginning of the chapter, we have motivated the representation of the n-point function at vanishing fields in terms of a vertex with n legs in (5.6). In this representation, the Green's functions are simply lines connecting vertices. For the different field species, they are given by double, dotted, solid and dashed lines for

gravitons, ghosts, fermions and scalars, respectively, according to

$= (\Gamma_k^{(hh)} + R_k^h)^{-1}$ 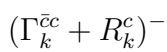
$= (\Gamma_k^{\bar{c}c} + R_k^c)^{-1}\,,$ (5.9)

$= (\Gamma_k^{\bar{\psi}\psi} + R_k^{\psi})^{-1}$ 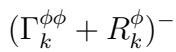
$= (\Gamma_k^{\phi\phi} + R_k^{\phi})^{-1}\,.$ (5.10)

The derivative of the regulator $\dot{R}_k$ is denoted by crossed circles via

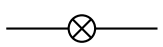
$= Z_\Phi \left(\dot{r}(p) - \eta_\Phi r(p)\right) K_\Phi(p)\,,$ (4.53)

where we use to momentum space representation. Different lines for the different field species are understood. What we see in the following, is that equation (5.5) and its higher order analogues can be represented in terms of simple diagrams just as in perturbative quantum field theory. For the higher order n-point functions, the derivation of the flow equation goes along the same lines as for the 2-point function given in (5.5). However, these expressions are much more complicated and we restrict ourselves to the second field variation. The result for the flow of the 3-point function is given only in terms of diagrams. Now, we derive the diagrammatic flow of the graviton 2-point function from (5.5) as an example. In this case, the indices **n** and **d** are bosonic. Therefore, the (-1) which would appear for fermionic indices in equation (5.5) vanishes. We fix the signs according to (5.5) and use the diagrammatic representation of the objects to write the flow of $\Gamma_k^{(hh)}$ as

$\dot{\Gamma}_k^{(hh)}[\Phi]\Big|_{\Phi=0} = \frac{1}{2}\Big($ 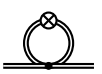 $+\,2$ 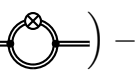 $\Big) - \Big(2$  $\Big)$

$- N_f \Big(-$  $+\,2$ 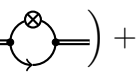 $\Big) + \frac{N_s}{2}\Big(-$  $+\,2$ 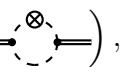 $\Big)\,,$ (5.11)

where we have suppressed the internal indices of the h fields, namely, spacetime indices and momenta. Two types of diagrams appear in (5.11). In the following, we call the first diagram in each of the brackets in (5.11) tadpole and the second one self-energy. The second and the third term in equation (5.5) both contribute equally to the self-energy diagram which yields the relative factor of two between the tadpole and self-energy. The fermionic loops carry a factor of 2 and an extra minus sign compared to the bosonic loops. The factor of two is due to the fact that both anti-fermion and fermion give the same contribution in the trace. Furthermore, the minus sign in fermionic loops originates from

$$G_{k,\mathbf{ab}} = (-1)(\Gamma_k^{(2)} + R_k)^{-1}_{\mathbf{ab}} \qquad \text{(for } (a,b) \text{ fermionic)}. \tag{5.12}$$

The additional factors of N_f and N_s result from number of fermion and scalar fields, respectively. Since these fields are completely decoupled from each other they enter only as a multiplicative factor for the loops. Along the same lines we can derive the

diagrammatic representation for the flow of the graviton 3-point function. It reads

$$\dot{\Gamma}_k^{(hhh)}[\Phi]\Big|_{\Phi=0} =$$

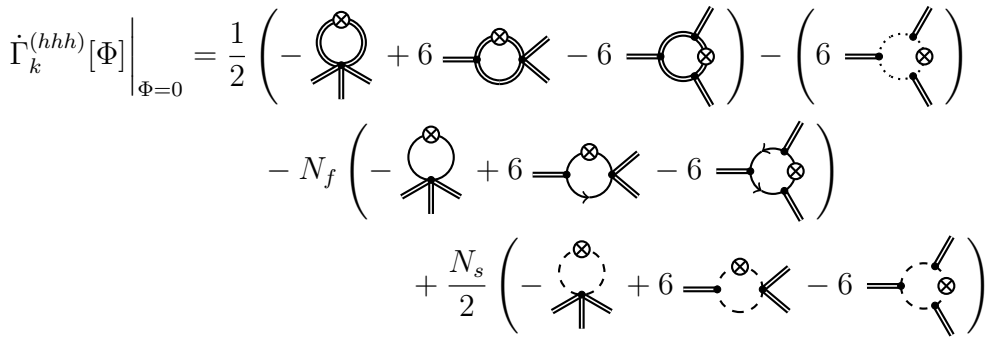

(5.13)

The loops in all diagrams represent traces over all remaining internal indices that appears in the flow equation (2.14). In particular, these traces involve the integration over momentum variables p. Note that due to the insertion of $\dot{R}_k$ the integrals are UV-regularized.

Thus, we have found a systematic way to derive flow equations for the n-point functions. Furthermore, we developed one-loop diagrammatics that allow to conveniently represent the flow equations. Loosely speaking the discussion in this section governs the right hand side of the flow equation (2.14). In order to extract the flow for the couplings of our truncation, we now consider the left-hand side of (2.14). The extraction of the flow of the couplings $\dot{\bar{u}}_n$ requires suitable projection procedures for the vertices that we discuss that are discussed in detail.

5.1 Connected Green's functions

One of the main ingredients to the flow equation are the connected Green's functions G_k which we calculate in the following. They are related to $(\Gamma_k^{(2)} + R_k)^{-1}$ by (2.13). Evaluating at $\Phi = 0$, we have

$$G_{k,\mathbf{ab}}[0] = (-1)^{\mathbf{ab}} (\Gamma_k^{(2)} + R_k)^{-1}_{\mathbf{ab}}\Big|_{\Phi=0} . \tag{5.14}$$

Note that the term $(-1)^{\mathbf{ab}}$ provides a minus sign for all fermionic indices $\mathbf{ab}$. Equation (5.14) can be conveniently expressed in terms of the components of the superfield as a matrix equation. The left-hand side is given by

$$G_{\mathbf{ab}} = \begin{pmatrix} G_k^{(hh)} & 0 & 0 & 0 & 0 & 0 \\ 0 & 0 & G_k^{(c\bar{c})} & 0 & 0 & 0 \\ 0 & G_k^{(\bar{c}c)} & 0 & 0 & 0 & 0 \\ 0 & 0 & 0 & 0 & G_k^{(\psi\bar{\psi})} & 0 \\ 0 & 0 & 0 & G_k^{(\bar{\psi}\psi)} & 0 & 0 \\ 0 & 0 & 0 & 0 & 0 & G_k^{(\bar{\phi}\phi)} \end{pmatrix} , \tag{5.15}$$

where we suppress the residual indices on the right-hand side of (5.15) for notational convenience. The right-hand side of (5.14) is expressed as the block-matrix

$$(-1)^{\mathbf{ab}}(\Gamma_k^{(2)}+R_k)^{-1}_{\mathbf{ab}}\Big|_{\Phi=0} = \begin{pmatrix} \mathbf{H} & 0 & 0 & 0 \\ 0 & \mathbf{C} & 0 & 0 \\ 0 & 0 & \mathbf{\Psi} & 0 \\ 0 & 0 & 0 & \mathbf{\Phi} \end{pmatrix}^{-1} = \begin{pmatrix} \mathbf{H}^{-1} & 0 & 0 & 0 \\ 0 & \mathbf{C}^{-1} & 0 & 0 \\ 0 & 0 & \mathbf{\Psi}^{-1} & 0 \\ 0 & 0 & 0 & \mathbf{\Phi}^{-1} \end{pmatrix}, \tag{5.16}$$

with the respective blocks are given by

$$\mathbf{H} = (\Gamma_k^{(hh)}+R_k^h)\big|_{\Phi=0}\,, \tag{5.17a}$$

$$\mathbf{C} = \begin{pmatrix} 0 & (\Gamma_k^{(\bar{c}c)}+R_k^c)\big|_{\Phi=0} \\ -(\Gamma_k^{(\bar{c}c)}+R_k^c)\big|_{\Phi=0} & 0 \end{pmatrix}, \tag{5.17b}$$

$$\mathbf{\Psi} = \begin{pmatrix} 0 & (\Gamma_k^{(\bar{\Psi}\Psi)}+R_k^\psi)\big|_{\Phi=0} \\ -(\Gamma_k^{(\bar{\Psi}\Psi)}+R_k^\psi)\big|_{\Phi=0} & 0 \end{pmatrix}, \tag{5.17c}$$

$$\mathbf{\Phi} = (\Gamma_k^{(\bar{\Phi}\Phi)}+R_k^\phi)\big|_{\Phi=0}\,. \tag{5.17d}$$

$$\tag{5.17e}$$

We used that the indices are antisymmetric under the exchange of Grassmann valued fields. In the last step, we can invert the block matrices by inverting each entry separately and adding the appropriate signs. We have

$$\mathbf{H}^{-1} = (\Gamma_k^{(hh)}+R_k^h)^{-1}\big|_{\Phi=0}\,, \tag{5.18a}$$

$$\mathbf{C}^{-1} = \begin{pmatrix} 0 & -(\Gamma_k^{(\bar{c}c)}+R_k^c)^{-1}\big|_{\Phi=0} \\ (\Gamma_k^{(\bar{c}c)}+R_k^c)^{-1}\big|_{\Phi=0} & 0 \end{pmatrix}, \tag{5.18b}$$

$$\mathbf{\Psi}^{-1} = \begin{pmatrix} 0 & -(\Gamma_k^{(\bar{\psi}\psi)}+R_k^\psi)^{-1}\big|_{\Phi=0} \\ (\Gamma_k^{(\bar{\psi}\psi)}+R_k^\psi)^{-1}\big|_{\Phi=0} & 0 \end{pmatrix}, \tag{5.18c}$$

$$\mathbf{\Phi}^{-1} = (\Gamma_k^{(\bar{\phi}\phi)}+R_k^\phi)^{-1}\big|_{\Phi=0}\,. \tag{5.18d}$$

Thus, the task of inverting the complicated expression in (5.14) of field indices has reduced to inverting the quantity $\Gamma_k^{(2)}+R_k$ and hence computing the Green's function, for each field separately. In the following, we calculate the Green's function for the graviton, the ghosts, the fermions and the scalar field.

5.1.1 Graviton Green's Function

We start by calculating the Green's function for the graviton field in momentum space. For gravitons (2.13) takes the form

$$G^h_{k,\mathbf{a_1a_2}} = (\Gamma_k^{(hh)}+R_k^h)^{-1}_{\mu\nu\rho\sigma}\big|_{\Phi=0} \tag{2.13}$$

The vertex $\Gamma_k^{(hh)}$ derives from variations of the classical action according to (4.3). For the graviton 2-point function we have

$$\Gamma^{(hh)}_{k,\mu\nu\rho\sigma}(p) = \frac{1}{32\pi}\left(K_{\mu\nu\rho\sigma}(p^2 - 2\Lambda_k^{(2)}) - \frac{2(1-\alpha)}{\alpha}p^\alpha p^\beta K_{\mu\nu\alpha}{}^\gamma K_{\rho\sigma\beta\gamma}\right). \tag{5.19}$$

Here, we have made the gauge choice $\beta = 1$ in order to get rid of extra terms. We will see that this choice is convenient also for the ghost propagator in the next section. The rank-4 tensor K proportional to second variation the $\sqrt{g}$ with respect to h according to

$$K_{\mu\nu\rho\sigma} = \frac{1}{2}\frac{\delta^2}{\delta h^{\mu\nu}\delta h^{\rho\sigma}}\sqrt{g}\bigg|_{g_{\mu\nu}=\delta_{\mu\nu}} = \frac{1}{2}(\delta_{\mu\nu}\delta_{\rho\sigma} - 2\delta_{\mu(\rho}\delta_{\sigma)\nu})\,. \tag{5.20}$$

The second 'cosmological constant' $\Lambda_k^{(2)}$ in equation (5.19) plays the role of a graviton mass. Therefore, we make the identification

$$m^2_{h,k} = -2\Lambda_k^{(2)}\,. \tag{5.21}$$

The regulator, is given by equation (4.49), reads for gravitons

$$R^h_{k,\mu\nu\rho\sigma}(p) = \Gamma^{(hh)}_{k,\mu\nu\rho\sigma}(p)\bigg|_{m_{h,k}=0} r_k(p)\,. \tag{4.49}$$

Having made the identification (5.21), we can express the graviton regulator via

$$R^h_{k,\mu\nu\rho\sigma}(p) = Z_h\frac{r_k(p)}{32\pi}\left(K_{\mu\nu\rho\sigma}p^2 - \frac{2(1-\alpha)}{\alpha}p^\alpha p^\beta K_{\mu\nu\alpha}{}^\gamma K_{\rho\sigma\beta\gamma}\right). \tag{5.22}$$

Consequently, the sum of (5.19) and (5.22) is given by

$$\begin{aligned}&\Gamma^{(hh)}_{k,\mu\nu\rho\sigma}(p) + R^h_{k,\mu\nu\rho\sigma}(p) = \\ &\frac{1}{32\pi}\left(K_{\mu\nu\rho\sigma}((1+r_k(p))p^2 + m^2_{h,k}) - \frac{2(1-\alpha)}{\alpha}(1+r_k(p))p^\alpha p^\beta K_{\mu\nu\alpha}{}^\gamma K_{\rho\sigma\beta\gamma}\right)\end{aligned} \tag{5.23}$$

This expression has be inverted in order to obtain the graviton Green's function G_k^h. Since α is a gauge parameter it will not contribute to any measurable quantities. Hence, we have the freedom to choose α.

Feynman–t'Hooft gauge

Equation (5.23) suggests setting $\alpha = 1$ which makes the second term vanish. Furthermore, as can easily be verified

$$K_{\mu\nu\rho\sigma}K^{\rho\sigma\alpha\beta} = \delta^{\alpha\beta}_{\mu\nu} = \mathbb{1} \tag{5.24}$$

$$K^{-1}_{\mu\nu\rho\sigma} = K_{\mu\nu\rho\sigma}\,. \tag{5.25}$$

Thus, in the case $\alpha = 1$ the inversion of (5.23) appears almost trivial and we can write

$$\begin{aligned} G^h_{k,\mu\nu\rho\sigma}(p) &= (\Gamma^{(hh)}_k(p) + R^h_k(p))^{-1}_{\mu\nu\rho\sigma} \\ &= \frac{32\pi}{(1+r_k(p))p^2 + m^2_{h,k}} K_{\mu\nu\rho\sigma} \qquad \text{for } (\alpha = 1) \end{aligned} \tag{5.26}$$

From this point of view, the gauge choice $\alpha = 1$ is computationally favorable. In fact, it has been primarily used in early RG-studies of quantum gravity [12]. However, the drawback of this choice is, that we do not have control over the RG flow of α for this gauge. Thus, α is subject to the RG-flow and the β-function for α is unknown. However, there is a striking arguments, why $\alpha_{=}0$ must be a fixed point of the renormalisation group flow for α [58].

Landau–DeWitt gauge

Hence, to circumvent the analysis of the flow of α, we set $\alpha = 0$. This way, it is at a fixed point and will stay constant with the flow. This argument makes $\alpha = 0$ the most convenient choice. Obviously, it is not possible to set $\alpha \to 0$ on the level of the 2-point function (5.19). Hence, the strategy is to invert (5.19) for general α first and then take the limit in a well defined way. However, the task of inverting (5.23) for general α is much harder to accomplish. In the present work, this is done by introducing a set of orthogonal projectors in momentum space $\{\mathbb{P}_i\}$. With respect to this basis, the inversion is merely an inversion of a 4×4-matrix which can be performed easily. As basic quantities for the orthogonal basis of projectors of rank four, we choose the rank 2 transverse and longitudinal projectors according to

$$\mathbb{P}^{\mathrm{T}}_{\mu\nu} = \delta_{\mu\nu} - \frac{p_\mu p_\nu}{p^2} \tag{5.27a}$$

$$\mathbb{P}^{\mathrm{L}}_{\mu\nu} = \frac{p_\mu p_\nu}{p^2} \tag{5.27b}$$

A complete set of tensors of rank 4 is then given by [59]

$$\mathbb{P}^{(2)}_{\mu\nu\rho\sigma} = \mathbb{P}^{\mathrm{T}}_{\mu(\rho}\mathbb{P}^{\mathrm{T}}_{\sigma)\nu} - \frac{1}{3}\mathbb{P}^{\mathrm{T}}_{\mu\nu}\mathbb{P}^{\mathrm{T}}_{\rho\sigma}\,, \tag{5.28a}$$

$$\mathbb{P}^{(1)}_{\mu\nu\rho\sigma} = 2\mathbb{P}^{\mathrm{T}}_{(\mu(\rho}\mathbb{P}^{\mathrm{L}}_{\sigma)\nu)}\,, \tag{5.28b}$$

$$\mathbb{P}^{(0-\mathrm{T})}_{\mu\nu\rho\sigma} = \frac{1}{3}\mathbb{P}^{\mathrm{T}}_{\mu\nu}\mathbb{P}^{\mathrm{T}}_{\rho\sigma} \qquad \mathbb{P}^{(0-\mathrm{L})}_{\mu\nu\rho\sigma} = \mathbb{P}^{\mathrm{L}}_{\mu\nu}\mathbb{P}^{\mathrm{L}}_{\rho\sigma}\,, \tag{5.28c}$$

$$\mathbb{P}^{(0-\mathrm{TL})}_{\mu\nu\rho\sigma} = \frac{1}{\sqrt{3}}\mathbb{P}^{\mathrm{T}}_{\mu\nu}\mathbb{P}^{\mathrm{L}}_{\rho\sigma} \qquad \mathbb{P}^{(0-\mathrm{LT})}_{\mu\nu\rho\sigma} = \frac{1}{\sqrt{3}}\mathbb{P}^{\mathrm{L}}_{\mu\nu}\mathbb{P}^{\mathrm{T}}_{\rho\sigma}\,. \tag{5.28d}$$

The first two projectors given by (5.28a) and (5.28b) are that of the transverse traceless (spin-two) and the traceless vector (spin-one) mode, respectively. The remaining

four correspond to spin-zero parts of the field. The system of projectors (5.28) form an orthorgonal basis for symmetric rank-four tensors that satisfy a projector algebra given [59]. Hence, we write $(\Gamma_k^{(hh)} + R_k)$ as

$$(\Gamma_k^{(hh)} + R_k) = \sum_i a_i \mathbb{P}^i \,, \tag{5.29}$$

where we suppress spacetime indices and momentum dependencies for convenience. This decomposition is sometimes called Stelle-decomposition. Equation (5.29) can be rewritten as a matrix in the basis of the projectors. We have

$$(\Gamma_k^{(hh)} + R_k) = \begin{pmatrix} a^{(2)} & 0 & 0 & 0 \\ 0 & a^{(1)} & 0 & 0 \\ 0 & 0 & a^{(0-\mathrm{T})} & a^{(0-\mathrm{TL})} \\ 0 & 0 & a^{(0-\mathrm{LT})} & a^{(0-\mathrm{L})} \end{pmatrix} . \tag{5.30}$$

The quantities a_i are given by the projection of the left hand side of equation (5.29) on the respective tensors according to

$$a_i = \frac{\mathrm{Tr}\left(\mathbb{P}^i \circ (\Gamma_k^{(hh)} + R_k)^{-1}\right)}{\mathrm{Tr}(\mathbb{P} \circ \mathbb{P})} \,. \tag{5.31}$$

Now we can invert the matrix in (5.30) and obtain the quantity G_k^h. The inverse is given by

$$G_k^h = (\Gamma_k^{(hh)} + R_k)^{-1} = \\ \frac{1}{Z_h} \begin{pmatrix} \frac{32\pi}{m_h^2 + p^2(r+1)} & 0 & 0 & 0 \\ 0 & \frac{32\pi\alpha}{\alpha m_h^2 + p^2(r+1)} & 0 & 0 \\ 0 & 0 & -\frac{16\pi}{m_h^2 + p^2(r+1)} & -\frac{16\pi\sqrt{3}}{m_h^2 + p^2(r+1)} \\ 0 & 0 & -\frac{16\pi\sqrt{3}}{m_h^2 + p^2(r+1)} & \frac{16\pi\left(\alpha m_h^2 + p^2(r+1)(4\alpha-3)\right)}{\left(m_h^2 + p^2(r+1)\right)\left(\alpha m_h^2 + p^2(r+1)\right)} \end{pmatrix} . \tag{5.32}$$

The contracted combination of regulator and Green's functions, $G\dot{R}_k G$, which enters the flow equation can be found in Appendix A.2. In order to set the gauge parameter to a fixed point, we can now take the limit $\alpha \to 0$. We observe, that the Green's function remains finite in this limit.

Before closing this section and turning to the calculation of the Green's function for the other fields, we consider the 2-point function $\Gamma_k^{(hh)}$ from (5.19) in Stelle decomposition. We write

$$\frac{\Gamma_k^{(hh)}}{Z_h} = \begin{pmatrix} \frac{1}{32\pi}\left(m_h^2 + p^2\right) & 0 & 0 & 0 \\ 0 & \frac{\left(\alpha m_h^2 + p^2\right)}{32\pi\alpha} & 0 & 0 \\ 0 & 0 & -\frac{\left(\alpha m_h^2 + p^2(4\alpha-3)\right)}{64\pi\alpha} & -\frac{\sqrt{3}\left(\alpha m_h^2 + p^2\right)}{64\pi\alpha} \\ 0 & 0 & -\frac{\sqrt{3}\left(\alpha m_h^2 + p^2\right)}{64\pi\alpha} & \frac{\left(\alpha m_h^2 + p^2\right)}{64\pi\alpha} \end{pmatrix} . \tag{5.33}$$

The transverse-traceless (spin-two) parts of G_k^h and $\Gamma_k^{(hh)}$ given by the (1,1)-components of the matrices (5.32) and (5.33), respectively are independent of the gauge parameter α. In Appendix A.2 we show that the transverse-traceless components of G_k^h and $\Gamma_k^{(hh)}$ are also inpendent of β. This suggests that the spin-two mode is entirely physical, i.e., contains no gauge-related information. Therefore, we consider only transverse-traceless external graviton modes as they are considered the physical ones. For the internal graviton fields that appear in the loops, however, all parts of the Green's functions contribute.

Remark: Flow of α

The fact that the transverse-traceless modes of G_k^h and $\Gamma_k^{(hh)}$ are gauge independent has another implication. It allows to extract the flow of m_h^2 and Z_h independently from the flow of α. We know that $\alpha = 0$ is a fixed point of $\dot{\alpha}$ for all choices of β. However, if we want to extract the full flow of α from e.g. the (2,2)-components of G_k^h and $\Gamma_k^{(hh)}$, the independence of the transverse-traceless mode from the gauge parameters implies that this is indeed possible.

In short, we extract the flow of m^2 and Z_h from the transverse-traceless component. Then it is possible consider the flow of the vector component to extract the flow of α independently.

Ghosts

By taking variations of the ghost action (4.18) with respect to the ghost fields we get the ghost 2-point function

$$\Gamma_{k,\mu\nu}^{(\bar{c}c)} = Z_c p^2 \left(\delta_{\mu\nu} + \frac{1-\beta}{2} \frac{p_\mu p_\nu}{p^2} \right) . \tag{5.34}$$

Since the ghost field is massless, the ghost regulator in given by

$$R_{k,\mu\nu}^c = Z_c r_k^c(p^2) \Gamma_{k,\mu\nu}^{(\bar{c}c)} \tag{5.35}$$

In turn, we can write the sum of (5.34) and (5.35) as

$$(\Gamma_k^{(\bar{c}c)} + R_k^c)_{\mu\nu} = Z_c (1 + r_k^c) p^2 \left(\delta_{\mu\nu} + \frac{1-\beta}{2} \frac{p_\mu p_\nu}{p^2} \right) . \tag{5.36}$$

The comparably simple structure allows to invert (5.34) without the decomposition in orthogonal tensors. By making the Ansatz

$$(\Gamma_k^{(\bar{c}c)} + R_k^c)_{\mu\nu}^{-1} = \frac{1}{Z_c (1 + r_k^c) p^2} \left(A \delta_{\mu\nu} + B \frac{p_\mu p_\nu}{p^2} \right) \tag{5.37}$$

and we can determine the the constants A and B and find

$$-G_{k,\mu\nu}^c(p^2) = (\Gamma_k^{(\bar{c}c)} + R_k^c)_{\mu\nu}^{-1} = \frac{1}{Z_c (1 + r_k^c) p^2} \left(\delta_{\mu\nu} - \frac{1-\beta}{3-\beta} \frac{p_\mu p_\nu}{p^2} \right) \tag{5.38}$$

The ghost Green's function G_k^c in (5.38) still depends on the gauge-parameter β. A convenient choice is $\beta = 1$ since makes the second term vanish. Note that we have made this choice also for the simplification of the graviton 2-point function. Thus, the ghost Green's function used within this work is given by

$$-G^c_{k,\mu\nu}(p^2) = (\Gamma_k^{(\bar{c}c)} + R_k^c)^{-1}_{\mu\nu} = \frac{1}{Z_c(1 + r_k^c)p^2}\delta_{\mu\nu} \qquad (\text{for } \beta = 1)\,. \tag{5.39}$$

For external ghost fields that enter in the ghost 2-point functions $\Gamma_k^{(\bar{c}c)}$ we will consider only the transverse modes of (5.34). This part is obtained by contracting the indices of (5.34) with the transverse-traceless projector (5.27a) and dividing by the projector norm. The transverse component of $\Gamma_k^{(\bar{c}c)}$ reads

$$\Gamma^{(\bar{c}c)}_{k,T}(p^2) = Z_c p^2\,. \tag{5.40}$$

5.1.2 Fermion Green's Function

The fermion 2-point function in momentum space is given by

$$\Gamma_k^{\bar{\psi}\psi}(p) = Z_\psi(-i\not{p} + m_\psi \mathbb{1})\delta_{ab}\,. \tag{5.41}$$

The fermion regulator reads

$$R_k^\psi(p) = r_k^\psi(p)\Gamma_k^{(\bar{\psi}\psi)}(p)\Big|_{m_\psi=0} = Z_\psi r_k^\psi(p)(-i\not{p})\delta_{ab}\,. \tag{5.42}$$

Altogether, we thus invert

$$\Gamma_k^{\bar{\psi}\psi} + R_k^\psi = Z_\psi(-i\not{p}(1 + r_k^\psi(p)) + m_\psi)\delta_{ab}\,, \tag{5.43}$$

in order to arrive at the fermion Green's function. Using $\gamma_\mu\gamma_\nu p^\mu p^\nu = p^2$ it is easily verified that

$$-G_k^\psi(p) = (\Gamma_k^{\bar{\psi}\psi} + R_k^\psi)^{-1} = \frac{i\not{p}(1 + r_k^\psi) + m_\psi}{p^2(1 + r_k^\psi(p))^2 + m_\psi^2}\delta_{ab}\,. \tag{5.44}$$

We obtain imaginary fermion momenta due to our conventions for the fermionic action with a real kinetic term. We shall see that the used conventions, however, do not lead to complex couplings.

5.1.3 Scalar Green's Function

The scalar Green's function is given by

$$\Gamma_k^{(\phi\phi)}(p^2) = Z_\phi(p^2 + m_\phi^2)\delta_{ab}\,. \tag{5.45}$$

The scalar regulator reads

$$R_k^\phi(p^2) = r_k^\phi(p^2)\Gamma_k^{(\phi\phi)}(p^2)\Big|_{m_\phi=0} = Z_\phi r_k^\phi(p^2)p^2\delta_{ab}\,. \tag{5.46}$$

In the scalar case the inversion of the sum of (5.45) and (5.46) is trivial. We have for the Green's function

$$G_k^\phi(p^2) = (\Gamma_k^{\phi\phi} + R_k^\phi)^{-1} = \frac{1}{Z_\phi(p^2(1 + r_k^\psi(p^2))) + m_\phi^2)}\delta_{ab} \tag{5.47}$$

The scalar Green's function complete the set of Green's function we need for solving the right hand side of the flow equation (2.14). We proceed with the analysis of the left hand side of (2.14).

5.2 Flow of 2-point Functions

In this section we consider the relation between the flow of the 2-point function and the flow of the couplings. We will extract separate information, namely the anomalous dimension and the flow of the mass from the momentum dependent and momentum independent parts, respectively. In the following, we derive the flows for these quantities for each of the fields.

5.2.1 Graviton 2-point Function

As discussed at the end of section 5.1.1 the transverse-traceless (spin-two) part of the graviton is the component which is regarded as physical. As can be read off from equation (5.32), the transverse-traceless part of $\Gamma_k^{(hh)}$ is given by

$$\Gamma_{k,\mathrm{TT}}^{(hh)}(p) = \frac{1}{32\pi}Z_h(p^2 + m_h^2)\,. \tag{5.48}$$

Taking the derivative with respect to t and multiplying both sides with $\frac{32\pi}{Z_h}$, we get

$$\frac{32\pi}{Z_h}\dot{\Gamma}_{k,\mathrm{TT}}^{(hh)}(p) = -\eta_h(p^2 + m_h^2) + \dot{m}_h^2\,, \tag{5.49}$$

where we denote derivatives with respect to t with a dot. The momentum dependent and momentum independent parts of the flow of the graviton 2-point function are proportional to the flow of the graviton mass $\dot{m}_h^2$ and the graviton anomalous dimension, respectively. We extract these quantities by making a Taylor expansion of the left hand side around vanishing momentum $p = 0$ according to

$$\frac{32\pi}{Z_h}\dot{\Gamma}_{k,\mathrm{TT}}^{(hh)}(0) + \frac{32\pi}{Z_h}\frac{1}{2}\frac{\partial^2\dot{\Gamma}_{k,\mathrm{TT}}^{(hh)}(p)}{\partial p^2}\Big|_{p=0} p^2 = (\dot{m}_h^2 - \eta_h m_h^2) - \eta_h p^2\,. \tag{5.50}$$

We omit the term linear in p on the left hand side, since it has no counter part on the right hand side. It can be shown to always vanish on the left hand side. Now we compare the coefficients of the expansion on the left and one the right hand side and extract the quantities η_h and $\dot{m}_k^2$. By introducing the dimensionless squared graviton mass, μ_h, and its flow

$$\mu_h = \frac{m_k^2}{k^2}\,, \tag{5.51a}$$

$$\dot{\mu}_h = -2\mu_h + \frac{\dot{m}_k^2}{k^2}\,, \tag{5.51b}$$

we express the relations obtained from (5.50) in terms of dimensionless quantities via

$$\dot{\mu}_h = -(2-\eta_h)\mu_h + \frac{32\pi}{Z_h k^2}\dot{\Gamma}^{(hh)}_{k,\mathrm{TT}}(0)\,, \tag{5.52a}$$

$$\eta_h = -\frac{16\pi}{Z_h}\frac{\partial^2 \dot{\Gamma}^{(hh)}_{k,\mathrm{TT}}(p)}{\partial p^2}\bigg|_{p=0}\,. \tag{5.52b}$$

We now have to treat the transverse-traceless part of the flow for the graviton 2-point function governed by the diagrams on the right hand side of

$\dot{\Gamma}^{(hh)}_k(p) = \frac{1}{2}\Big(-$ 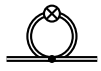 $+\,2\,$ $\Big) - \Big(2\,$ 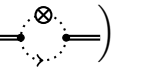 $\Big)$

$- N_f\Big(-$  $+\,2\,$ 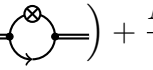 $\Big) + \frac{N_s}{2}\Big(-$  $+\,2\,$ 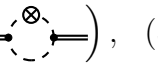 $\Big)\,,$ (5.11)

according to (5.52) in order to derive η_h and $\dot{\mu}_h$. Thus, the vertex construction together with a suitable projection on the spacetime and momentum indices allows to extract the flows for these quantities from the graviton 2-point function.

Remark: Flow for α Revisited

The same procedure can be applied to the flow of the vector (spin-1) part of the graviton 2-point function, in order to get an equation for flow of the gauge parameter α. The vector-part of the graviton 2-point function governed by the $(2,2)$ component of the matrix in (5.32) reads

$$\Gamma^{(hh)}_{k,\mathrm{V}} = \frac{Z_h}{32\pi}\left(\frac{1}{\alpha}p^2 + m_h^2\right)\,. \tag{5.53}$$

As before we take a derivative with respect to t and bring the prefactor $\frac{32\pi}{Z_h}$ to the left hand side:

$$\frac{32\pi}{Z_h}\dot{\Gamma}^{(hh)}_{k,\mathrm{V}} = -\eta_h\left(\frac{1}{\alpha}p^2 + m_h^2\right) - \frac{\dot{\alpha}}{\alpha^2}p^2 + \dot{m}_h^2 \tag{5.54}$$

Expanding the left hand side in p around $p = 0$ to second order we get an equation for the flow of α. It is given by

$$\dot{\alpha} = -\alpha \left(\eta_h + \alpha \frac{16\pi}{Z_h} \frac{\partial^2 \dot{\Gamma}^{(hh)}_{k,\mathrm{V}}}{\partial p^2} \bigg|_{p=0} \right) . \tag{5.55}$$

Equation (5.55) confirms the statement, that $\alpha = 0$ is a fixed point of its flow. The only quantities that contain α on the right hand side of the flow equation (2.14), are the graviton Green's functions. That is, because the gauge fixing term (4.19) in the graviton action is linear in the fluctuating field h. The graviton Green's function (5.32) contains only terms which do either not depend on, or are of linear order in α. Hence, both terms on the right hand side of equation (5.55) contain terms from zeroth to third order in α, dependent on the number of graviton Green's functions in the diagrams. Therefore, $\alpha = 0$ is a fixed point of (5.55).

From the flow equation (5.55) we can easily derive the linear stability of the fixed point in α-direction. We take the derivative of (5.55) with respect to α and evaluate at $\alpha = \alpha* = 0$. We have

$$\frac{\partial \dot{\alpha}}{\partial \alpha} \bigg|_{\alpha=0} = -\eta_h \bigg|_{\alpha=0} . \tag{5.56}$$

The right hand side is minus the graviton anomalous dimension η_h in Landau–deWitt gauge. Hence, the fixed point is UV-stable in the α-direction as long as the graviton anomalous dimension is positive.

5.2.2 Ghost 2-point Function

Along the same lines as in the case of the graviton 2-point function we extract the anomalous dimension of the transverse ghost field. The transverse ghost 2-point function is given by (5.40)

$$\Gamma^{(\bar{c}c)}_{k,T}(p^2) = Z_c p^2 . \tag{5.40}$$

As before, we take the derivative with respect to t and devide by Z_c to obtain

$$\frac{\dot{\Gamma}^{(\bar{c}c)}_{k,T}(p^2)}{Z_h} = -\eta_c p^2 . \tag{5.57}$$

Thus, by expanding the right hand side of equation (5.57) in a Taylor series in p around $p = 0$ and comparing the coefficients, we get the relation for η_c. It reads

$$\eta_c = -\frac{1}{2Z_c} \frac{\partial^2 \dot{\Gamma}^{(\bar{c}c)}_{k,\mathrm{T}}(p^2)}{\partial p^2} \bigg|_{p=0} . \tag{5.58}$$

In the diagrammatic representation, the transverse part of the flow of $\Gamma_k^{\bar{c}c}$ is given by

$$\dot{\Gamma}^{(\bar{c}c)}_{k,\mathrm{T}}(p^2) = \frac{1}{\mathrm{Tr}(\mathbb{P}_\mathrm{T} \circ \mathbb{P}_\mathrm{T})} \,\mathrm{Tr}\, \mathbb{P}_\mathrm{T} \circ \Big(+ \Big) \,. \tag{5.59}$$

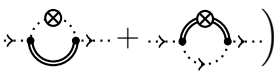

Similarly to the analysis of flow of the graviton 2-point function, we have derived a relation between the anomalous dimension of the ghosts η_c and the flow of the ghost 2-point function.

5.2.3 Fermion 2-point Function

The fermion 2-point function was derived in section 5.1.2. We will omit the flavor indices in the following since they only enter trivially. The fermion 2-point function is given by

$$\Gamma_k^{\bar{\psi}\psi}(p) = Z_\psi(-i\not{p} + m_\psi \mathbb{1})\,. \tag{5.41}$$

Taking the scale derivative ∂_t and deviding by Z_ψ we obtain

$$\frac{\dot{\Gamma}_k^{\bar{\psi}\psi}(p)}{Z_\psi} = -\eta_\psi(-i\not{p} + m_\psi \mathbb{1}) + \dot{m}_\psi \mathbb{1} \tag{5.60}$$

Here, we make use of the spinor structure of the fermionic flow, in order to derive equations for the anomalous dimension and the flow of the fermion mass. The part of (5.60) proportional to p and η_ψ is proportional to the traceless γ-matrices. On the other hand, the part proportional to the flow of the mass is proportional to the identity matrix with non-vanishing trace. We take the trace of (5.60) on the one hand and multiply both sides of (5.60) with $\not{p}$ and then take the trace on the other hand. Again, we formulate the flow equation for the fermion mass in terms of dimensionless squared fermion mass,

$$\mu_\psi = \frac{\dot{m}_\psi^2}{k^2}, \tag{5.61}$$

the flow of which relates to the flow of m_ψ via

$$\begin{aligned} \dot{\mu}_\psi &= -2\mu_\psi + \frac{\dot{m}_\psi^2}{k^2} \\ \dot{\mu}_\psi &= -2\mu_\psi + 2\sqrt{\mu_\psi}\frac{\dot{m}_\psi}{k}. \end{aligned} \tag{5.62}$$

Altogether, we arrive at the flow equation for the dimensionless fermion mass and the equation for the fermion anomalous dimension:

$$\dot{\mu}_\psi = -2(1-\eta_\psi)\mu_\psi + \frac{\sqrt{\mu_\psi}}{2Z_\psi k}\,\mathrm{Tr}\,\dot{\Gamma}_k^{\bar{\psi}\psi}(p) \tag{5.63a}$$

$$\eta_\psi = \frac{i}{8Z_\psi}\frac{\partial^2\,\mathrm{Tr}\left(\not{p}\Gamma_k^{\bar{\psi}\psi}(p)\right)}{\partial p^2}\bigg|_{p=0} \tag{5.63b}$$

The flow of of the fermion 2-point function from the right hand side of the flow equation is given by

$$\dot{\Gamma}_k^{\bar{\psi}\psi}(p) = \frac{1}{2}\Big(-$$  $$+\,2$$ 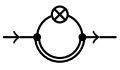 $$+\,2$$ 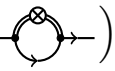 $$\Big)\,. \tag{5.64}$$

5.2.4 Scalar 2-point Function

For the scalar fields the 2-point function is given by

$$\Gamma_k^{\phi\phi}(p) = Z_\phi(p^2 + m_\phi^2)\,, \tag{5.65}$$

where we again omit the color indices since they only enter trivially. Since the graviton transverse-traceless mode of the graviton is just a scalar field, we have the same derivation as in section 5.2.1. For the scalar anomalous dimension η_ψ and the flow of the dimensionless scalar mass μ_ϕ we write

$$\dot{\mu}_\phi = -(2-\eta_\phi)\mu_h + \frac{1}{Z_\phi k^2}\dot{\Gamma}_k^{(\phi\phi)}(0)\,, \tag{5.66a}$$

$$\eta_\phi = -\frac{1}{2Z_\phi}\frac{\partial^2\dot{\Gamma}_k^{(\phi\phi)}(p)}{\partial p^2}\bigg|_{p=0}\,. \tag{5.66b}$$

The flow for the scalar two point function that originates from the right hand side of the flow equation is reads

$$\dot{\Gamma}_k^{\bar{\phi}\phi}(p) = \frac{1}{2}\Big(-$$  $$+\,2$$ 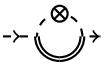 $$+\,2$$ 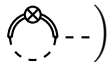 $$\Big)\,. \tag{5.67}$$

The relations for the scalar anomalous dimension η_ϕ and the flow of the scalar mass μ_ϕ complete the set of quantities we extract from the 2-point functions. For a closed system of differential equations for the couplings, the only thing missing is the flow of Newton's coupling G_N.

5.3 Flow of the Graviton 3-point Function

The graviton 2-point function is independent of G_N. Thus we study the graviton 3-point function for the investigation of the flow of G_N. We derived diagrams which govern the flow of the graviton 3-point function in equation (5.13). The vertex construction (4.47) relates the 3-point function to the respective couplings G_N and $\Lambda^{(3)}$ by

$$\Gamma_k^{(hhh),\mathbf{a_1a_2a_3}} = (Z_h)^{\frac{3}{2}} G_N^{\frac{1}{2}} \mathcal{T}^{\mathbf{a_1a_2a_3}}(\Lambda_k^{(3)}). \tag{5.68}$$

Here, we denoted with the multi-indices $\mathbf{a_i} = (\mu_i, \nu_i, p_i)$ the combinations of space-time and momentum indices of the graviton field h. Before proceeding further, let us make some remarks about the tensor $\mathcal{T}$ here.

Properties of $\mathcal{T}^{\mathbf{a_1 a_2 a_3}}$

1. The definition of $\mathcal{T}^{\mathbf{a_1 a_2 a_3}}$ is given in general by equation (4.48). For the specific case of the graviton 3-point function, it is given by

$$\mathcal{T}^{\mathbf{a_1 a_2 a_3}} = \frac{\delta^3 S_{\mathrm{EH}}(G_N = 1, \Lambda = \Lambda_k^{(3)})}{\delta h_{\mathbf{a_1}} \delta h_{\mathbf{a_2}} \delta h_{\mathbf{a_3}}} \tag{5.69}$$

2. Expression (5.69) has $3 \times 2 = 6$ spacetime indices and $3 \times 1 = 3$ momentum indices. Hence, it is a complicated object, which is difficult to handle. In principle, we expect that $\mathcal{T}$ admits a representation in terms of orthogonal tensors. However, an orthogonal basis for tensors of this rank is unknown. Therefore, we have find another way to extract the physically relevant parts of $\mathcal{T}$ which govern the flow of the couplings G_N and $\Lambda^{(3)}$.

3. Apart from the spacetime indices, $\mathcal{T}$ also depends on the three momenta of the graviton fields. In the most general case, two of these momenta are arbitrary. The third one can be eliminated by momentum conservation. Hence, along with the choice of the projection procedure for the spacetime indices we also have find a of a projection for the momenta at which equation (5.68) is evaluated. The simplest possible choices for the combination of three momenta which obey momentum conservation are:

   - A momentum configuration where one of the momenta, e.g., p_3 is zero. In this case p_2 is fixed by p_1 by momentum conservation $p_2 = -p_1$. We call this the asymmetric configuration.
   - A configuration where the norms of all three momenta are equal. Momentum conservation then fixes the three momenta to lie in a 2-dimensional plane and to be distributed with an angle of $\frac{2\pi}{3}$ between each other. We refer to this choice as symmetric configuration.

4. Since the tensor $\mathcal{T}$ is obtained by taking the third variation of the Einstein-Hilbert action, it is at most quadratic in the field momenta. More precisely, is comprises the two parts

$$S_{\mathrm{EH}}(G_N = 1, \Lambda = \Lambda_k^{(3)}) = \frac{1}{32\pi} \int \underbrace{2\sqrt{g}\Lambda_k^{(3)}}_{\text{no derivatives}} - \underbrace{\sqrt{g}R}_{\text{quadratic derivatives}} \quad d^4x\,. \tag{5.70}$$

   one of which contains no spacetime derivatives and is proportional to the 3rd 'cosmological constant' $\Lambda_k^{(3)}$. The other term is quadratic in spacetime derivatives. Thus, in momentum space $\mathcal{T}$ decomposes into

$$\mathcal{T}^{\mathbf{a_1 a_2 a_3}}(p_1, p_2, p_3, \Lambda_k^{(3)}) = \mathcal{T}^{\mathbf{a_1 a_2 a_3}}(p_1, p_2, p_3, 0) + \Lambda_k^{(3)} \mathcal{T}^{\mathbf{a_1 a_2 a_3}}(0, 0, 0, 1). \tag{5.71}$$

The tensor $\mathcal{T}^{(3)}$ thus contains a part which is proportional to $\Lambda_k^{(3)}$ and momentum independent. The second part is quadratic in the momenta and independent of running couplings. We use the decomposition given in (5.71) for the construction of projectors for the flow of the graviton 3-point function.

5.3.1 Spacetime Projection

In order to extract the relevant part of the flow of Newton's coupling G_N, we have to identify the physical parts of the flow. Therefore, we construct two projection tensors from the Einstein-Hilbert action. One, which is used for the projection onto the momentum independent part and another one for the momentum dependent part. According to (5.71) we write

$$\tilde{\Pi}_\Lambda^{\mathbf{a_1a_2a_3}} = \mathcal{T}^{\mathbf{a_1a_2a_3}}(0,0,0,1)\,, \tag{5.72a}$$

$$\tilde{\Pi}_G^{\mathbf{a_1a_2a_3}} = \mathcal{T}^{\mathbf{a_1a_2a_3}}(p_1,p_2,p_3,0)\,. \tag{5.72b}$$

Now, analogous to case of the 2-point function we identify the transverse-traceless parts of the graviton as the physical modes. Hence, we contract the spacetime indices of the projectors $\tilde{\Pi}_\Lambda$ and $\tilde{\Pi}_G$ with transverse traceless projectors. We expand the multi indices and write

$$\Pi_\Lambda^{\mu\nu\rho\sigma\omega\tau} = \mathbb{P}^{(2)}(p_1)^{\mu\nu}{}_{\alpha\beta}\mathbb{P}^{(2)}(p_2)^{\rho\sigma}{}_{\gamma\delta}\mathbb{P}^{(2)}(p_3)^{\omega\tau}{}_{\epsilon\phi}\tilde{\Pi}_\Lambda^{\alpha\beta\gamma\delta\epsilon\phi}\,, \tag{5.73a}$$

$$\Pi_G(p_1,p_2,p_3)^{\mu\nu\rho\sigma\omega\tau} = \mathbb{P}^{(2)}(p_1)^{\mu\nu}{}_{\alpha\beta}\mathbb{P}^{(2)}(p_2)^{\rho\sigma}{}_{\gamma\delta}\mathbb{P}^{(2)}(p_3)^{\omega\tau}{}_{\epsilon\phi}\tilde{\Pi}_G(p_1,p_2,p_3)^{\alpha\beta\gamma\delta\epsilon\phi}\,. \tag{5.73b}$$

The projectors Π_G and Π_Λ are used to map out the physically relevant parts of the flow for G_N and $\Lambda_k^{(3)}$, respectively. To this end, we consider the flow of the graviton 3-point function. We take a t-derivative of equation (5.68) and multiply both sides with $2\sqrt{\frac{G_N}{Z_h^3}}$. We have

$$2\sqrt{\frac{G_N}{Z_h^3}}\dot{\Gamma}_k^{hhh,\mathbf{a_1a_2a_3}} = \left(-3\eta_h + \dot{G}_N\right)\mathcal{T}^{\mathbf{a_1a_2a_3}} + 2G_N\partial_t\mathcal{T}_{.3}^{\mathbf{a_1a_2a_3}} \tag{5.74}$$

Due to the momentum structure of $\mathcal{T}$ the contraction with the projectors in (5.73) yields

$$\mathrm{Tr}(\Pi_i \circ \mathcal{T}_3) = M_i(p_1,p_2,p_3) + N_i\Lambda_k^{(3)}\,, \tag{5.75}$$

where $i \in \{\Lambda, G\}$. The expression on the right hand side of (5.75) defines the complete pairwise contraction of all spacetime indices on Π_i and $\mathcal{T}$. In general M_i is a function quadratic in the graviton momenta. In particular

$$M_i(0,0,0) = 0. \tag{5.76}$$

Furthermore, since the projectors (5.73) are independent of t and, thus

$$[\partial_t, \Pi_i] = 0, \tag{5.77}$$

we can write

$$\mathrm{Tr}(\Pi_i \circ \partial_t \mathcal{T}_3) = N_i \dot{\Lambda}_k^{(3)}. \tag{5.78}$$

Contracting the spacetime indices of equation (5.74) with Π_i and using (5.75) and (5.78) we obtain

$$2\sqrt{\frac{G_N}{Z_h^3}}\,\mathrm{Tr}(\Pi_i \circ \dot{\Gamma}_k^{hhh}) = \left(M_i(p_1,p_2,p_3) + N_i \Lambda_k^{(3)}\right)(\dot{G} - 3\eta_h G_N) + \\ + 2N_i \dot{\Lambda}_k^{(3)} G_N\,. \tag{5.79}$$

The Flow of $\Lambda^{(3)}$

The flow equation for $\Lambda_k^{(3)}$ is governed by the momentum independent part of $\mathcal{T}$ projected with Π_Λ. We evaluate equation (5.79) at vanishing graviton momenta and use (5.76). The resulting flow equation for $\Lambda_k^{(3)}$ reads

$$\dot{\Lambda}_k^{(3)} = \frac{1}{N_\Lambda}\frac{1}{\sqrt{G_N Z_h^3}} \lim_{(p_i)\to 0} \mathrm{Tr}(\Pi_\Lambda \circ \dot{\Gamma}_k^{hhh}) + \frac{\Lambda_k^{(3)}}{2}\left(-\frac{\dot{G}_N}{G_N} + 3\eta_h\right), \tag{5.80}$$

$$\dot{\lambda}_k^{(3)} = -\left(1 - \frac{3}{2}\eta_h + \frac{\dot{g}}{2g}\right) + \frac{1}{N_\Lambda k^2}\frac{1}{\sqrt{G_N Z_h^3}} \lim_{(p_i)\to 0} \mathrm{Tr}(\Pi_\Lambda \circ \dot{\Gamma}_k^{hhh}), \tag{5.81}$$

where we introduced the dimensionless variables

$$\lambda_k^{(3)} = \frac{\Lambda_k^{(3)}}{k^2} \tag{5.82}$$

$$g = G_N k^2, \tag{5.83}$$

in the last step.

The second term on the right hand side of equation (5.81) is calculated with help of the right hand side of the flow equation. In diagrammatic language, it is given by (5.13). The constant N_Λ is obtained from equation (5.75) at vanishing momenta. Note that (5.81) contains the flow of $\dot{g}$ which is discussed in the following.

The Flow of G_N

In order to obtain a scalar flow equation for the couplings G_N we employ the projector Π_G. In this section, it is important to distinguish between the momentum vectors $\boldsymbol{p}$ and their respective norms p. First of all, we note that due to momentum conservation at the vertex the graviton momentum $\mathbf{p_3}$ can be eliminated. We have

$$M_G(\mathbf{p_1}, \mathbf{p_2}, \mathbf{p_3}) = M_G(\mathbf{p_1}, \mathbf{p_2}) = M_G(p_1, p_2, x = \cos\theta), \tag{5.84}$$

where θ is the angle between the momenta $\mathbf{p_1}$ and $\mathbf{p_2}$. The functions M_G and N_G are obtained with help of equation (5.75). Since the projector Π_G is quadratic in the graviton momenta, M_G and N_G are quartic and quadratic in the momenta, respectively. In order make the $\dot{\Lambda}_k^{(3)}$-part of (5.79) momentum independent, we divide out the extra momentum dependence coming from the projector Π_G. To this end, we divide equation (5.79) by N_G according to

$$2\sqrt{\frac{G_N}{Z_h^3}}\frac{\mathrm{Tr}(\Pi_G \circ \dot{\Gamma}_k^{hhh})}{N_G} = \left(\frac{M_G}{N_G} + \Lambda_k^{(3)}\right)(\dot{G} - 3\eta_h G_N) + \dot{\Lambda}_k^{(3)} G_N \,. \tag{5.85}$$

Now, we take the Hessian of (5.85) with respect to (p_1, p_2) which yields

$$\sqrt{\frac{G_N}{Z_h^3}}\left(\partial_{p_a}\partial_{p_b}\frac{\mathrm{Tr}(\Pi_G \circ \dot{\Gamma}_k^{hhh})}{N_G}\right) = M_{ab}(\dot{G} - 3\eta_h G_N)\,, \tag{5.86}$$

with

$$M_{ab} = \frac{1}{2}\left(\partial_{p_a}\partial_{p_b}\frac{M_G}{N_G}\right)(p_1, p_2, x), \tag{5.87}$$

and $a, b \in \{1, 2\}$. Equation (5.86) is a matrix equation for the flow of G_N. A scalar flow is obtained e.g. by taking its trace with respect to the indices $\{a, b\}$. Doing this and transforming to dimensionless quantities we arrive at the scalar flow equation for g

$$\dot{g} = (2 + 3\eta_h)g + \frac{1}{M_{aa}}\sqrt{\frac{gk^2}{Z_h^3}}\left(\partial_{p_a}\partial_{p_a}\frac{\mathrm{Tr}(\Pi_G \circ \dot{\Gamma}_k^{hhh})}{N_G}\right)(p_1, p_2, x)\,, \tag{5.88}$$

where the sum over a is understood.

Hence, we have derived a flow equation for g considering a general momentum configuration. In this generality, equation (5.88) is very hard to solve and can in particular not be solved analytically. However, (5.88) simplifies considerably if we choose particularly simple momentum configurations. Furthermore, analytic results for these configurations can be obtained, using Litim's cutoff in the limit of vanishing momenta.

5.3.2 Momentum Configurations

In the previous section we derived flow equations for the dimensionless couplings λ_3 and g. The momentum configuration for which $\dot{g}$ is evaluated turns out to be relevant. Since the flow equation for λ_3, (5.81), contains $\dot{g}$ the flows for both couplings are dependent on the momentum configuration. In this section we consider two particularly simple momentum configurations and evaluate the flow (5.88) for

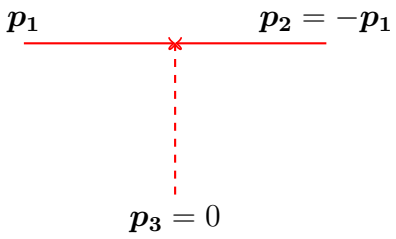

Figure 5.1: Sketch of the asymmetric momentum configuration. The momentum $\boldsymbol{p_3}$ (dashed line) is zero in this limit.

these choices. Generally, a natural way to simplify the equations is by identifying the two momentum norms

$$p = p_1 = p_2. \tag{5.89}$$

For this choice, we have for M_{aa}

$$M_{aa}(x) = \left(\partial_p^2 \frac{M_G}{N_G}\right)(x) \qquad (\text{for } p_1 = p_2 = p). \tag{5.90}$$

M_N and N_Λ are quartic and quadratic in p, respectively. Since p is the only momentum norm, p^2 can be factored out. The second derivative removes the remaining quadratic momentum dependence. This way M_{aa} only depends on x for the choice (5.89). Having this, we express the corresponding flow equation for g as

$$\dot{g} = (2 + 3\eta_h)g + \frac{2}{M_{aa}(x)}\sqrt{\frac{gk^2}{Z_h^3}}\left(\partial_p^2 \frac{\mathrm{Tr}(\Pi_G \circ \dot{\Gamma}_k^{hhh})}{N_G}\right)(p, x)\,. \tag{5.91}$$

In order to simplify (5.91) further, we fix the angle x. We distinguish two different cases for these choices which we refer to as asymmetric configuration for $x = -1$ and symmetric configuration for $x = -\frac{\sqrt{3}}{2}$. In the following we discuss the two configurations in more detail.

Asymmetric Configuration: $x = -1$

The choice $p = p_1 = p_2$, $x = \cos\theta = -1$ corresponds to the limit $\boldsymbol{p_3} = 0$. In Figure 5.1 the momentum configuration is shwon schematically. In a coordinate system where $\boldsymbol{p_1}$ is defined along the p_x-axis, we write

$$\boldsymbol{p_1} = \begin{pmatrix} p \\ 0 \\ 0 \\ 0 \end{pmatrix}, \quad \boldsymbol{p_2} = \begin{pmatrix} -p \\ 0 \\ 0 \\ 0 \end{pmatrix}, \quad \boldsymbol{p_3} = 0 \quad (\text{asymmetric configuration}) \tag{5.92}$$

The requirement can only be reached asymptotically and has some further implications. For instance, we have complete freedom to choose the angle between $\boldsymbol{p_3}$ and

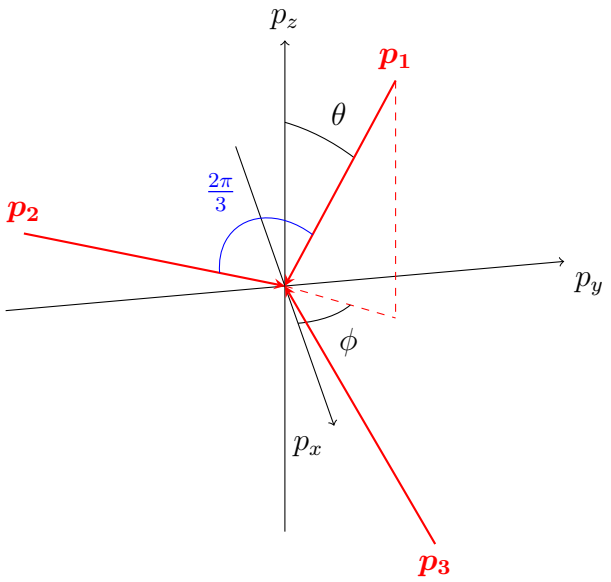

Figure 5.2: Sketch of the symmetric momentum configuration. The position of all three vectors is fully determined by its norm, and two angles. Hence, the integrals in the loops can be evaluated analytically by identifying the two angles with the integration angles.

$\boldsymbol{p_1}$ which corresponds to the choice which initial configuration for which the limit is taken. Furthermore, for $\boldsymbol{p_3}$ the notion of a transverse-traceless projector is not sensible any more. Therefore, we replace the transverse traceless projector for $\boldsymbol{p_3}$ by another one which does not suffer from these ambiguities. We define

$$\mathbb{P}^{\mathrm{T}}(\boldsymbol{p}=0) = \delta_{\mu\nu} \tag{5.93}$$

$$\mathbb{P}^{(2)}(\boldsymbol{p}=0) = \delta_{\mu(\rho}\delta_{\sigma)\nu} - \frac{1}{3}\delta_{\mu\nu}\delta_{\rho\sigma}, \tag{5.94}$$

in order to have a well defined limit in all cases. With this choice we enable an analytic evaluation of the loop integrals for $p = 0$.

Symmetric Configuration: $x = -\frac{\sqrt{3}}{2}$

In the symmetric configuration we have $x = \cos\theta = -\frac{3}{2}$ and hence, $\theta = \frac{2\pi}{3}$. Together with $p = p_1 = p_2$, this amounts to the fully symmetric momentum configuration where all momenta have the same norm. In Figure 5.2 the symmetric configuration is given schematically. In a coordinate system in which $\boldsymbol{p_1} = p\boldsymbol{e}_{\boldsymbol{p_x}}$ momenta can be

written as:

$$\boldsymbol{p_1} = p \begin{pmatrix} 1 \\ 0 \\ 0 \\ 0 \end{pmatrix}, \ \boldsymbol{p_2} = p \begin{pmatrix} -\frac{1}{2} \\ -\frac{\sqrt{3}}{2} \\ 0 \\ 0 \end{pmatrix}, \ \boldsymbol{p_3} = p \begin{pmatrix} -\frac{1}{2} \\ \frac{\sqrt{3}}{2} \\ 0 \\ 0 \end{pmatrix} \quad \text{(symmetric configuration)} \tag{5.95}$$

The ambiguities which we described for the asymmetric configuration in the previous section are absent here. The symmetric configuration, i.e. the position of all momenta, is fully determined by two angles. These angles are denoted θ and ϕ in Figure 5.2. This suggests, that in the coordinate system defined by (5.95), the loop integration can be simplified in a similar way as in the asymmetric case by identifying the angles of with the integration. For $p = 0$ we get analytic flow equations for Litim's cutoff.

Flow of g for fixed momentum configurations

Once x is fixed, equation (5.91) loses its angle dependence. This results in a flow equation for g which solely depends on the momentum norm p. We have

$$\dot{g} = (2 + 3\eta_h)g + \frac{2}{M_{aa}} \sqrt{\frac{gk^2}{Z_h^3}} \left(\partial_p^2 \frac{\mathrm{Tr}(\Pi_G \circ \dot{\Gamma}_k^{hhh})}{N_G} \right)(p). \tag{5.96}$$

As a first approximation we evaluate at $p = 0$. This allows to compute equation (5.96) analytically. However, it will turn out to be a rather bad choice in section 7.3.2. Thus, we propose an improved momentum projection scheme there.

5.4 Evaluating the Diagrams

The task of deriving flow equations for the coupling has now reduced to the evaluation of the diagrams introduced in the beginning of this chapter. In general extract different quantities from momentum dependent and the momentum independent parts of the n-point flow diagrams. In this section, we will briefly explain how the diagrams are evaluated. We discuss the simple example of the fermion-loop diagram contributing to the transverse-traceless graviton 2-point function. It reads

$$\dot{\Gamma}^{(hh)}_{\mathrm{TT},k} \sim \mathrm{Tr} \left(\mathbb{P}^{(2)} \circ \right) . \tag{5.97}$$

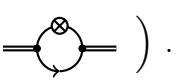

This diagram is particularly easy to evaluate. We first collect all the vertices and Greens functions which are needed. We have

$$A \xrightarrow{\ p\ } B = -G^{\psi}_{k;AB}(p) = \frac{1}{Z_\psi}\frac{i(1+r^{\psi}_k)\not{p}_{AB} + m_\psi \mathbb{1}_{AB}}{p^2(1+r^{\psi}_k(p))^2 + m^2_\psi}\,, \tag{5.44}$$

$$\begin{aligned} A \xrightarrow{\ p\ } \otimes \xrightarrow{} B &= G^{\psi}_{k;AC}(p) R^{\psi}_{k;CD}(p) G^{\psi}_{k;DB}(p) = \\ &= G^{\psi}_{k;AC}(p)(-i\not{p}(1+r^{\psi}_k(p)))_{CD} G^{\psi}_{k;DB}(p)\,, \end{aligned} \tag{5.98}$$

$\mu\nu$ — B / A

$$= -\frac{\delta_{\mu\nu}}{2}\left(m_\psi \mathbb{1} - \frac{i}{2}\left(\not{p}_{\bar{\psi}} + \frac{1}{2}\not{p}_h\right)\right)_{AB} + \frac{i}{4}\left(p^{(\mu}_{\bar{\psi}}\gamma^{\nu)} + \frac{1}{2}p^{(\mu}_h\gamma^{\nu)}\right)_{AB}\,. \tag{5.99}$$

As the shape function $r^{\psi}_k(p)$ we choose Litim's cutoff. It reads

$$r^{\psi}_k(p) = \left(\frac{k}{p} - 1\right)\theta(k^2 - p^2)\,. \tag{5.100}$$

Expanding the momentum trace we get for the diagram

$$\begin{aligned} \mathrm{Tr}\left(\mathbb{P}^{(2)} \circ \right) = \mathbb{P}^{(2)}(p)_{\mu\nu\rho\sigma} \int_{\mathbb{R}^4} \Gamma^{h\bar{\psi}\psi;\mu\nu}_{AB}(p,q) R^{\psi}(q)_{BC} G^{\psi}_{k;CD}(q) \times \\ \Gamma^{h\bar{\psi}\psi;\rho\sigma}_{DE}(-p, p+q) G^{\psi}_{k;EA}(p) d^4q\,. \end{aligned} \tag{5.101}$$

Now we expand the expression and use the trace theorems for spinors. The contraction of the indices is done with *FORM*. We get for the content of the integral

$$\begin{aligned} &\frac{1}{G_N Z_h}\,\mathrm{Tr}\left(\mathbb{P}^{(2)} \circ \right) = \\ &-G_N \int_0^1 \int_{-1}^1 \left(\frac{2\left(x^2-1\right)q^2(\eta_f(q-1)+1)}{15\left(m^2_\psi+1\right)^2 l_\psi(p,q,x)} k_\psi(p,q,x)\right)\frac{\sqrt{1-x^2}q^3}{4\pi^3} dx dq\,, \end{aligned} \tag{5.102}$$

where

$$\begin{aligned} k_\psi(p,q,x) = \Big(\left(m^2_\psi - 1\right)\left(\sqrt{p^2+q^2+2pqx} - 1\right)\theta\left(1 - (p^2+q^2+2pqx)\right) \times\ , \\ \left(4x^2q + 5xp + q\right) + \sqrt{p^2+q^2+2pqx}\left(-m^2_\psi\left(4x^2q + 5xp + q - 10\right)\ ,\right. \\ \left. +4x^2q + 5xp + q\right)\Big)\,. \end{aligned} \tag{5.103}$$

$$\begin{aligned} l_\psi(p,q,x) = \sqrt{p^2+q^2+2pqx}\Big(\left(\sqrt{p^2+q^2+2pqx} - 1\right)^2\theta\left(1 - (p^2+q^2+2pqx)\right)^2 \\ -2\left(\sqrt{p^2+q^2+2pqx} - 1\right)\sqrt{p^2+q^2+2pqx}\,\theta\left(1 - (p^2+q^2+2pqx)\right) \\ \left. +m^2_\psi + (p^2+q^2+2pqx)\right) \end{aligned} \tag{5.104}$$

Using equations (5.52) extract the fermionic contribution to the flow of the graviton mass and the gravtion anomalous dimension from the diagram.

5.4.1 Evaluation at $p = 0$

The task of evaluating the integral (5.101) is fulfilled easiest by setting $p = 0$. Hence, following equation (5.52a) we arrive at

$$\dot{\mu}_h \sim 32\pi \,\mathrm{Tr}\left(\mathbb{P}^{(2)} \circ \right)\Big|_{p=0} =$$

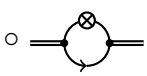

$$= 32\pi G_N \int_0^1 \int_{-1}^1 \left(\frac{2\left(x^2-1\right) q^2 \left(4x^2\left(m_\psi^2-1\right) - 9m_\psi^2 - 1\right)\left(\eta_f(q-1)+1\right)}{15\left(m_\psi^2+1\right)^3} \right) \times \frac{\sqrt{1-x^2}q^3}{4\pi^3} dx dq \,, \quad (5.105)$$

$$\eta_h \sim -16\pi \frac{\partial^2}{\partial p^2} \,\mathrm{Tr}\left(\mathbb{P}^{(2)} \circ \right)\Big|_{p=0} =$$

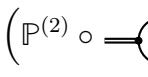

$$= -32\pi G_N \int_0^1 \int_{-1}^1 \left(-\frac{\left(x^2-1\right)^2 \left(12x^2+1\right)\left(m_\psi^2-1\right)\left(\eta_f(q-1)+1\right)}{15\left(m_\psi^2+1\right)^3} \right) \times \frac{\sqrt{1-x^2}q^3}{4\pi^3} dx dq + \text{distributitive corrections} \,. \quad (5.106)$$

The distributive correction in the latter equation is due δ-functions that arise when we take a second derivative of the non-analytic integral kernel. This is explained in more detail in Appendix A.3. The correction term for the present diagram is given by

$$\text{distributive corrections} =$$

$$= -32\pi G_N \int_{-1}^1 \left(\frac{x^2\left(x^2-1\right)\left(4x^2\left(m_\psi^2-1\right)^2 + m_\psi^4 + 18m_\psi^2 + 1\right)}{30\left(m_\psi^2+1\right)^4} \right) \times \frac{\sqrt{1-x^2}q^3}{4\pi^3} dx \quad (5.107)$$

We evaluate the integrals in order to obtain its contribution to the flow of the graviton mass and the anomalous dimension. The integration is performed with *Mathematica*. The analytic result in dimensionless quantities is given by

$$\dot{\mu}_h \sim -\frac{g(\eta_f - 7)\left(5\mu_\psi + 1\right)}{63\pi\left(\mu_\psi+1\right)^3} \quad (5.108a)$$

$$\eta_h \sim \frac{g(\eta_f - 5)\left(\mu_\psi - 1\right)}{48\pi\left(\mu_\psi+1\right)^3} + \frac{g\left(\mu_\psi^2 + 6\mu_\psi + 1\right)}{24\pi\left(\mu_\psi+1\right)^4}, \quad (5.108b)$$

where the second term in (5.108b) corresponds to the distributive corrections. In general this term carries the highest power in $(1+\mu_i)^{-1}$ because it results from a derivative of the Green's function G_k^i with respect to p.

5.4.2 Anomalous Dimensions

Equation (5.108b) shows the general structure in which the anomalous dimensions appear in the flow. Each anomalous dimension η_Φ consists on two parts. One part is linear in all other anomalous dimensions. The second part, is independent of them. Thus, for the ensemble of fields Φ we can express the anomalous dimensions in terms of

$$\boldsymbol{\eta} = \begin{pmatrix} \eta_h \\ \eta_c \\ \eta_\psi \\ \eta_\phi \end{pmatrix} = g\left(\boldsymbol{A}(\lambda_3, \mu_i)\boldsymbol{\eta} + \boldsymbol{C}(\lambda_3, \mu_i)\right), \tag{5.109}$$

where $\boldsymbol{A}$ is a general matrix and $\boldsymbol{c}$ is a vector which does not depend on the anomalous dimensions. Hence, the vector $\boldsymbol{\eta}$ can be written as

$$\boldsymbol{\eta} = g\Big((\mathbb{1} - g\boldsymbol{A})^{-1}\boldsymbol{C}\Big)(g, \lambda_3, \mu_i) \tag{5.110}$$

This equation reflects the non-perturbative nature of the flow equation. The matrix $(\mathbb{1} - g\boldsymbol{A})^{-1}$ depends non-trivially on the couplings g, λ_3 and the masses μ_i. Hence, a solution of (5.110) is in general a complicated function of the couplings and the masses. Since the $\boldsymbol{\eta}_i$ feed back into the flow for the couplings and the masses, the inversion of $(\mathbb{1} - g\boldsymbol{A})$ gives rise to non-perturbative terms in g and λ_3 in the flow which can not be obtained by perturbation theory.

Remark: Anomalous Dimensions in Integrals

We close this section with a short remark. So far, we have considered the anomalous dimension as constant with respect to the momentum variable. Thus, anomalous dimensions could be moved out of the loop integrals in the previous section. However, we see in section 7.3.2, that this approximation is not always justified. The next best approximation is, thus, to evaluate η_Φ at the value of p, where the integrand is peaked. This is typically the case at $p = k$. We employ this improved procedure in section 7.3.2.

5.5 The Analytic Flow Equations

In the following, we evaluate the 2-point functions for all fields and the graviton 3-point function to obtain flow equations for all the quantities that appear in the system. We choose $p = 0$ and Litim's cutoff to obtain analytic expressions for the flows.

5.5.1 Couplings

For the analytic equations for the dimensionless couplings λ_3 and g we use the graviton 3-point function. In particular, the flow of g is extracted by employing the

symmetric momentum configuration for $p = 0$. We have

$$\begin{aligned}
\dot{g} =&(2+3\eta_h)g + \frac{g^2}{19\pi}\Bigg(- \frac{47(6-\eta_h)}{6(1+\mu_h)^2} + \frac{16(1-3\lambda_3)\lambda_4}{(1+\mu_h)^4} \\
&+ \frac{45(8-\eta_h) + 472(6-\eta_h)\lambda_4 - 120\lambda_3(2(6-\eta_h) + 3(4-\eta_h)\lambda_4)}{18(1+\mu_h)^3} \\
&+ \frac{147(10-\eta_h) - 1860(8-\eta_h)\lambda_3 + 3380(6-\eta_h)\lambda_3^2 + 25920(4-\eta_h)\lambda_3^3}{90(1+\mu_h)^4} \\
&+ 2\frac{-299 + 1780\lambda_3 - 3640\lambda_3^2 + 2336\lambda_3^3}{15(1+\mu_h)^5} - \frac{50-53\eta_c}{10}\Bigg) \\
&- \frac{g^2 N_\psi}{38\pi}\left(\frac{3(5-\eta_\psi)\,(1-\mu_\psi)}{4\,(1+\mu_\psi)^3} + \frac{3\left(1+6\mu_\psi+\mu_\psi^2\right)}{2\,(1+\mu_\psi)^4}\right. \\
&\left. + \frac{(6-\eta_\psi)\,(521+529\mu_\psi)}{450\,(1+\mu_\psi)^4} - \frac{1-32\mu_\psi-9\mu_\psi^2}{5\,(1+\mu_\psi)^5}\right) \\
&- \frac{g^2 N_\phi}{95\pi}\left(\frac{50+\eta_\phi}{12\,(1+\mu_\phi)^4} + \frac{3}{(1+\mu_\phi)^5}\right)
\end{aligned} \tag{5.111}$$

$$\begin{aligned}
\dot{\lambda}_3 =& - \left(1 + \frac{\dot{g}}{2g}\right)\lambda_3 + \frac{g}{2\pi}\Bigg(\frac{12-\eta_c}{5} + \frac{8-\eta_h-4(6-\eta_h)\lambda_5}{4(1+\mu_h)^2} \\
&+ \frac{3(8-\eta_h)\lambda_4 - 16(6-\eta_h)\lambda_3\lambda_4}{3(1+\mu_h)^3} \\
&- \frac{11(12-\eta_h) - 72(10-\eta_h)\lambda_3 + 120(8-\eta_h)\lambda_3^2 - 80(6-\eta_h)\lambda_3^3}{120(1+\mu_h)^4}\Bigg) \\
&+ \frac{gN_\psi}{8\pi}\left(\frac{17(6-\eta_\psi) + (378-79\eta_\psi)\mu_\psi}{30\,(1+\mu_\psi)^2} - \frac{(7-\eta_\psi)\,(1+5\mu_\psi)}{7\,(1+\mu_\psi)^3}\right. \\
&\left. + \frac{(8-\eta_\psi)\left(1+4\mu_\psi-\mu_\psi^2\right)}{28\,(1+\mu_\psi)^4}\right) \\
&+ \frac{gN_\phi}{16\pi}\left(\frac{8-\eta_\phi-4(6-\eta_\phi)\mu_\phi}{6\,(1+\mu_\phi)^2} - \frac{10-\eta_\phi}{5\,(1+\mu_\phi)^3} + \frac{12-\eta_\phi}{30\,(1+\mu_\phi)^4}\right)
\end{aligned} \tag{5.112}$$

5.5.2 Masses

The flows for masses are obtained from the momentum independent parts of the 2-point functions. They read

$$\begin{aligned}\dot{\mu}_h =&(\eta_h-2)\mu_h+\frac{g}{\pi}\left(\frac{8(6-\eta_h)\lambda_4-3(8-\eta_h)}{12(1+\mu_h)^2}\right.\\&\left.+\frac{21(10-\eta_h)-120(8-\eta_h)\lambda_3+320(6-\eta_h)\lambda_3^2}{180(1+\mu_h)^3}-\frac{10-\eta_c}{5}\right)\\&+\frac{gN_\psi}{3\pi}\left(-\frac{5(6-\eta_\psi)+(90-19\eta_\psi)\mu_\psi}{10\,(1+\mu_\psi)^2}+\frac{(7-\eta_\psi)\,(1+5\mu_\psi)}{21\,(1+\mu_\psi)^3}\right)\\&+\frac{gN_\phi}{12\pi}\left(\frac{(6-\eta_\phi)\mu_\phi}{(1+\mu_\phi)^2}+\frac{10-\eta_\phi}{10\,(1+\mu_\phi)^3}\right)\end{aligned}\tag{5.113}$$

$$\begin{aligned}\dot{\mu}_\psi =&(2\eta_\psi-2)\mu_\psi+\frac{g\mu_\psi}{\pi}\left(\frac{6-\eta_h}{(1+\mu_h)^2}\right.\\&\left.-\frac{2408-349\eta_h+1120(6-\eta_h)\mu_\psi}{1120\,(1+\mu_\psi)\,(1+\mu_h)^2}-\frac{133-23\eta_\psi+28(24-5\eta_\psi)\mu_\psi}{140\,(1+\mu_\psi)^2\,(1+\mu_h)}\right)\end{aligned}\tag{5.114}$$

$$\begin{aligned}\dot{\mu}_\phi =&(\eta_\phi-2)\mu_\phi\\&+\frac{g\mu_\phi}{2\pi}\left(\frac{6-\eta_h}{(1+\mu_h)^2}-\frac{(6-\eta_h)\mu_\phi}{(1+\mu_h)^2\,(1+\mu_\phi)}-\frac{(6-\eta_\phi)\mu_\phi}{(1+\mu_h)\,(1+\mu_\phi)^2}\right)\end{aligned}\tag{5.115}$$

5.5.3 Anomalous Dimensions

We derive the anomalous dimension from the momentum dependent parts of the respective 2-point functions. Note that the equations for the anomalous dimensions have the structure given generically in (5.109).

$$\begin{aligned}\eta_h =&\frac{g}{4\pi}\left(\frac{6-\eta_h}{(1+\mu_h)^2}-\frac{6(8-\eta_h)+8(6-\eta_h)\lambda_3-36(4-\eta_h)\lambda_3^2}{9(1+\mu_h)^3}\right.\\&\left.+\frac{17+8\lambda_3(9\lambda_3-8)}{3(1+\mu_h)^4}-\eta_c\right)\\&+\frac{gN_\psi}{24\pi}\left(\frac{(5-\eta_\psi)\,(1-\mu_\psi)}{2\,(1+\mu_\psi)^3}+\frac{1+6\mu_\psi+\mu_\psi^2}{(1+\mu_\psi)^4}\right)\\&-\frac{32gN_\phi}{315\pi\,(1+\mu_\phi)^4}\end{aligned}\tag{5.116}$$

$$\eta_c =-\frac{g}{9\pi}\left(\frac{8-\eta_h}{(1+\mu_h)^2}+\frac{8-\eta_c}{1+\mu_h}\right)\tag{5.117}$$

$$\eta_\psi = \frac{g}{4\pi}\left(\frac{9(7-\eta_h)+12(10-\eta_h)\mu_\psi}{20\,(1+\mu_\psi)\,(1+\mu_h)^2} - \frac{9(6-\eta_h)}{8(1+\mu_h)^2} + \frac{6-\eta_\psi+(54-11\eta_\psi)\mu_\psi}{5\,(1+\mu_\psi)^2\,(1+\mu_h)}\right) \tag{5.118}$$

$$\eta_\phi = \frac{g\mu_\phi}{2\pi}\left(\frac{6-\eta_h}{(1+\mu_h)^2\,(1+\mu_\phi)} + \frac{6-\eta_\phi}{(1+\mu_h)\,(1+\mu_\phi)^2} - \frac{6\mu_\phi}{(1+\mu_h)^2\,(1+\mu_\phi)^2}\right) \tag{5.119}$$

5.5.4 Solving the Flow

The complete flow for $p = 0$ in the symmetric momentum configuration is solved numerically for given initial condition. First, however, we identify

$$\lambda_3 = \lambda_4 = \lambda_5\,, \tag{5.120}$$

in order to close the system. Now, the system of anomalous dimensions (5.116) is solved by means of the matrix equation (5.110). The solution is substituted back into (5.113) and (5.111). The complete system of flowing parameters defined this way is given by

$$(g, \lambda_3, \mu_h, \mu_\psi, \mu_\phi) \qquad \text{(complete set of flowing parameters)}\,. \tag{5.121}$$

In order to study the UV-behavior of the theory, we solve the fixed point equation

$$\boldsymbol{\beta} = (\dot{g}, \dot{\lambda}_3, \dot{\mu}_h, \dot{\mu}_\psi, \mu_\phi)^{\mathrm{T}} = 0\,. \tag{5.122}$$

We solve this equation to obtain fixed point coordinates $P^* = (g^*, \lambda_3^*, \mu_h^*, \mu_\psi^*, \mu_\phi^*)$. Now, the fixed point is analysed by means of a linear stability analysis which leads to the critical exponents $(\theta_1, \ldots, \theta_6)$. This way, we obtain global information about the UV and IR behavior without solving the flow equation explicitly.

Masses of the Matter fields

Throughout most of this work we will set the masses of the matter fields to zero. This leads to a major simplification of the flow since we lose two flowing parameters in (5.122). It is justified by the observation that $\mu_\psi = 0$ and $\mu_\phi = 0$ are fixed points of the flow.

6 Pure Gravity Setup

Before considering the complete system of quantum gravity with matter we first discuss some important features of the pure gravity system. To this end we, investigate the locality in momentum space of the flow for the graviton 2- and 3-point functions. Furthermore, we compare the different momentum configurations, namely asymmetric and symmetric configuration, for the flow of Newton's coupling g. We also determine UV-fixed points for the pure gravity system.

Here and in the following, all momenta p are given in units of the cutoff k. More precisely, we make the redefinition

$$p \to p = \frac{p}{k}\,. \tag{6.1}$$

6.1 Locality of the Flow in Momentum Space

An important property that we observe for the flow of the graviton 2- and 3-point functions is locality in momentum space. In general, we require for the flow of a general observable $\mathcal{O}$ that is of lower asymptotic order in the field momenta than the observable itself. Hence, for the limit $p \to \infty$ we require that the quotient of $\dot{\mathcal{O}}$ and $\mathcal{O}$ goes to zero. We write

$$\lim_{p\to\infty} \frac{\dot{\mathcal{O}}(p)}{\mathcal{O}(p)} = 0\,. \tag{6.2}$$

This relation suggests that the UV-properties of the theory do not alter its IR flow. As was discussed in section 3.3 this property is particularly important in quantum gravity. There, the flow towards the UV and, thus, beyond the initial regularization scale of the path integral is only possible because of the locality of the flow. Otherwise, the theory would pick up a spurious dependence on the regularization scale even in the deep UV which we regard as unphysical. For our system we require locality on the basis of the graviton n-point functions. Consequently,

$$\lim_{p\to\infty} \frac{\Gamma_k^{(n)}(p)}{\Gamma_k^{(n)}(p)} = 0. \tag{6.3}$$

In particular, for this relation to hold, all external field momenta involved need to go to infinity. This property is trivially fulfilled for theories with momentum independent vertices. For Yang-Mills-theories the couplings are only linear in the momenta. Thus, the propagators suppress the momentum dependence of the vertices. For gravity, the vertices are quadratic in field momenta. Therefore, the n-point function

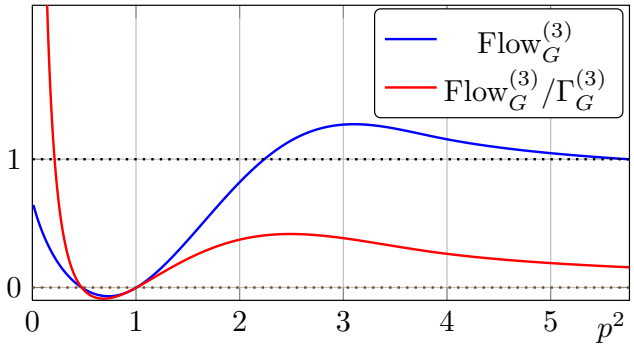

Figure 6.1: The flow of the graviton three-point function for values of λ_3, g and μ_h as a function of the dimension field momenta p (blue curve) which goes to a constant for $p \gg 1$. The red curve shows the ratio of the flow and three point function itself. It decays rapidly which suggests locality in momentum space

in gravity scales with p^2. This requires for the flow on the graviton n-point function to approach a constant as $p \to \infty$. In this section we will to show that the graviton 3-point function exhibits this asymptotic behaviour. For the 2-point function, it was already observed in [27]. Note, that the behaviour (6.2) is non-trivial since it does not hold for all theories with interactions quadratic in the momenta. Therefore, we account this behaviour for the diffeomorphism invariance of the theory. Furthermore, in case of the flow for the graviton n- point function (6.2) ensures that the flow of the respective couplings involved will also be local in momentum space. Consider the flow of the general n-point function as obtained from the flow equation

$$\dot{\Gamma}_k^{(n)} = \text{Flow}(\Gamma_k^{(n)}), \tag{6.4}$$

where we suppress all indices. The function $\text{Flow}(\Gamma_k^{(n)})$ represents the diagrammatic contributions originating from the right hand side of the flow equation. For example, in case of the 2-point function $\text{Flow}(\Gamma_k^{(hh)})$ is given by

$$\text{Flow}(\Gamma_k^{(hh)}) = -\frac{1}{2}$$ 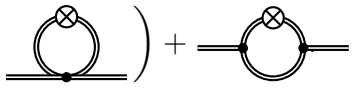 $$+$$ (6.5)

Now, in order to extract a general dimensionful coupling $\bar{w}_n$ from equation (6.4) we apply a suitable projection represented by Π_w to both sides of (6.4).

$$\dot{\bar{w}}_n(\Pi_w \circ \dot{\Gamma}_k^{(n)}(1)) = \Pi_w \circ \text{Flow}(\Gamma_k^{(n)}) \tag{6.6}$$

where we used

$$\Pi_w \circ \dot{\Gamma}_k^{(n)}(\bar{w}) = \dot{\bar{w}} \left(\Pi_w \circ \Gamma_k^{(n)}(1) \right) . \tag{6.7}$$

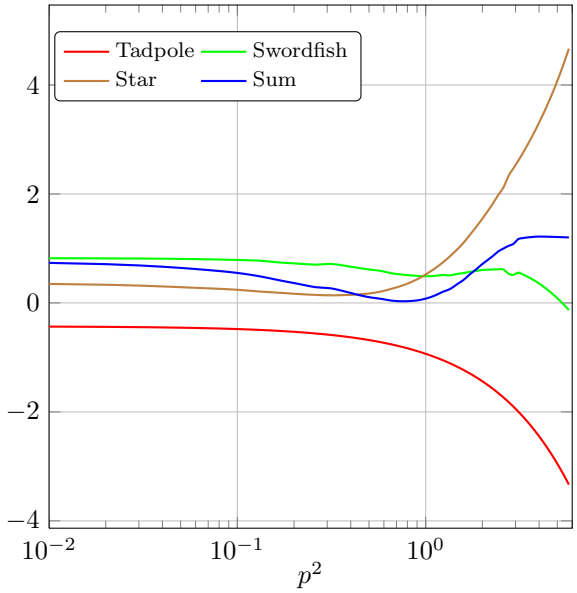

Figure 6.2: Contributions of the three relevant diagrams contributing to the flow of the graviton 3-point function. For large $p \gg 1$ the sum of the diagrams approaches a constant.

In our truncation, we can convince ourselves that $\Gamma_k^{(n)}(1)$ will asymptotically scales like the n-point function itself. In the limit of large momenta, we have

$$\lim_{p\to\infty} \dot{\Gamma}_k^{(n)}(1) = \mathcal{C} \lim_{p\to\infty} \Gamma_k^{(n)}(\bar{w})\,, \tag{6.8}$$

with a undefined constant $\mathcal{C}$. Together with (6.2), this implies

$$\lim_{p\to\infty} \dot{\bar{w}}(p) = 0\,. \tag{6.9}$$

Hence, due to (6.2) the flow of $\bar{w}$ is local in momentum space. This implies that the integration of modes at scale k has an impact only on the coupling at scales in a local neighborhood around $p \approx 1$ and below. This is statement lies at the heart of the Wilsonian idea of integrating out momentum shells.

6.2 Locality of the Graviton 3-point Function

The locality in momentum space for the graviton 2-point function was shown in [27]. What we address here the locality in momentum space of the flow for the 3-point function $\mathrm{Flow}(\Gamma_k^{(hhh)})$. To this end, we consider the projection of $\mathrm{Flow}(\Gamma_k^{(hhh)})$ as obtained from the contraction with Π_G. We write

$$\mathrm{Flow}_G(\Gamma_k^{(hhh)}) = \mathrm{Tr}\left(\Pi_G \circ \mathrm{Flow}(\Gamma_k^{(hhh)})\right) \tag{6.10}$$

We consider the three diagrams that contribute to the flow of Γ_k^{hhh}. These are

$$\mathrm{Flow}(\Gamma_k^{(hhh)}) = -\frac{1}{2}$$ 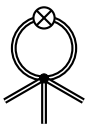 $$+ 3$$ 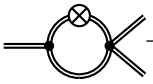 $$- 3$$ 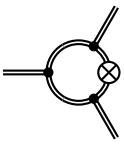 $$+ 6$$ 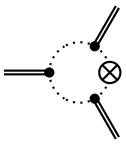 $$. \qquad (6.11)$$

6.2.1 Symmetric Momentum Configuration

In order to simplify the presentation, we consider here only the symmetric momentum configuration introduced in 5.3.2. However, the property (6.3) also holds for arbitrary momentum configurations as long as all momenta involved go to infinity. The asymptotic momentum scaling of the diagrams in (6.11) is given by

$$-\frac{1}{2}$$ 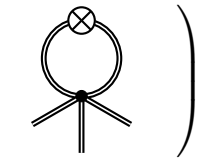 $$\overset{p\gg 1}{\approx} -752 g^2\pi^2 \int_0^1 \frac{(2+\eta_h(-1+q^2))}{19\,(1+\mu_h)^2} q^3 dq \times p^2 \qquad (6.12a)$$

$$3$$ 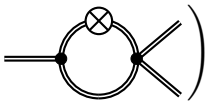 $$\overset{p\gg 1}{\approx} 1232 g^2\pi^2 \int_0^1 \frac{(2+\eta_h(-1+q^2))}{19\,(1+\mu_h)^2} q^3 dq \times p^2 \qquad (6.12b)$$

$$-3$$ 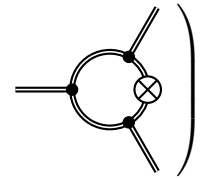 $$\overset{p\gg 1}{\approx} -480 g^2\pi^2 \int_0^1 \frac{(2+\eta_h(-1+q^2))}{19\,(1+\mu_h)^2} q^3 dq \times p^2 \qquad (6.12c)$$

Obviously, the three terms in (6.12) cancel, even before having integrated out q. Hence, after averaging over the solid angle the asymptotic scaling proportional to p^2 vanishes. Interestingly, all diagrams that contribute to the flow of $\Gamma_k^{(3)}$ minus the ghost contribution are involved in the cancellation. Figure 6.2 shows the cancellation of the three contributions as a function of p. As long as all momenta go to infinity the flow of the graviton three point function assumes a constant in the limit of large momenta. Consequently, for all momentum configurations (6.3) will be satisfied. For the dimensionless Newton constant g, this suggests that its flow decays rapidly with the field momenta. Thus, only fluctuations of the order of $p = 1$ and below will contribute to its flow.

6.2.2 Asymmetric Momentum Configuration

For a momentum configuration where one of the momenta is zero, locality of the flow of the three-point function does not hold. Hence, $\mathrm{Flow}_G(\Gamma_k^{(hhh)})$ scales with p^2 for large momenta and diverges asymptotically. To understand this behaviour we note that setting one of the momenta to zero is inherently different than any configuration in which all momenta go to infinity, regardless the ratio of momenta or the angles involved. The limit of one graviton momentum equal zero is comparable

to the emittance of soft (photon) bremsstrahlung in QED. Consider the process of an electron radiating a photon in an eternal field. In the limit of vanishing photon energy the cross section for this process diverges and we observe an infrared singularity. Stressing this analogy the divergence of the flow of the graviton three-point function is regarded as an infrared divergence due to the radiation of soft graviton bremsstrahlung. Thus, the limit of infinite momenta in the asymmetric momentum configuration is not associated with ultraviolet physics. Therefore, we do not obtain information about the ultraviolet behaviour of the theory from the asymmetric momentum configuration. Therefore, the flow for g obtained from the asymmetric momentum configuration is not local in momentum space.

We have shown that locality in momentum space holds for the graviton 3-point function. Similarly, it also holds for the graviton two-point function which was shown in [27]. Conversely, locality in momentum space is not fulfilled for momentum configurations where one of the external graviton momenta is zero. This configuration however, was identified as reflecting an inherently infrared process which makes it inappropriate for the study of ultraviolet properties.

We argue that by this result, the symptomatic momentum configuration is not trustworthy for ultraviolet studies. We will see in the sequel, that in fact the UV fixed-point structures of the different configurations vary significantly.

7 Flow of the Gravity-Matter System

We now turn to the fixed point analysis of the gravity-matter system. In the first parts we only consider the limit $p = 0$. It may seem contra-intuitive to study the UV behaviour of a theory in a limit where all external momenta go to zero. In fact, the approximation $p = 1$ considered later will lead to more consistent results. However, the $p = 0$ allows to formulate the flow in terms of the analytic equations (5.111), (5.113) and (5.116). This makes a systematic analysis much more simple. We start by considering a simple but yet physically relevant subsystem and restrict ourselves to the pure-gravitiy. Then, we successively introduce matter fields and eventually consider the properties of the complete system.

7.1 Simplified Pure-Gravity System

For a first and simple analysis of the pure-gravity system for $p = 0$ we will make the identification

$$\lambda_3 = -\frac{1}{2}\mu_h \qquad \text{(simplified pure-gravity system)}, \tag{7.1}$$

which, since $\mu_h = -2\lambda_2$, amounts to the identification

$$\lambda_2 = \lambda_3 = \lambda_4 = \dots . \tag{7.2}$$

In this case, the truncation basically reduces to an improved Einstein-Hilbert truncation which was also studied in [24–27]. We also include the anomalous dimensions η_h and η_c into the analysis. The identification (7.1) reduces the number of flowing parameter to two, namely

$$(g, \mu_h) \qquad \text{(set of flowing parameters the simplified system)}\,. \tag{7.3}$$

These two couplings define a two dimensional parameter space which can be represented by means of a two-dimensional phase diagram. Figure 7.1 depicts the phase

FP-Number	g^*	μ_h^*	$\theta_{1,2}$
1	0	0	$\{-2, 2\}$
2	0.943	-0.707	$\{-26.4 \pm 54.1i\}$

Table 7.1: Fixed points for the gravity system with identified λ_3 obtained from the symmetric momentum configuration. FP 2 is UV-attractive whereas the Gaussian fixed point (FP1) has one UV-unstable direction.

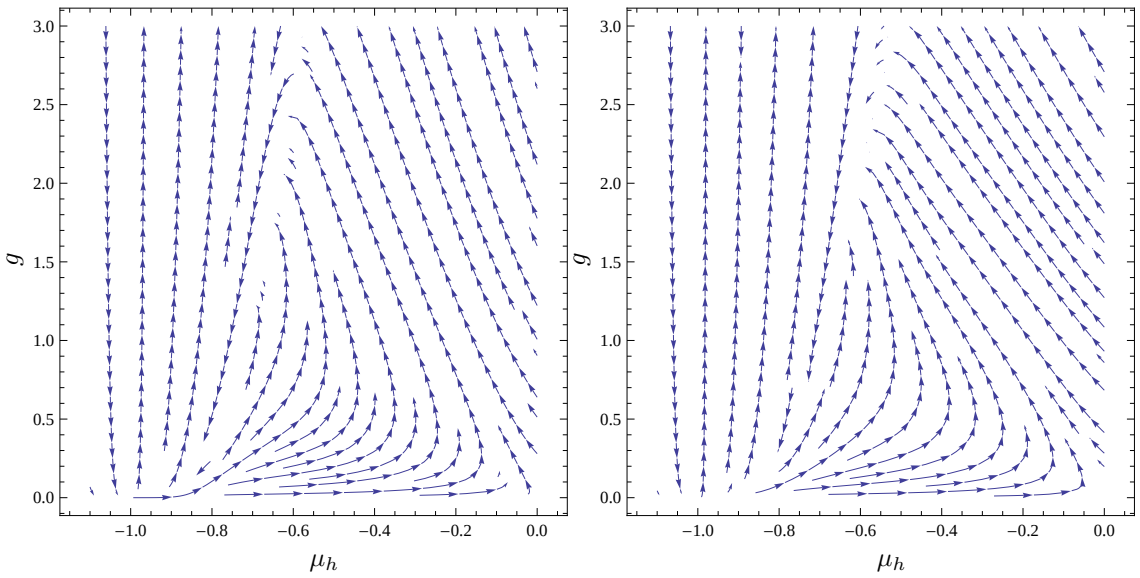

Figure 7.1: Phase diagrams of a truncated pure gravity systems. The left panel depicts the flow obtained from the asymmetric momentum configuration at $p = 0$. In the right panel, the symmetric momentum configuration for $p = 0$ is shown. Although both phase diagrams look similar, only the symmetric momentum configuration admits a non-Gaussian fixed point.

diagrams for (g, μ_h) for the two different momentum configurations. In the left panel the phase diagram for the asymmetric momentum configuration is shown. The right panel depicts the phase diagram in case of the symmetric momentum configuration. Interestingly, although both phase diagrams look very similar at first sight, only the symmetric momentum configuration (right panel) admits a non-Gaussian fixed point. We suspect, that in case of the asymmetric momentum configuration a meant-to-be non-Gaussian fixed point is hidden behind a line of singularities of the β-function. In Table 7.1 the fixed points and their critical exponents for the symmetric system is given. The fixed point's critical exponents are given by a complex conjugate pair with negative real parts. They are much bigger that 1 which can be interpreted as an incompleteness of the truncation [17]. We conjecture that the inclusion of the higher order coupling λ_3 lowers these eigenvalues by an order of magnitude.

In this simple study, we found a non-Gaussian fixed point for the simplified pure-gravity system in the symmetric momentum configuration with the identification $\lambda_3 = -\frac{1}{2}\mu_h$. Surprisingly, the corresponding flow for the asymmetric momentum configuration does not admit a non-Gaussian fixed point. In the previous section we already discussed the non-locality of the flow of g for this momentum configuration. This property was accounted for the infrared-nature of the corresponding scattering process. Thus, together with non-existence of a UV-fixed point for the pure-gravity system we declare the asymmetric momentum configuration as not appropriate for UV studies of quantum gravity. Therefore, we drop the it in the sequel and consider

only the flow of g from the symmetric momentum configuration.

7.2 Simplified Gravity-Matter System

In this section, we couple matter to the simplified pure-gravity system discussed in the previous section. In this study we consider N_f fermionic and N_s bosonic fields which are non-interacting and massless. By successively increasing the number of matter fields we construct an analytic continuation of the fixed point of the simplified pure-gravity system discussed above. This way, we study the impact of matter on the UV behaviour of quantum gravity.

The inclusion of matter amounts to adding matter loop contributions to the flow of the graviton 2-and 3-point functions functions. Furthermore, we introduce anomalous dimensions for the respective matter fields. The extra contributions to the graviton 2- and 3-point functions are directly proportional to the number of the respective matter fields

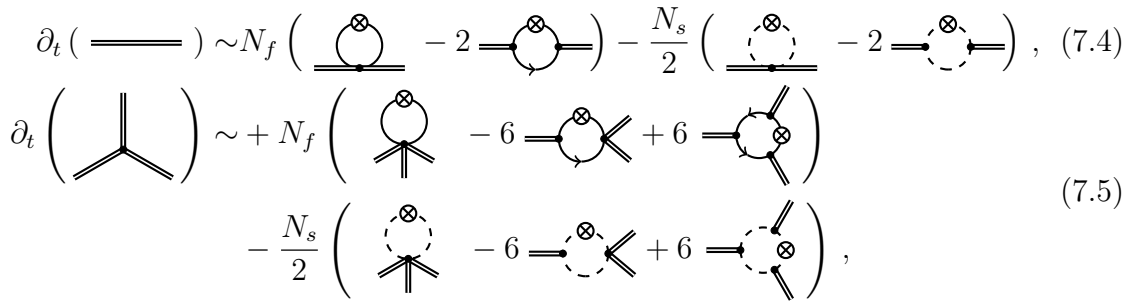

(7.4)

(7.5)

leading to the matter contributions to the flow equations in (5.111), (5.113) and (5.116). On the other hand, there are graviton-loop contributions to the matter two-point functions which contribute the matter anomalous dimensions. All of these interactions result in a complex interacting system even for this comparably simple model.

7.2.1 One-Loop β-Functions

The contributions of the diagrams (7.4) lead to complicated and non-perturbative expressions, once the anomalous dimensions are taken into account. However, in order to obtain an effective one-loop result, we set all anomalous dimensions to zero. If we assume, that the anomalous dimensions remain small, the resulting flow equations give a good approximation of the complete system of β-functions. Furthermore, it allows to easily compare the results with other renormalisation group calculations. In our approach, the one-loop contributions from the matter fields are

given by

$$\beta_g \sim \quad 2g + g^2\left(-\frac{3599}{11400\pi}N_f - \frac{43}{570\pi}N_s\right) \quad \approx g^2\left(-0.316N_f - 0.0754N_s\right)\,, \quad (7.6a)$$

$$\beta_{\mu_h} \sim \quad -2\mu_h + g\left(-\frac{8}{9\pi}N_f + \frac{1}{12\pi}N_s\right) \qquad \approx g\left(-0.283N_f + 0.0265N_s\right)\,. \quad (7.6b)$$

Obviously, in both equations fermions have a stronger effect on the β-functions than scalars. In (7.6a) both contributions have the same sign but differ by a factor of four. In (7.6b), however, the contributions even have opposite signs and differ by a factor of about ten. Since the canonical running term in β_g is positive, on one-loop level, fermions and scalar are in favor of a fixed point of the flow of g. For β_{μ_h}, the canonical running is negative. Matter in (7.6b) can both disfavor and favor a fixed point, depending on the sign of μ_h. For the fixed point we are considering in the simplfied-pure gravity setup we have $\mu_h^* < 0$, see Table 7.1. It follows that fermions favor this particular fixed point whereas scalars disfavor it. Furthermore, the existence and stability of fixed points of the simplified gravity-matter system is found to be very sensitive to variations of the β-function for μ_h rather than variations of β_g. From this naïve one-loop analysis we expect that fermions and scalars fields have very different impacts on the non-Gaussian UV fixed point of quantum gravity.

The one-loop results in (7.6) are compared with one-loop results from ordinary renormalisation group theory. There, the β-function for Newton's constant reads [60, 61]

$$\beta_g \sim g^2\left(\frac{1}{3\pi}N_f + \frac{1}{6\pi}N_s\right) \approx 0.0531N_f + 0.106N_s\,. \quad (7.7)$$

Surprisingly, both contributions have opposite signs compared to our findings. The flow for g and $\mu_h = -2\lambda_2$ was also calculated in [19, 20]. While the one-loop β-function for g in these works agree with (7.7) the one-loop flow for μ_h is given by

$$\beta_{\mu_h} \sim -2\mu_h + g\left(\frac{24}{\pi}N_f - \frac{6}{\pi}N_s + \mu\left(\frac{4}{\pi}N_f + \frac{2}{\pi}N_s\right)\right) \quad (7.8)$$

If we again assume fixed point values in the range $-1 < \mu < 0$, the fermion and scalar fields in (7.7) have exactly the opposite effect compared to what we find in (7.6). In (7.8), scalars are in favor of a fixed point for the flow of μ whereas fermions tend to disfavor it. The reason why the signs are different is unclear. The results from [19, 20] are based on background field flows where one needs to identify the background and the fluctuating fields. This can pose severe problems which is known from pathological examples in QCD [62, 63]. Also, the results in [19, 20] are evaluated in a curved (maximally symmetric) background. Different expansion points of the curvature R could lead to different signs for the β-functions.

We discussed the important one-loop approximation of our theory. Surprisingly, it does not agree with what has been found in the literature. On one-loop level, fermions stabilize the UV fixed point of quantum gravity, whereas scalar fields destabilize it in our approach. In the sequel, we study whether this behaviour persists beyond one loop.

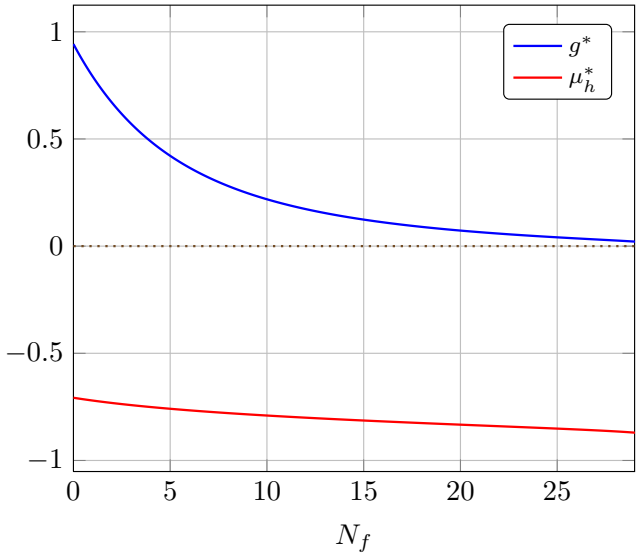

Figure 7.2: The fixed point values for the quantum gravity system in the presence of a different number of fermion fields. An increasing number of fermions lowers the fixed point value g^*. The fixed point value μ_h^* is driven towards the pole of the propagator at $\mu_h = -1$.

7.2.2 Beyond One-Loop

In this section we discuss the whole non-perturbative impact that matter fields have on the simplified gravity system. To this end, we to discuss the impact of fermions and scalar fields separately.

Fermion Fields

First, we study the effect of fermions on the non-Gaussian fixed point of the simplified gravity system. Thus, we successively increase the number of fermions by increasing the parameter N_f in (7.4). Clearly, the variation of one of the terms in the flow equation perturbs the non-Gaussian fixed point. With increasing N_f we follow the fixed point value of the system through parameter space. In Figure 7.2 the fixed point values $g*$ and μ_h^* are depicted as a function of the number of fermions N_f. After the inclusion of an arbitrary number of fermion fields, the fixed point persist. However, an increasing fermion number leads to a decrease of both fixed point values g^* and μ_h^*. Thus, g^* approaches zero with increasing N_f whereas μ_h^* is driven towards $\mu_h = -1$. There, the flow equations (5.111) exhibit a singularity because of the pole of the graviton propagator. In a detailed scaling analysis where the influence of higher order vertices in the infrared was modeled, an IR fixed point was found for a very similar system in [27] at

$$(g_{\mathrm{IR}}^* = 0, \mu_{\mathrm{IR}}^* = -1) \qquad (\text{IR fixed point})\,. \tag{7.9}$$

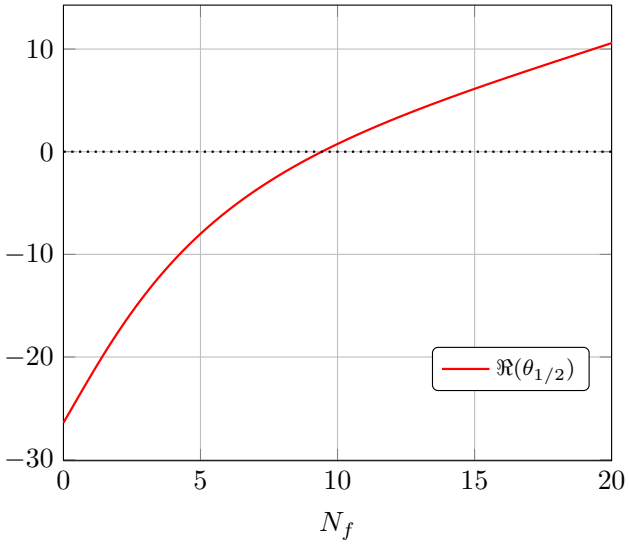

Figure 7.3: The real parts of the complex conjugate pair of eigenvalues for the simplified gravity-matter system. The fixed point is attractive without fermions but loses its attractivity and becomes repulsive at $N_f \approx 10$.

For the present system we have not made such an analysis. For now, we assume that the fixed point exists which is supported by the phase diagram in Figure 7.1 and by the numerical calculations of trajectories. Hence, the inclusion of fermions into the system drives the non-Gaussian UV fixed point towards the infrared fixed point. This suggests that fermions have a shielding effect on gravity in the UV. They weaken the coupling in the UV and push the system towards the IR fixed point.

Interestingly, the inclusion of fermions not only changes the fixed point values (g^*, μ_h^*) but also has a strong influence on the attractivity at the fixed point, i.e., its critical exponents. In Figure 7.3 the real parts of the two critical exponents are shown. The exponents appear in a complex conjugate pair. Therefore they have identical real parts. The plot suggests that at a fermion number of about $N_f = 10$ the ultraviolet fixed point loses its attractivity and becomes repulsive. If we take this limit seriously, it suggests that more that 10 fermions are not compatible with the asymptotic safety scenario. A similar limit has been observed in [20] where at about $N_f \approx 10$ the truncation breaks down and the fixed point vanishes.

We discussed the inclusion of fermions into the simplified gravity system with $\lambda_3 = -\frac{1}{2}\mu_h$. We found that the fixed point persists under the inclusion of an arbitrary number of fermions. Fermions weaken gravity in the UV by moving the fixed point to lower values of g. This is consistent with our finding on the basis of the effective one-loop approximation in section 7.2.1. Furthermore, fermion fields drive the UV-physics of the system towards the IR. This is interpreted as fermionic shielding of gravity in the UV.

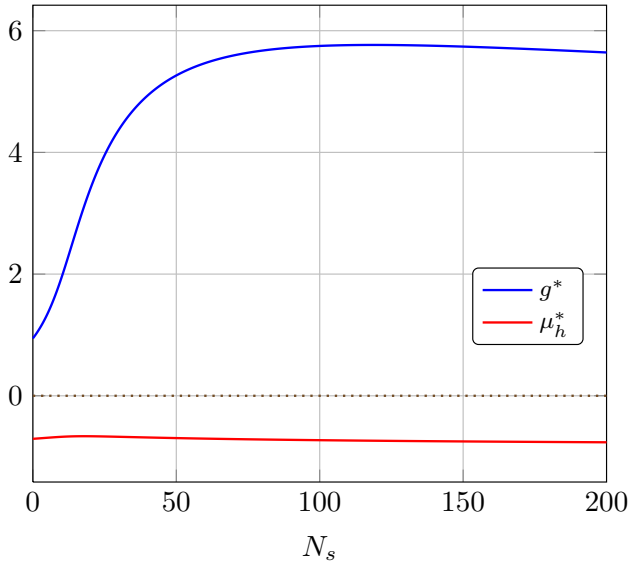

Figure 7.4: The fixed point values for the quantum gravity system in the presence of a different number of scalar fields. Scalars tend to increase the gravitational coupling. The fixed point value for μ_h is not affected by the number of scalar fields.

7.2.3 Scalar Fields

In this section we successively increase the number of scalar fields N_s. Doing so we observe impact of N_s on the position and the properties of the non-Gaussian fixed point in the simplified gravity-matter system. In Figure 7.4 the fixed point values of the simplified gravity-matter system is shown under the inclusion of a different N_s fields. We observe that scalar fields drive the non-Gaussian fixed point towards higher values for Newton's coupling g. However, the increase of g^* saturates at $N_s \approx 130$ where it slowly starts decreasing again. At the same time, the fixed point value for μ_h remains almost constant even for a large N_s. Thus, as we discussed in section 7.2.1, scalar fields disfavor a non-Gaussian fixed point. However, the system remains stable even for a large number of scalar fields. The extra-contribution in disfavor of the fixed point are balanced by the graviton parts of β_g and β_{μ_h}. We can confirm that the effect of scalar fields is in general is much less pronounced than that of scalar fields. This is in agreement with the effective one loop result. It is true most obviously for μ_h^* which remains stable even under the inclusion of 200 scalar fields.

In Figure 7.5 the critical exponents $\theta_{1,2}$ are plotted as a function of the number of scalar fields. They are always negative, i.e., the fixed point is always attractive. At $N_s \approx 17$ the complex conjugate pair of eigenvalues turns into two separate real eigenvalues. One of them (θ_1 in the Figure 7.5) runs to very large negative values for $N_s > 17$. Large critical exponents were also observed in pure-gravity systems [17, 64]. They indicate a loss of reliability for the truncation in this region. This

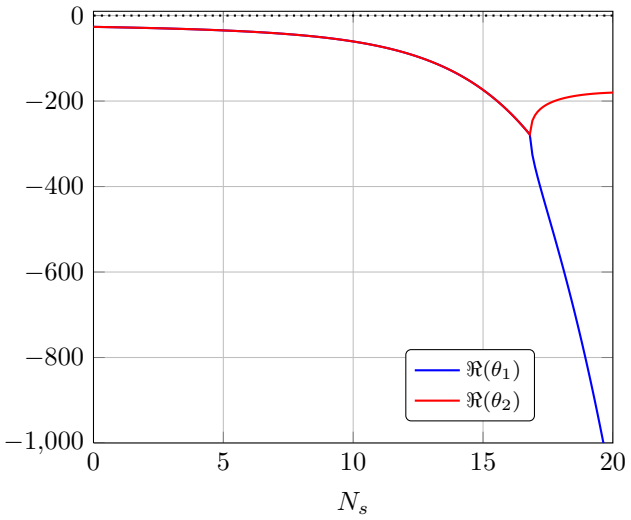

Figure 7.5: The critical exponents for the simplified quantum gravity system in the presence of a varying number scalar fields. In this picture, scalar fields increase the stability of the fixed point. At $N_f \approx 17$ the complex conjugate pair of eigenvalues bifurcates into two real negative critical exponents.

finding indicates that the simplified quantum gravity model is not sufficient to cover the whole dynamics of the gravity-matter system. We discuss this in more detail in the next section.

In sum, scalar fields have a very different effect on the simplified gravity-matter system than fermions. Scalars drive the non-Gaussian fixed point to larger values, thus, they make gravity stronger coupled in the UV. This is accounted for the fixed-point disfavoring property of scalar fields which we observed in the effective one-loop analysis in section 7.2.1. Still, the fixed point of the simplified gravity-matter system admits an arbitrary number of scalar fields N_s. Thus, the gravity contributions to the β-functions stabilize the system and prevent g^* from running towards infinity. The linear stability of the fixed point is increased by scalar fields. However, one of the critical exponents is driven towards large negative values for increasing N_s. This is interpreted as an insufficiency of the truncation.

7.2.4 Insufficiencies of the Simplified Gravity-Matter System

In the previous section we observed the running of one of he critical exponents θ to large negative values with increasing N_s.This indicates that the simplified gravity-matter system is an insufficient truncation to study the complex interaction of gravity and matter. A problem that we have ignored until now is that even without the inclusion of matter the simplified gravity system with the identification $\lambda_3 = -\frac{1}{2}\mu_h$ exhibits large graviton anomalous dimensions η_h. In section 4.3.2 we formulated an upper bound of 2 for the anomalous dimensions of bosons. However, in the simplified gravity system we have $\eta_h^* \approx 3 > 2$ at the non-Gaussian fixed point. This remains

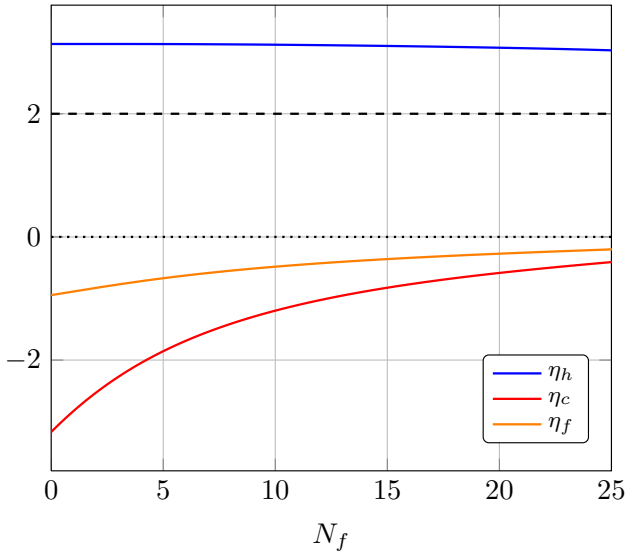

Figure 7.6: Anomalous dimensions at the non-Gaussian fixed point for the inclusion of a different number of fermion fields N_f. Over the whole range, the fermion anomalous dimension remains above 2 which we consider as a critical number for bosons. All other anomalous dimensions quickly go to zero for increasing fermion number.

true for arbitrary N_f and N_s. In Figure 7.6 the relevant anomalous dimensions at the fixed point are shown as a function of the fermion number.

The situation is even more alarming for the inclusion of scalar fields. As is shown in Figure 7.7 not only the graviton anomalous dimension at the non-Gaussian fixed point η_h^* stays above the critical value of 2. Furthermore, the ghost anomalous dimension η_c^* is driven towards large negative values. Together with the large negative value for the critical exponent we find that we lose control over the system upon including matter fields into the simplified gravity system.

The simplified gravity model with matter has questionably high anomalous dimension without matter already. This gets worse for the inclusion of scalar fields $N_s \neq 0$. Although in all cases, the non-Gaussian fixed point persists, it loses its attractivity for $N_f \approx 10$ and the critical exponents as well as the anomalous dimensions are driven towards large negative values for $N_s \approx 17$. We assume that this effect is nothing physical but rather an artifact of the insufficient truncation. The inclusion of higher order vertices such as the inclusion of an independent λ_3 is expected to improve the results considerably.

7.3 Complete Pure-Gravity System

We now turn to the complete full gravity system without and with the inclusion of matter. We refer to the complete gravity system as the one where all parame-

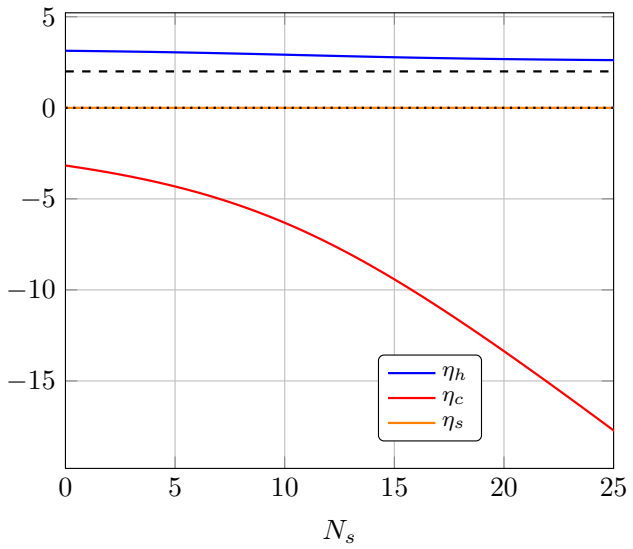

Figure 7.7: Anomalous dimensions at the non-Gaussian fixed point for the relevant fields. The ghost anomalous dimension η_c quickly runs to very large negative values for $N_s > 17$ whereas the graviton anomalous dimension stays above 2 over the whole range.

ters including λ_3 are flowing quantities. As we have seen in the previous chapters, the flow of g as obtained from asymmetric momentum configuration suffers from inconsistencies such as non-locality of the flow in momentum space and the absence of the non-Gaussian fixed point in the corresponding simplified system. Therefore, we again restrict ourselves to the flow obtained from the symmetric momentum configuration.

7.3.1 Flow Equations at $p = 0$

First, we consider the flow of the complete pure gravity system in the limit $p = 0$. Using Litim's cutoff we obtain the flow equations given by (5.111), (5.113) and (5.116) with zero fermion and zero scalar fields. Surprisingly, these equations do not admit an attractive non-Gaussian fixed point for $\eta_h \neq 0$ and $\eta_c \neq 0$. There are two possible reasons for that

1. The non-Gaussian fixed point which we found in the simplified gravity system is merely an artifact of the insufficient truncation and there really is no fixed point in the complete system.

2. The extraction of the flow of g and that of η_h by taking derivatives of the graviton 3- and 2-point functions is not an accurate reflection real momentum dependence of the flow in the region of $0 < p < 1$. Thus, the non-existence of the non-Gaussian fixed point for the projection $p = 0$ is an insufficiency of

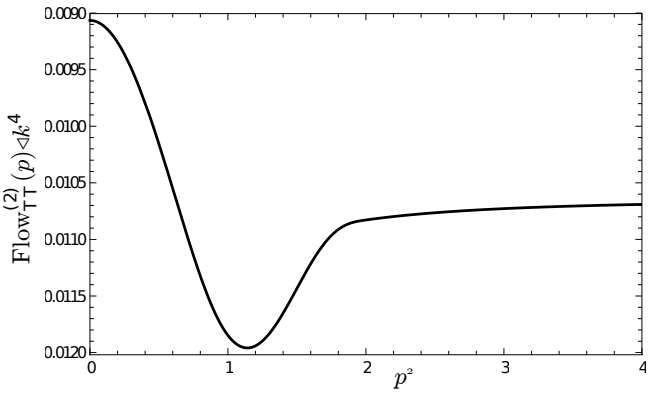

Figure 7.8: Schematic momentum dependence of the graviton 2-point function. The flow has a minimum at around $p = 1$ and is flat at $p = 0$. Hence, the second derivative with respect to p of the curve at $p = 0$ and $p = 1$ will give results of different signs. Taken from [25].

the truncation. In this case, an improvement of the p-projection for $\dot{g}$ and η_h is required.

The non-existence of a non-Gaussian fixed point would pose severe problems since is in contradiction to all reported findings regarding the asymptotic safe scenario of quantum gravity. Thus, we have to consider the exact momentum dependence of $\mathrm{Flow}(\Gamma_k^{hh})$ and $\mathrm{Flow}(\Gamma_k^{hhh})$ to decide whether the chosen momentum approximation scheme is reliable.

7.3.2 Improved Momentum Projection Scheme

The insufficiency of the second derivative with respect to p at $p = 0$ for the flow of the graviton 2-point function has already been reported in [25, 27]. In Figure 7.9 the momentum dependence of the flow of the graviton 2-point function is given. It exhibits a minimum at $p = 1$ and a maximum at $p = 0$. Thus, the momentum dependence in the region $0 < p < 1$ is not accurately modeled by a parabola centered at $p = 0$. Hence, for the extraction of η_h from the momentum dependent part of the graviton 2-point it is necessary to go beyond a second derivative approximation of the $\mathrm{Flow}(\Gamma_k^{(hh)})$ at $p = 0$. In [27] this problem was solved by extracting $\eta_h(p)$ by the finite difference:

$$\eta_h(p) = -\frac{\frac{\partial_t \Gamma_k^{(hh)}(p^2)}{Z_h(p^2)} - \frac{\partial_t \Gamma_k^{(hh)}(-\mu_h)}{Z_h(-\mu_h)}}{(p^2 + \mu_h)} \tag{7.10}$$

which can be evaluated numerically. The corresponding equation for the ghost anomalous dimension $\eta_c(p)$ reads

$$\eta_c(p) = -\frac{\partial_t \Gamma_k^{(cc)}(p^2)}{Z_c(p) p^2}. \tag{7.11}$$

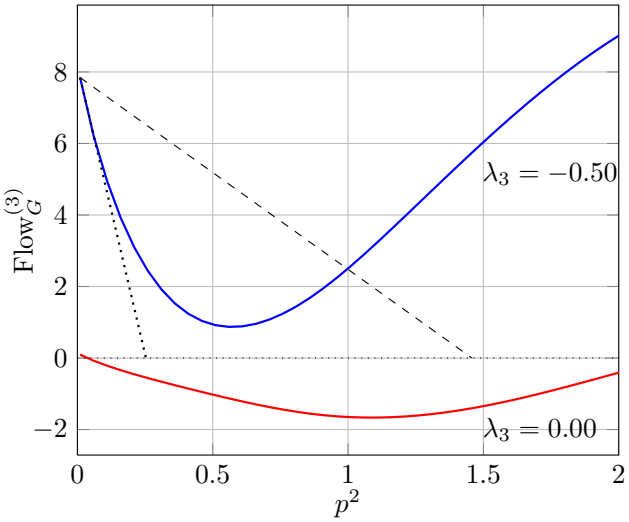

Figure 7.9: Momentum dependence of the graviton 3-point function for different values of λ_3 and $\mu_h = -0.5$. The momentum dependence varies significantly with varying λ_3. The dotted and dashed lines represent the different approximation procedures of taking the derivative with respect to p^2 at $p^2 = 0$ and a finite difference between $p^2 = 1$ and $p^2 = 0$, respectively.

Since we know that the integrants in the loop integrals are always peaked around $p = 1$ we approximate $\eta_h(p) = \eta_h(k)$, see section 4.3.2. Now we can move the anomalous dimensions out of the integrals. All calculations are performed numerically for a grid of the parameter μ_h.

For the graviton 3-point function, the picture is similar. Derivatives at $p = 0$ do not reflect the momentum dependence of the flow of the 3-point function in the physical region $0 < p < 1$. In Figure 7.9 the momentum dependence is shown for $\mu_h = -0.5$ and two different values of λ_3. Apparently, for different values of λ_3 the momentum decencies are very different. While for $\lambda_3 = 0$ the derivative with respect to p^2 at $p^2 = 0$ is an accurate approximation, for $\lambda_3 = -0.5$ it is certainly not. Modeling the momentum dependence of $\mathrm{Flow}(\Gamma_k^{(hhh)})$ with a derivative at $p^2 = 0$ is represented by the dotted line in Figure 7.9. The dashed line represents the modeling of the flow by means of a finite difference between the flow at $p^2 = 1$ and $p^2 = 0$. For both λ_3 the finite difference is a better approximation. Using such a finite difference we have to find a formula for the extraction of the flow of $\dot{g}$. We choose the symmetric momentum configuration and evaluate (5.85) at $p = 1$ and $p = 0$ and subtract both formulae from one another. We keep the graviton anomalous dimensions momentum dependent as suggested by (7.10). Rearranging

FP-Number	g^*	λ_3^*	μ_h^*		$\theta_{1,2,3}$
1	0	0	0	$\{-2, 2, 2\}$	
2	0.98	0.29	-0.33	$\{-4.0 \pm 8.7i, -3.3\}$	
3	0.96	-0.024	-0.35	$\{-2.1 \pm 2.4i, 5.8\}$	

Table 7.2: Fixed point values of the complete pure gravity system within the one-loop approximation. The system with vanishing anomalous dimensions admits two non-trivial fixed point. FP 2 is fully UV attractive whereas FP exhibits one UV repulsive direction.

the terms we get for the flow of g:

$$\dot{g} = (2 + 3\eta_h(1))g + 3\lambda_3 N_G(1) \left(\frac{\eta_h(1) - \eta_h(0)}{M_G(1)} \right) g + 2 \left(\frac{\mathrm{Tr}\left[\Pi_G \circ \frac{\dot{\Gamma}_k^{(hhh)}(1)}{Z_h^{3/2}(1)} \right] - \mathrm{Tr}\left[\Pi_G \circ \frac{\dot{\Gamma}_k^{(hhh)}(0)}{Z_h^{3/2}(0)} \right]}{M_G(1)} \right) \sqrt{g} \quad (7.12)$$

The functions $M_G(p)$ and $N_G(p)$ are given by

$$M_G(p) = \frac{171 p^4}{2^{12}\pi}, \qquad N_G(p) = -\frac{p^2}{2^8 \pi}. \quad (7.13)$$

The last term in (7.12) reflects the linear interpolation in p^2 between the flows at $p = 1$ and $p = 0$ in the region $0 < p < 1$. It represents the slope of the dashed line in Figure 7.9.

We conclude, that we found an improved procedure for the extraction of $\dot{g}$ from the flow of the graviton 3-point function in terms of a finite difference. For the $\eta(p)$ we apply an improved scheme, that was introduced in [27]. These projection procedure reflect the actual momentum dependencies of the graviton 3- and 2-point functions in a substantially more accurate way. The evaluation of $\dot{g}$ with (7.12) leads to different results for the flow of g already in the effective one-loop approximation without anomalous dimensions. We discuss the one-loop case in the following.

7.3.3 Complete Pure Gravity System at One-Loop

We employ the improved momentum approximation scheme in order to derive an improved flow equation for g. For the moment, we restrict ourselves to the one-loop approximation, thus, we set the graviton and ghost anomalous dimensions, η_h and η_c, to zero. A vanishing graviton anomalous dimension simplifies equation (7.12) considerably. The resulting effective one-loop system admits three fixed points in the relevant regime. Table 7.2 depicts the fixed point values and their critical exponents. FP 1 is the usual Gaussian fixed point. The two other fixed points, FP 2 and FP

3, are both non-trivial and have three and two UV relevant directions, respectively. The values for g^* and μ_h^* compare well with the results from the simplified pure gravity system discussed in section 7.1. However, for the complete gravity system with improved momentum approximation scheme all critical exponents are of the order of 1. Thus, the indications for an insufficient truncation that we found for the simplified gravity system are absent in the present complete system. The appearance of another non-Gaussian fixed point is explained by the extension of the truncation. Thus, the fixed point equation $\beta_{\lambda_3} = 0$ is a higher order algebraic equation which admits more solutions. At this point, it is unclear which of these fixed points is physical. We decide decide on this by going beyond one loop and investigating which of the fixed points in Table 7.2 is still present. Due to improvements for critical exponents we are confident that we improved the truncation considerably by introducing the extra coupling λ_3.

The one-loop approximation of the complete pure gravity system using the improved momentum approximation scheme led to two new fixed points one of which has a repulsive direction. The results are more trustworthy than the ones found for the simplified pure gravity system. Now, we study if these findings persist when going beyond one-loop by introducing non-vanishing anomalous dimensions.

7.3.4 Beyond One-Loop

In this section we include anomalous dimensions for the graviton and the ghosts according to (7.10) and (7.11). This way, we make full use of the improved momentum approximation scheme. Solving the system numerically we find one non-trivial fixed point which represents our high-end result for the complete pure-gravity system beyond one loop. It reads

$$(g^*, \lambda_3^*, \mu_h^*) = (0.60, 0.097, -0.57)\,, \tag{7.14}$$

$$(\theta_{1/2}, \theta_3) = (-0.52 \pm 4.1i, 12)\,. \tag{7.15}$$

The inclusion of the anomalous dimension leads to a reduction in the number of non-Gaussian fixed points. Only one non-trivial fixed point persists beyond one-loop which has only two UV relevant directions. The values for g^*, and λ_3^* are considerably smaller than in the one loop case in the previous section. However, μ_h^* is bigger by almost a factor of two compared to FP 2 and FP 3 in Table 7.2. As in the one-loop case we have a complex conjugate pair of eigenvalues with negative real parts. The real parts here are much smaller than in the one-loop case. The negative eigenvalue, however, is much bigger than in the one loop calculation. The appearance of a UV unstable direction with an eigenvalue of the order of ten is surprising. We expected that the eigenvalues would decrease with the introduction of anomalous dimensions. Since the fixed point we found in our high-end solution has one unstable direction, we also consider FP 3 from the one loop case (see Table 7.2) the physically relevant one. The anomalous dimensions at the fixed point are

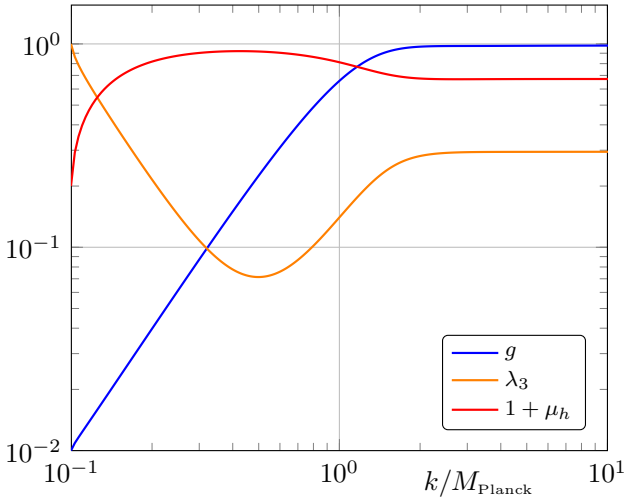

Figure 7.10: Running of the couplings from the IR to the UV in the complete pure gravity system at one-loop. In the vicinity of the IR fixed point, g scales classically. The variable k is rescaled with respect to the Planck mass M_{Planck}.

given by

$$(\eta_h^*(0), \eta_h^*(1), \eta_c^*) = (1.5, 0.43, -1.4), \tag{7.16}$$

which is well below the critical number of 2 in all cases. From calculations of the full momentum dependence [27] and from the locality of the graviton 2-point function we know that η_h quickly goes to zero for $p \gg 1$.

We have introduced the coupling λ_3 and employed an improved momentum projection scheme. This way we solved almost all of the problems that we had in the simplified pure gravity system, such as large anomalous dimensions and large critical exponents. However, we still have one large critical exponent. We expect that a further extension of the truncation, i.e., the inclusion of λ_4 lowers this value considerably. The stabilizing effect of higher order operators on the critical exponents was also found in [17, 64].

7.3.5 IR behaviour

We have analyzed the UV behaviour of the pure gravity system in much detail in the previous section, let us now briefly discuss the behaviour of the complete pure-gravity theory in the infrared. The IR behaviour was found to be unaffected by a change of truncation. Therefore, we will discuss the IR running of the three couplings only for the one loop approximation of the complete pure gravity system. As was mentioned before, all systems that we discussed so far exhibit an infrared fixed point at

$$(g_{\text{IR}}^*, \lambda_{3,\text{IR}}^*, \mu_{h,\text{IR}}^*) = (0, \infty, -1), \tag{7.17}$$

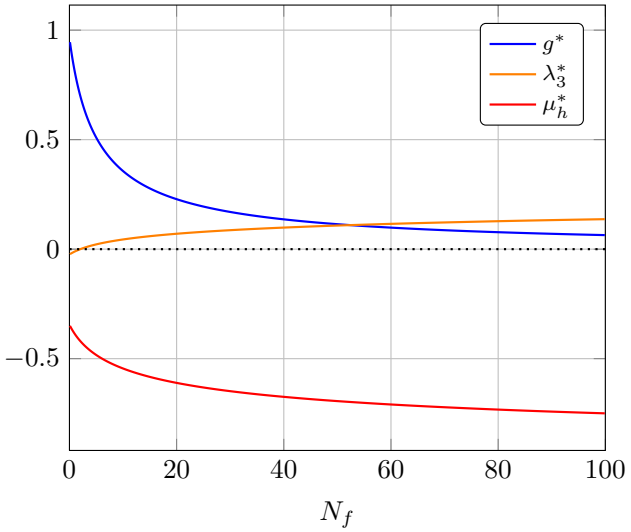

Figure 7.11: The impact of fermions on the non-Gaussian fixed point in the complete gravity system at one loop. Increasing the number of fermions weakens the gravitational coupling at the UV fixed point. While μ_h^* approaches -1, λ_3^* is driven towards to higher positive values and saturates at ≈ 0.2.

which is IR attractive. Around this fixed point we find g to scale classically, thus, according to $g \sim G_N k^2$. Following [14, 27], we determine the Planck mass from the scaling of g in the infrared. In Figure 7.10 trajectories for the running quantities are shown as functions of k/M_{Planck} starting in the infrared and ending at the fully attractive UV fixed points. The classical scaling of g in the vicinity of the IR fixed point is indicated by the linear slope in the double-logarithmic plot.

Thus, classical scaling is retained in the infrared for our theory. We regard this as is an important consistency check. Furthermore, there exist global trajectories from the IR to the UV which connect the IR and UV fixed points.

7.4 Complete Gravity-Matter System at One-Loop

Now we include matter into the complete pure gravity system. Since we found the approximation $p = 0$ is inconsistent for pure gravity, we employ the improved momentum approximation scheme for the inclusion of matter. We will restrict ourselves to the one-loop approximation here. Thus, we set $\eta = 0$ for all fields. As in section 7.2.2 we start by discussing the impact of fermions on the fixed point, followed by the investigation of scalars.

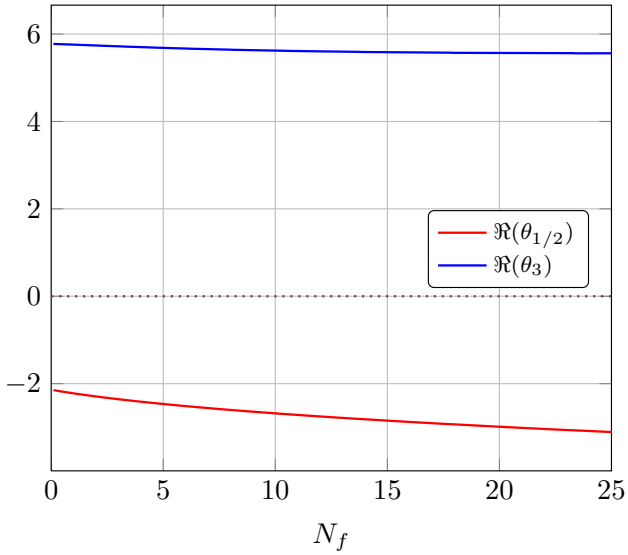

Figure 7.12: Real parts of critical exponents for the non-Gaussian fixed point as a function of fermion fields. An increase of the fermion number results in a decrease of the reals parts of the complex conjugate pair of critical exponents to larger negative values. The positive critical exponent decreases slighty.

7.4.1 Fermions

We successively increase the number of fermion fields in the complete gravity-matter model. We consider the effect of fermions on FP 3 in the pure gravity system according to Table 7.2. This has one repulsive direction and is considered physical, since it is found in all truncations. In Figure 7.11 the effect of fermions on FP 3 is shown as a function of N_f. The inclusion of fermions reduces the fixed point value g^*. Thus, g^* approaches 0 asymptotically with $N_f \to \infty$. The fixed point value μ_h^* is driven towards -1. This agrees with the findings in the simplified gravity-matter system discussed in section 7.2.2, The fixed point value λ_3^* is driven towards slightly larger positive values.

The observations regarding the fixed point values of the complete gravity-matter system are in good agreement with the simplified gravity-matter system. However, the picture is completely different for the critical exponents $\theta_{1,2,3}$. In Figure 7.12 the real parts of the critical exponents for the non-Gaussian fixed point are given as a function of the number of fermions N_f. The real parts of the complex conjugate pair of eigenvalues are negative and approach slightly higher negative values for large N_f. The positive critical exponent decreases slightly to lower positive values. Hence, the fixed point does not lose its attractivity as in case of the simplified system.

Fermions weaken gravity in the UV at the non-Gaussian fixed point in the complete gravity-matter system. This finding is consistent with the results of the simplified gravity-matter system. However, we observe that the behaviours of the critical

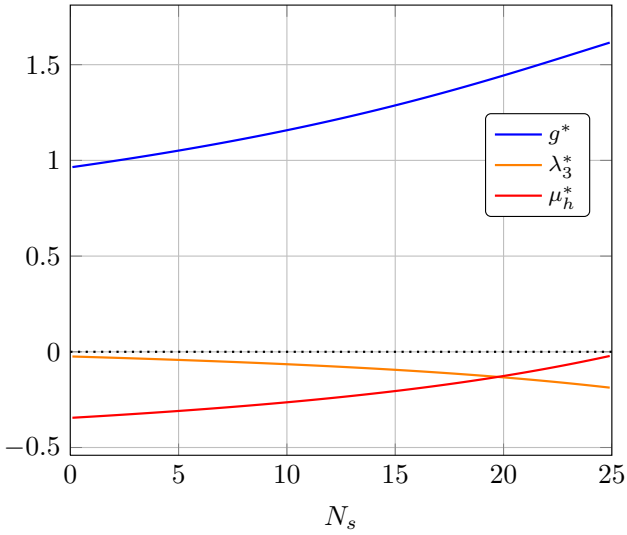

Figure 7.13: The impact of scalar on the non-Gaussian fixed point in the complete gravity system at one loop. Increasing the number of scalar enhances the gravitational coupling at the UV fixed point. While μ_h^* approaches 0 and becomes positive for $N_s \approx 25$, λ_3^* decreases to larger negative values.

exponents differ significantly. We are confident that this fact reflects the improvement of our truncation. In sum, the complete gravity-matter system admits a UV fixed point which is attractive in two out of three directions for an arbitrary number of fermions.

7.4.2 Scalars

Now we study the evolution of fixed point FP 3 in the complete gravity-matter system under the increase of the number of scalar fields. In Figure 7.13 the fixed point values $(g^*, \lambda_3^*, \mu_h^*)$ are shown as a function of N_s. The fixed point persists for an arbitrary number of scalars. The inclusion of scalar fields yields an increase of the fixed point values g^* and μ_h^* while λ_3^* remains constant. At $N_s \approx 25$, μ_h^* changes sign and becomes constant. Hence, scalars enhance the gravitational coupling at the UV fixed point. This finding is again, consistent with the results of the simplified gravity-matter system in section 7.2.2. The fixed point value λ_3^* decreases with increasing number of scalars. The real parts of the critical exponents do not vary significantly as a function of the number of scalar fields. For complex conjugate pair they increases slightly. The positive critical exponent decreases to lower positive values. These findings for the critical exponents are again in great difference to what was found for the simplified gravity-matter system in section 7.2.2. Here there we do not have large eigenvalues which is in favor of the reliability of the truncation.

In sum, we found that arbitrary numbers of scalar fields are consistent with the existence of the non-Gaussian fixed point. Scalars increase the fixed point values $g*$

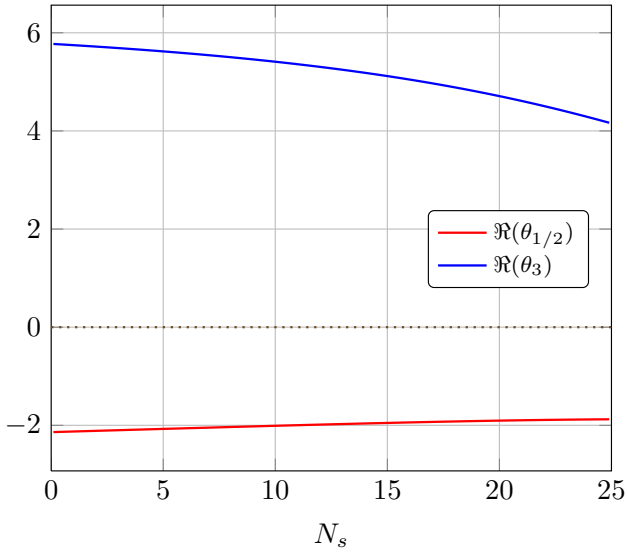

Figure 7.14: Real parts of critical exponents for the non-Gaussian fixed point as a function of scalar fields. The increase of N_s results in a increase of the real parts of the real parts of the complex conjugate pair of criitcal exponents to smaller negative values. The positive critical exponent decreases to lower positive values.

and μ^*, whereas λ_3^* decreases. Therfore, scalars support gravitational coupling in the UV. The fixed point values are consistent with the findings of the simplified matter-gravity system. The critical exponents of both systems, however, vary significantly.

7.5 Conclusions and Outlook

We found in this chapter a consistent picture of how massless matter affects the dynamics of asymptotically safe quantum gravity. In all truncations that admit a non-Gaussian fixed point of pure gravity the fixed point remains stable under the inclusion of an arbitrary number of matter fields. This is in contradiction to the findings in [20, 21], where only a small number of fermions is consistent before the fixed point vanishes or the truncation breaks down. It was suggested by the naïve one-loop analysis that fermions are in favor of UV fixed point. According to our findings fermions in fact weaken the gravitational coupling at the UV fixed point. They drive the fixed point values for g and μ_h^* towards its IR fixed point. We interpret this behaviour as fermionic shielding of quantum gravity at high energies. Scalars have the exact opposite effect. They force the gravitational coupling at the fixed point to higher values, thus enhancing gravity in the UV. Also, the μ_h^* at the assumes higher values and eventually changes sign. For all considered particle species λ_3^* exhibits always the exact opposite behaviour to μ_h^* which reflects that

approximately, the classical relation

$$\lambda_2 = \lambda_3 = \dots \tag{7.18}$$

is fulfilled. The extension of the truncation by introducing λ_3 and using an improved momentum projection scheme for the flow of g improves the behaviour of the system considerably. This reflected in smaller anomalous dimensions and smaller critical exponents. The inclusion of the full dynamics of the graviton 3-point function by means of an accurate approximation of its momentum dependence and the consideration of its constant part are necessary for a consistent picture of asymptotically safe quantum gravity in the vertex expansion.

In order to further improve the truncation gravity-matter system beyond one-loop should be considered by including the anomalous dimensions of the gravity, ghost and matter fields. Furthermore, the consideration of non-zero masses for the matter fields could be interesting. The truncation of the pure gravity system would receive a major improvement by the inclusion of the full momentum dependence of the anomalous dimensions [27] and that of g. The inclusion of higher order terms in the scalar curvature R in the classical gravity action could help to stabilize the critical exponents. This was observed in [17, 64].

Part III

Gravity and Interacting Matter

Motivation

So far, we considered matter, i.e, fermions and scalar fields, that are minimally coupled to dynamical gravity. Minimal coupling suggests that interaction vertices of the theory are constructed only from the metric variations of the kinetic terms. For gravity, this leads to vertices with an arbitrary number of graviton legs for any field species. These vertices generate all $2n$-order interactions among matter fields on one-loop level due to diagrams of the type

$$\partial_t \left(\quad \right) \sim \quad . \tag{7.19}$$

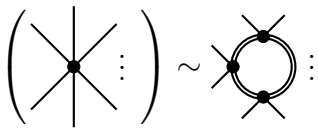

Therefore, minimally coupled matter theories without matter-self interactions become interacting after one RG-step due to induced self-interactions [22, 23, 65]. In the first part of this the truncation was chosen such that no interactions among matter fields are considered. In order to obtain a more realistic description matter in the universe, we consider models in which matter interaction are included. Simple models of gravity and interacting matter are seen as an important stepping stone for the inclusion of gravity into the Standard Model. To that end, we discuss models with 4-fermion interactions in the first chapter of this part. This type of interaction that generated in the RG flow by graviton loops. Induced 4-fermion interactions at the Planck scale could be inconsistent with the observation of light fermions at low energies [22]. Therefore, the present analysis has important implications for the general consistency of fermion fields and the asymptotic safety scenario.

In the second chapter we discuss the Yukawa interaction which is an interaction between a fermion-antifermion pair and a scalar field. Since three fields are involved in this process, it is not of the type given in (7.19). Thus, Yukawa interactions are not generated by the RG-flow of minimally coupled matter. However, there is a close connection between the Yukawa interaction and a momentum dependent 4-fermion interaction. Since both of these types of matter interactions play an important role in particle and solid state physics, it is an interesting question how the presence of gravity interactions affects their behavior.

8 4-fermion Interactions

In the Standard Model without gravity, the fermions are chiral, i.e. massless at high energies. The fermion masses that are observed at lower energies arise are due to spontaneous symmetry breaking of the Higgs field in the electroweak sector and chiral symmetry breaking in the strong sector. Chiral symmetry breaking is the spontaneous generation of fermion masses triggered by strong correlations between fermions. In the Standard Model, these correlations are induced by the exchange of gluons. A process like this can be represented by box diagrams like the one shown in Figure 8.1. According to the Standard Model, spontaneous chiral symmetry breaking at the QCD-scale Λ_{QCD} induced by gluon fluctuations is responsible for the generation of most of the mass in the universe. Hence, gauge-field induced fermion self-interactions are of fundamental importance for our understanding of the origin of fermion masses in the Standard Model. Gravity is known to interact with matter in a very similar manner as Yang-Mills theories which model the strong interactions in the Standard Model. Therefore, it can be conjectured that there exists a similar effect of mass generation due to gravity-induced fermion self-interactions in the ultraviolet. Chiral symmetry breaking induced by gauge fields typically occurs when the gauge-coupling exceeds a critical value [22]. Gravity is known to be very weakly coupled at low energies. However, asymptotic safety implies, that gravity becomes strongly interacting in the UV. If a mass generation due to gravity-induced chiral symmetry breaking takes place, it will occur at energies of or beyond the Planck scale $\Lambda_{\mathrm{Planck}}$. Chiral symmetry breaking at such high energies however, implies fermion masses in the IR of the order of $\Lambda_{\mathrm{Planck}}$, in contrast to observation. Hence, we expect a mechanism that prevents chiral symmetry to take place at such high energies. This way, light fermions are consistent with the asymptotic safety scenario of quantum gravity.

In the following, we briefly discuss the concept of chiral symmetry breaking. In the sequel the impact of graviton fluctuations on the flow of the 4-fermion (also called 4-Fermi) coupling will be calculated. What we will find is, that due to the vertex structure of the 4-Fermi interactions we get a simple condition for chiral symmetry breaking. Furthermore, this condition is not satisfied in any case. This mechanism

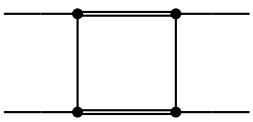

Figure 8.1: Gluon-induced 4-fermion interaction diagram. In this diagram the double lines represent gluons and the solid line fermions.

generalises to an arbitrary number of fermion flavors N_f. It makes the considered model fully consistent with the asymptotic safety scenario. Thus, the model admits light fermions (compared to the Planck scale) in the universe.

8.1 NJL-Model

8.1.1 Chiral Symmetry breaking

First, we briefly discuss the main concepts of chiral symmetry breaking. In general, chiral symmetry is defined as the invariance of the action with respect to axial phase transformations. For the fermion fields $\bar{\psi}(x)$ and $\psi(x)$ the transformation reads

$$\psi(x) \to \psi(x) e^{i\gamma_5 \alpha}\,, \tag{8.1a}$$

$$\bar{\psi}(x) \to e^{i\gamma_5 \alpha} \bar{\psi}(x)\,. \tag{8.1b}$$

A necessary condition for a chiral symmetry of a fermionic action is that it does not contain an explicit fermion mass term $\approx m_f \bar{\psi}\psi$. Chiral symmetry can be spontaneously broken if a finite vacuum expectation value $< \bar{\psi}\psi >$ is generated by quantum fluctuations. The generation of such a term is indicated by the breakdown of the pointlike fermionic truncation. Hence, at least one of the 4-Fermi couplings divergences [66]. We have

$$\frac{1}{\lambda} \to 0 \quad \text{(chiral symmetry breaking)}. \tag{8.2}$$

We understand this better in a bosonised description with a bosonic field ϕ that couples to a fermion bilinear. There, λ is related to the mass of the respective boson according to

$$\lambda \sim \frac{1}{m_\phi^2}. \tag{8.3}$$

Thus, the divergence of λ indicates that the mass for ϕ changes sign. This is the case when the effective potential for ϕ acquires a Mexican hat shape. Consequently, a non-zero vacuum expectation values for ϕ and, therefore, $\bar{\psi}\psi$ are generated.

8.1.2 NJL-model without gravity

We consider the NJL-model without gravity adopting the notation in [66]. First, we naively introduce a simple fermionic truncation that is chirally symmetric. We have

$$\Gamma = \int Z_\psi \left\{ \bar{\psi} \not{\partial} \psi - \frac{1}{2} \bar{\lambda}_\sigma \left[(\bar{\psi}\psi)^2 - (\bar{\psi}\gamma_5\psi)^2 \right] \right\} d^4x\,. \tag{8.4}$$

Obviously, this action is invariant under phase transformations and axial phase transformations (see (8.1)). In the flow of Γ_k all operators that are compatible

FP-Number	λ_σ^*	λ_v^*	$\theta_{1,2}$
1	0	0	$\{2, 2\}$
2	$-64\pi^2$	$32\pi^2$	$\{10, -2\}$
3	$6\pi^2$	$2\pi^2$	$\{\frac{5}{2}, -2\}$

Table 8.1: Fixed points for the NJL-model without gravity for Litim's cutoff. FP 1 is fully IR attractive. FP 2 and FP 3 have one IR attractive and one IR repulsive direction, respectively.

with the symmetries of the action are generated. Hence, (8.4) is not complete since quantum fluctuations induce other chirally symmetric 4-Fermi couplings. The investigation of chiral symmetry breaking is only sensible if we consider a complete set of 4-fermion interactions. This seems like an extensive task on first sight. However, these operators are not independent. Instead, they obey Fierz-ambiguities of the kind

$$\left[(\bar{\psi}\psi)^2 - (\bar{\psi}\gamma_5\psi)^2\right] = \frac{1}{2}\left[(\bar{\psi}\gamma_\mu\gamma_5\psi)^2 - (\bar{\psi}\gamma_\mu\psi)^2\right], \tag{8.5}$$

which we for now just accept as ambiguities in the formulation of tensor products. A proof and the complete set of Fierz ambiguities can be found, e.g., in [66, 67]. One can show, that for one fermion species, $N_f = 1$, we have a Fierz-complete basis by adding the interaction $\sim (\bar{\psi}\gamma_\mu\gamma_5\psi)^2$ to (8.4). Our model of the 4-Fermi interaction now reads

$$\Gamma_{\text{NJL}} = \int Z_\psi \left\{\bar{\psi}\partial\!\!\!/\psi - \frac{1}{2}\bar{\lambda}_\sigma\left[(\bar{\psi}\psi)^2 - (\bar{\psi}\gamma_5\psi)^2\right] + \frac{1}{2}\bar{\lambda}_v\left[(\bar{\psi}\gamma_\mu\psi)^2\right]\right\} d^4x\,, \tag{8.6}$$

which is also known as the NJL-model for 4-fermi interactions. In the remainder of this chapter, we will consider the dimensionless couplings $\lambda_{\sigma/v}$. They are related to the dimensionfull couplings $\bar{\lambda}_{\sigma/v}$ by

$$\lambda_{\sigma/v} = \bar{\lambda}_{\sigma/v} k^2 \tag{8.7}$$

To conclude, without proof, we have stated that chiral symmetry breaking is indicated by the breakdown of the 4-Fermi (point-like) truncation. If the truncation breaks down, at least one of the couplings diverges.

8.1.3 Flow equations

We get the diagrammatic flow for the dimensionless couplings λ_σ and λ_v from the flow equation of fermion 4-point function. It reads

∂_t 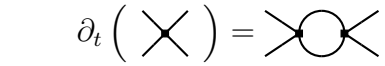 (8.8)

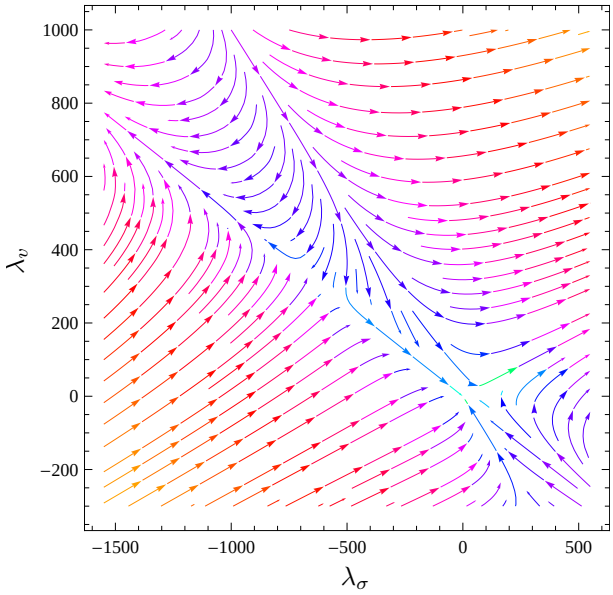

Figure 8.2: Phase diagram for the flow towards the IR of the two couplings in the NJL-model. The three fixed points are all located in the center of the plot.

Using Litim's cutoff we get the flow for the two couplings

$$\beta_{\lambda_\sigma} = 2\lambda_\sigma(1+\eta_\psi) - \frac{5-\eta_\psi}{40\pi^2}(\lambda_\sigma^2 + 4\lambda_\sigma\lambda_v + 3\lambda_v^2) \tag{8.9a}$$

$$\beta_{\lambda_v} = 2\lambda_v(1+\eta_\psi) - \frac{5-\eta_\psi}{80\pi^2}(\lambda_\sigma^2 + 2\lambda_\sigma\lambda_v + \lambda_v^2), \tag{8.9b}$$

which agrees with [66]. Note that for the NJL-model without gravity the anomalous dimension of the fermion is zero $\eta_\psi = 0$ in the limit $p = 0$, because all vertices are momentum independent. This ceases to be true for the NJL-model with gravity. The system (8.9) of differential equations has three fixed points which are given in Table 8.1. The Gaussian fixed point (FP 1) is IR-attractive whereas the two non-Gaussian fixed points (FP 2 and FP 3) both have one IR unstable direction.

By plotting the equation for λ_σ for λ_v set to zero we examine some of the properties of the full system. Figure 8.3 depicts schematically the β_{λ_σ}-function for $\lambda_v = 0$. Due to the quadratic structure of the flow (8.9), there are two fixed points. One of them is the IR-attractive Gaussian fixed point, the other one is repulsive in the IR-direction. In particular, if the initial value for λ_σ is too high i.e. the flow starts in the UV beyond the IR-repulsive non-Gaussian fixed point, it will flow to infinity. According to (8.2) this implies chiral symmetry breaking. Consider the subsystem of one only coupling λ_σ. If the initial value for λ_σ is too high, chiral symmetry will break spontaneously when flowing towards the IR. Extra-couplings that appear in the loops of the flow and do not depend on λ_σ or λ_v (like Newton's coupling g) potentially shift the curve upwards and downwards. In case of a shift downwards the was-to-be-Gaussian and the non-Gaussian fixed points approach each other. If

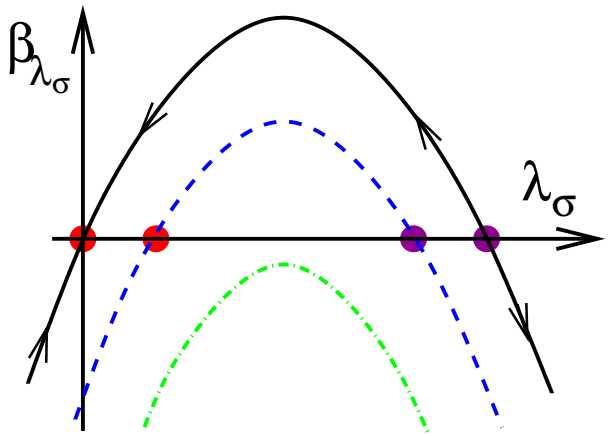

Figure 8.3: Schematic behavior of the β-function for one of the 4-Fermi couplings. The 4-Fermi coupling is set to zero (black solid line). The interaction with gravity shifts the parabola down (blue line). If the gravitational coupling is strong enough two fixed points annihilate (Taken from [22]).

the shift is large enough this effect can lead to an annihilation of the fixed points in Figure 8.3. Then β_{λ_σ} becomes negative for all λ_σ. Thus, chiral symmetry breaking takes place for arbitrary initial couplings. Since gravity is always attractive, we conjecture that it favors the onset of chiral symmetry breaking. The question is whether the gravitational interaction at the UV fixed point is strong enough to move the parabola curve in Figure 8.3 below zero. For our study, we assume chiral fermions in the vicinity of the non-Gaussian fixed point of quantum gravity, i.e., at energies of and below the Planck-scale. Thus, we assume the initial 4-Fermi couplings at the Planck scale are zero. Our condition for chiral symmetry breaking is therefore annihilation of fixed points.

8.2 Gravity-Matter interactions

We now introduce gravity-fermion interactions. The complete effective action of the NJL-model for N_f which we consider in the following is given by

$$\Gamma_{\text{NJL,grav}} = \Gamma_{\text{ferm,grav}} + \int Z_\psi \left\{ -\frac{1}{2}\lambda_\sigma \left[(\bar{\psi}\psi)^2 - (\bar{\psi}\gamma_5\psi)^2 \right] + \frac{1}{2}\lambda_v \left[(\bar{\psi}\gamma_\mu\psi)^2 \right] \right\} \sqrt{g} d^4x \,. \tag{8.10}$$

The NJL-action is coupled to gravity via the $\sqrt{g}$-term which makes the action integral diffeomorphism invariant. Also we have the usual kinetic term for the fermion. We have

$$\Gamma_{\text{ferm,kin}} = \int Z_\psi \bar{\psi} \not{\nabla} \psi d^4x \,, \tag{8.11}$$

which is absorbed into $\Gamma_{\text{ferm,grav}}$. Note that the fermion masses are zero, $m_f = 0$, in the UV. The coupling of the fermion kinetic term and the 4-Fermi interaction terms to gravity lead to interactions of 2 and 4 fermions with an arbitrary numbers of gravitons, respectively . The diagrammatic flow equation for the NJL-gravity model is given by

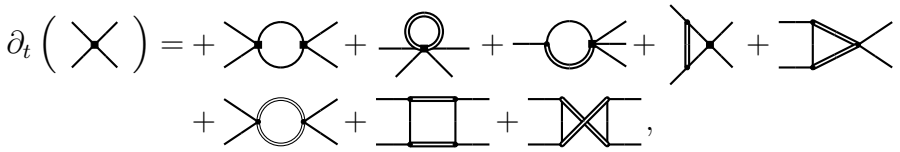

(8.12)

with the appropriate signs and symmetry factors. Consequently, the β-functions for λ_σ and λ_v are much more complicated than in(8.9) and involve powers in g up to two. Generically, they are given by

$$\begin{aligned}\beta_{\lambda_i} &= \beta_{\lambda_i,\text{NJL}}(\eta_\psi) + 2\mathfrak{f}_i(g)\lambda_i + \mathfrak{g}_i(g^2)\,,\\ \beta_{\lambda_i} &= a_i\lambda_i^2 + 2(1+\eta_\psi+\mathfrak{f}_i(g)+b_i\lambda_j)\lambda_i + c_i\lambda_j^2 + \mathfrak{g}_i(g^2)\,,\end{aligned} \tag{8.13}$$

where $i \in \{\sigma, v\}$ and $i \neq j$. The coefficients a_i, b_i and c_i are read off from the equations (8.9). We have

$$(a_\sigma, b_\sigma, c_\sigma) = A\cdot(2,4,6)\,, \tag{8.14}$$

$$(a_v, b_v, c_v) = A\cdot(1,1,1)\,, \tag{8.15}$$

where the negative number A can be written in terms of the threshold-functions defined in [33, 66] as

$$A = -4v_4 l_1^{(\text{F}),(4)}(0;\eta_\psi) = -\frac{1}{8\pi^2} l_1^{(\text{F}),(4)}(0;\eta_\psi)\,, \tag{8.16}$$

$$A < 0\,. \tag{8.17}$$

For example, for a fermionic Litim's cutoff (8.16) reads

$$A = -\frac{5-\eta_\psi}{80\pi^2} \qquad \text{(Litim's cutoff)}\,. \tag{8.18}$$

Due to structure of the fermionic truncation (8.10) the coefficients $\mathfrak{f}_i$ and $\mathfrak{g}_i$ are not independent. Instead, they obey the relations

$$\mathfrak{f}_v = \mathfrak{f}_\sigma =: \mathfrak{f}\,, \tag{8.19}$$

$$\mathfrak{g}_\sigma = -2\mathfrak{g}_v =: \mathfrak{g}\,. \tag{8.20}$$

These expressions can be written in terms of threshold functions. The function $\mathfrak{f}$ does not have a fixed sign since it originated from a sum of diagrams. However, $\mathfrak{g}$ is always negative since it stems from only one diagram. We write

$$\mathfrak{g} = -120\pi^2 v_4 l_3^{(4)}(0,\eta_h) = -\frac{15}{4} l_3^{(4)}(0,\eta_h)\,, \tag{8.21}$$

$$\mathfrak{g} < 0\,. \tag{8.22}$$

For Litim's cutoff $\mathfrak{f}$ and $\mathfrak{g}$ are given by

$$\mathfrak{f} = \frac{g}{70\pi}\left(\frac{(2\eta_\psi - 7)}{(\mu_h + 1)} - \frac{(79\eta_h - 448)}{8\,(\mu_h + 1)^2}\right), \tag{8.23}$$

$$\mathfrak{g} = -g^2 \frac{5(8 - \eta_h)}{16\,(\mu_h + 1)^3}\,. \tag{8.24}$$

The 4-Fermi interaction is momentum independent and we evaluate at vanishing momenta, $p = 0$. Therefore, the 4-Fermi contribution to the fermion anomalous dimension

 (8.25)

is zero. Hence, the 4-Fermi sector decouples completely from the rest of the gravity-fermion system. Consequently, we analyse the flow of the 4-Fermi coupling independently from the rest of the gravity-fermion system. Using the relations (8.19) it is possible to make statements about chiral symmetry breaking of the 4-Fermi interaction in a completely regulator independent. We substitute the relations (8.19) into the flow equations (8.13). Now, the fixed points are expressed in a closed form as functions of $\mathfrak{f}$, $\mathfrak{g}$ and A via

$$\lambda^*_{\sigma,1} = \frac{-\sqrt{2A\mathfrak{g} + 4(\eta_\psi + \mathfrak{f} + 1)^2} + 2\,(\eta_\psi + \mathfrak{f} + 1)}{A}\,, \tag{8.26a}$$

$$\lambda^*_{v,1} = \frac{\sqrt{2A\mathfrak{g} + 4(\eta_\psi + \mathfrak{f} + 1)^2} - 2\,(\eta_\psi + \mathfrak{f} + 1)}{2A}\,, \tag{8.26b}$$

$$\lambda^*_{\sigma,2} = \frac{\sqrt{2A\mathfrak{g} + 4(\eta_\psi + \mathfrak{f} + 1)^2} + 2\,(\eta_\psi + \mathfrak{f} + 1)}{A}\,, \tag{8.26c}$$

$$\lambda^*_{v,2} = -\frac{\sqrt{2A\mathfrak{g} + 4(\eta_\psi + \mathfrak{f} + 1)^2} + 2\,(\eta_\psi + \mathfrak{f} + 1)}{2A}\,, \tag{8.26d}$$

$$\lambda^*_{\sigma,3} = -\frac{2A\mathfrak{g} + 3(\eta_\psi + \mathfrak{f} + 1)^2}{8A(\eta_\psi + \mathfrak{f} + 1)}\,, \tag{8.26e}$$

$$\lambda^*_{v,3} = -\frac{-2A\mathfrak{g} + (\eta_\psi + \mathfrak{f} + 1)^2}{8A(\eta_\psi + \mathfrak{f} + 1)}\,. \tag{8.26f}$$

We identify the first fixed point $\mathrm{FP}_1 = (\lambda^*_{\sigma,1}, \lambda^*_{v,1})$ as the Gaussian fixed point in the limit $g \to 0$. Then we have $\mathfrak{f} \to 0$ and $\mathfrak{g} \to 0$ and the Gaussian fixed point is recovered. For $g \neq 0$, FP_1 it is shifted to non-zero values and therefore becomes non-Gaussian.

The first two fixed points in (8.26) annihilate if the argument in the square roots become negative. This is the scenario for chiral symmetry breaking at the Planck scale, The condition for chiral symmetry breaking reads

$$A\mathfrak{g} + 2(\eta_\psi + \mathfrak{f} + 1)^2 < 0\,. \tag{8.27}$$

The functions A and $\mathfrak{g}$ are both manifestly negative and the remaining terms appear only quadratically. Therefore, condition 8.27 cannot be satisfied. A and $\mathfrak{g}$ are contributions from one diagram, respectively. Their sign is universal and cannot be changed by the choice of regulator. The sign of $\mathfrak{f}$ is irrelevant for this analysis, since this contribution enters (8.27) quadratically. Chiral symmetry breaking in our model is prevented by the relations (8.19), since they lead to general fixed points which can never annihilate.

For the fixed-point values of the simplified gravity-matter model with one fermion, the value for (8.27) is given by

$$2A\mathfrak{g} + 4(\eta_\psi + \mathfrak{g} + 1)^2 \Big|_{(g^*, \mu_h^*)} \approx 6 \qquad \text{(Litim's cutoff)}\,, \tag{8.28}$$

which is substantially bigger than zero.

In sum, we found a natural mechanism that prevents chiral symmetry breaking at the Planck scale for all regulators. It is traced back to the general structure of the 4-Fermi couplings. The relations (8.19) are regulator independent and lead to a cancellation of minus signs.

8.3 Multiple Fermion Flavours

In this section, we generalise the findings from the previous section to an arbitrary number of fermion flavours N_f. To obtain a truncation which is $\mathrm{SU}(N_f)_L \times \mathrm{SU}(N_f)_R$ chirally symmetric, the action (8.6) is modified. Instead of (8.6) we consider the fermionic contribution to the action given by

$$\Gamma_{k,N_f} = -\int Z_\psi \left\{ \bar{\lambda}_{-,k} \left[V - A \right] + \bar{\lambda}_{+,k} \left[V + A \right] \right\} \sqrt{g} d^4x\,. \tag{8.29}$$

where V and A read

$$V = (\bar{\psi}^i \gamma_\mu \psi^i)(\bar{\psi}^j \gamma^\mu \psi^j)\,, \tag{8.30a}$$

$$A = -(\bar{\psi}^i \gamma_\mu \gamma_5 \psi^i)(\bar{\psi}^j \gamma^\mu \gamma_5 \psi^j)\,, \tag{8.30b}$$

$$\tag{8.30c}$$

and i and j are the fermion flavour indices running from 1 to N_f. This action was used in a similar study in [22]. The flow equations for the truncation (8.29) are given by the same diagrams and have a generically identical structure. They are written as

$$\beta_{\lambda_i} = a_{N,i}\lambda_i^2 + 2(1 + \eta_\psi + \mathfrak{f}_{N,i}(g) + b_{N,i}\lambda_j)\lambda_i + c_{N,i}\lambda_j^2 + \mathfrak{g}_{N,i}(g^2)\,. \tag{8.31}$$

The coefficients $a_{N,i}$, $b_{N,i}$ and $c_{N,i}$ with $i \in \{+, -\}$ are given by

$$(a_{N,+}, b_{N,+}, c_{N,+}) = -2A \cdot (3, N_f + 1, 0)\,, \tag{8.32}$$

$$(a_{N,-}, b_{N,-}, c_{N,-}) = -2A \cdot (N_f - 1, 0, N_f)\,, \tag{8.33}$$

which agrees with [22, 68] For this truncation, the relations between $\mathfrak{f}_{N,i}$ and $\mathfrak{g}_{N,i}$ are given by

$$\mathfrak{f}_{N,+} = \mathfrak{f}_{N,-} =: \mathfrak{f}_N \,, \tag{8.34}$$

$$\mathfrak{g}_{N,+} = -\mathfrak{g}_{N,-} =: \mathfrak{g}_N \,. \tag{8.35}$$

The $\mathfrak{f}_N$ and $\mathfrak{g}_N$ expressed in terms of the $\mathfrak{f}$ and $\mathfrak{g}$ discussed in the previous section read

$$\mathfrak{f}_N = \mathfrak{f} \,, \tag{8.36}$$

$$\mathfrak{g}_N = \frac{1}{4}\mathfrak{g} \,. \tag{8.37}$$

Thus, there is a close relation between the flow equations in the case of $N_f = 1$ and for general N_f. We expect that for any 4-Fermi truncation of this type, there will be relations of the type (8.34). Again, due to the relations (8.34) we can express the fixed points in a closed form. Now it is, however, much more complicated than in the previous case of only one fermion. The complete fixed point equations are given in appendix A.4. For the present model, there are four fixed points. From the expressions for the fixed points we extract two relations, for which fixed points annihilate. They read

$$2A\mathfrak{g}_N(2N-1) + Q^2 < 0 \,, \tag{8.38a}$$

$$2A\mathfrak{g}_N(N-1)\left(2N^2+5N+9\right) + (N+3)^2Q^2 < 0 \,, \tag{8.38b}$$

with $Q = 1+\eta_\psi+\mathfrak{f}_N$. For $N \geq 1$ the left hand sides of the equations (8.38) are bigger than zero. As in case of the NJL model the minus signs of A and $\mathfrak{g}_N$ cancel. Chiral symmetry breaking in this model can only take place, if the number of fermions is smaller than one. Since N_f however counts Dirac fermions, the only possible choice for $N_f < 1$ is a theory with one Weyl fermion where $N_f = \frac{1}{2}$. This theory, however, is not chiral to begin with. This is in contradiction to our assumption of a chiral theory at the Planck scale.

8.4 Conclusions and Outlook

In conclusion, we have found that the general vertex structure 4-Fermi truncations leads to simple identifications between the resulting flow diagrams. For the discussed truncations these result in closed expressions for the fixed point values. From these expression we could derive simple conditions for chiral symmetry breaking. These relations led to the regulator independent statement that for the considered types of interactions chiral symmetry can not be broken by gravity at the Planck scale. This holds as long as we assume chiral fermions and vanishing 4-Fermi coupling in the UV. These findings generalise the findings in [22] not only by the inclusion of the fermion anomalous dimension η_ψ. Furthermore, our result is completely regulator

independent. We found that the anomalous dimension has no influence in this analysis since it always enters the conditions quadratically. Our statement is only valid for momentum independent vertices. Therefore, it will be interesting to investigate if these findings generalise to momentum dependent 4-Fermi interactions.

9 Systems with Yukawa-Interaction

In this chapter we consider the Yukawa interaction, which is an interaction between a scalar field and an antifermion-fermion field pair. It is an interaction between three fields and is represented by the vertices

$h_\sigma \mathbb{1} =$ 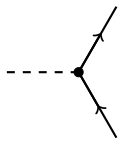 , $-h_\sigma i\gamma_5 =$ 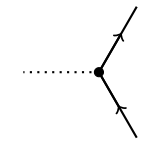 , (9.1)

for two scalar fields ϕ_1 and ϕ_2 of mass m_σ, respectively. We denote by h_σ the Yukawa coupling. We follow the notation in [66] and restrict ourselves to one fermion flavour, $N_f = 1$. In flat space without gravity, the interaction vertices (9.1) are connected to the 4-Fermion interaction given by

$\bar{\lambda}_\sigma(\mathbb{1} \otimes -\gamma_5 \otimes \gamma_5) =$ 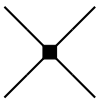 (9.2)

by means of a Hubbard-Strattonovich transformation [69, 70]. The two interactions (9.1) and (9.2) are related by

$$\bar{\lambda}_\sigma = \frac{h_\sigma^2}{m_\sigma^2}\,. \tag{9.3}$$

The procedure of identifying 4-Fermi interactions with an interaction mediated by a scalar field is called partial bosonisation. It is most commonly used to model the momentum dependence of the 4-Fermi interaction. Applications range from particle to condensed matter physics. Systems with Yukawa interaction are perturbatively renormalisable in 4 dimensions is of particular interest for the Standard Model of Particle Physics. There, perturbative renormalisability motivates the replacement of the Fermi theory of the beta-decay by a Yukawa-interaction of the leptons with a W or a Z boson [31]. At high energies, a marginal coupling as h_σ in the Yukawa theory, exhibits a logarithmic running towards a so-called Landau pole. At the scale of the Landau pole, 'new physics' is expected that prevents the coupling from running into that pole. Many studies propose quantum gravity as the source of 'new physics' in this context [29]. In this chapter we show that the asymptotic safety scenario prevents the Yukawa coupling from running into the Landau pole. Therefore, the unification of the Yukawa model with asymptotically safe quantum gravity allows for a consistent UV limit of the theory.

The flow of h_σ^2 towards the Landau pole is driven by the anomalous dimensions of the fermions and scalar fields. In Figure 9.1 the β-function of h_σ^2 is shown as a

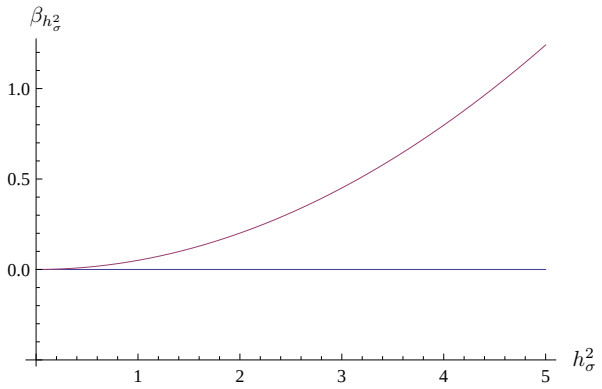

Figure 9.1: The β-function for the coupling h_σ^2 for $\mu_\sigma = 0$, The blue curve represents β_σ^2 without including anomalous dimensions. For the red curve the anomalous dimensions are included. In both cases, we have only a Gaussian fixed point. The coupling is marginal which is reflected by the vanishing first derivative around zero.

function of h_σ with and without the inclusion of anomalous dimensions (red and blue curve, respectively). There is only the Gaussian fixed point in both cases and the linear approximation around $h_\sigma^2 = 0$ is zero. This suggests that h_σ^2 is perturbatively marginal. This picture changes when we include gravity interactions. As we will see, asymptotically safe quantum gravity coupled to the Yukawa system turns the marginal Yukawa coupling into a perturbatively relevant coupling in the UV. The transition of perturbatively marginal couplings to relevant or irrelevant ones within the asymptotic safety scenario was observed for other theories [23]. In the following we consider the contributions to the flow of the Yukawa system. They originate from interactions of the system with gravity. We consider the square of the Yukawa-coupling h_σ^2, following [66]. A typical contribution to the flow of h_σ^2 is given by the triangle diagram

$$\partial_t h_\sigma^2 \sim 2h_\sigma \left(\quad \right) \sim h_\sigma^2 g\,. \tag{9.4}$$

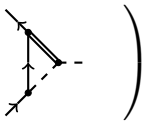

All gravity-Yukawa diagrams will contribute terms $\sim h_\sigma^2 g$ to $\partial_t h_\sigma^2$. Since h_σ^2 is marginal, all contributions to $\partial_t h_\sigma^2$ are at least linear or of higher order in h_σ^2. Hence, $h_\sigma^2 = 0$ is a fixed point of the gravity-Yukawa theory. In order to understand what role the asymptotic safety scenario plays, we assume for the moment that there exists a non-Gaussian fixed point for the gravity-Yukawa system of the form

$$g* \neq 0 \qquad \mu_h^* \neq 0 \qquad h_\sigma^{2,*} = 0 \qquad \mu_\sigma^* = 0. \tag{9.5}$$

The existence of such a fixed point is probable, since the back-coupling of the Yukawa system to the non-interacting matter-gravity sub-system is of higher order in the couplings. Thus, the back-coupling takes place only on the level of anomalous dimensions. According to (9.4), gravity contributions are linear in h_σ^2. This suggests

FP-Number	μ_σ^*	h_σ^2	$\theta_{1,2}$
1	0	0	$\{-2, 0\}$

Table 9.1: Tabulated fixed point values for the Yukawa system without gravity. The system exhibits a Gaussian fixed point which is ultraviolet stable in the μ_σ-direction.

that g^* contributes to $\beta_{h_\sigma^2}$ at leading order in h_σ^2 at a fixed point of the kind (9.5). There are two possibilities. Either a cancellation between the diagrams leads to a vanishing sum of all contributions of gravity-Yukawa diagrams or there is a non-vanishing contribution. A non-vanishing gravity contribution to $\partial_t h_\sigma^2$ turns h_σ^2 into a perturbatively relevant or irrelevant coupling in the UV. In particular, a perturbatively relevant coupling suggests that an asymptotically safe Yukawa system does not run towards a Landau pole for large energies because the coupling becomes relevant before. Thus, the logarithmic flow of h_σ^2 is eventually stopped and reversed by the interaction with gravity. This mechanism allows for a sensible UV-limit of Yukawa systems, e.g., in the Standard Model.

Yukawa-System

In our study of the Yukawa interaction we consider massless fermions

$$m_\psi = 0\,.$$

The truncated effective action of the Yukawa-system reads

$$\Gamma_k = \int \sqrt{g}\left(\bar\psi \not\nabla \psi + \frac{1}{2}((\partial\phi_1)^2 + (\partial\phi_2)^2) + \frac{m_\sigma}{2}(\phi_1^2+\phi_2^2) - \right.$$
$$\left. - h_\sigma \bar\psi(\phi_1 \mathbb{1} - i\phi_2\gamma_5)\psi\right) d^4x\,. \quad (9.6)$$

As in the previous section, we absorb the fermion and scalar kinetic terms as well as the scalar mass terms into the fermion and scalar actions $S_{\text{ferm,k}}$ and $S_{\text{scal,k}}$, respectively. We are left with the Yukawa-interaction term

$$\Gamma_{\text{Yuk,k}} = \int \sqrt{g}\left(-h_\sigma \bar\psi(\phi_1\mathbb{1} - i\phi_2\gamma_5)\psi\right) d^4x\,. \quad (9.7)$$

9.1 Yukawa System without Gravity

First we consider the Yukawa system without gravity. In this case, the interactions (9.1) are the only interaction among the matter fields $(\bar\psi, \psi, \phi_1, \phi_2)$. Consequently, the only contributions to the flow of the fermion 2-point function are given by the diagrams

∂_t ( )$_{\text{Yuk}}$ = 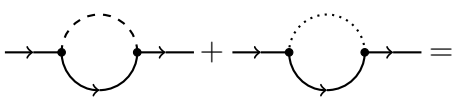 $= \frac{1}{Z_\psi}\eta_\psi i\not{p}\,.$ (9.8)

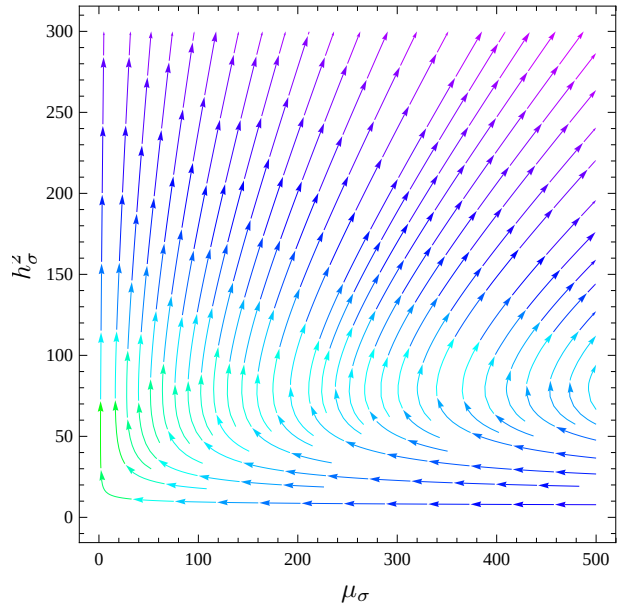

Figure 9.2: Stream plot of the Yukawa-system without gravitational interactions. The Gaussian fixed pointhas one perturbatively irrelevant and one marginal direction. In the marginal h_σ^2-direction the fixed point is weakly repulsive which is suggested the slow RG-running of the couplings in this region (green arrows).

Both diagrams give the same result, due to the Yukawa-vertex structure. Similarly, the flow of the scalar propagator reads

$$\partial_t \,(\text{ - - - - - - })_{\text{Yuk}} = -2 \quad = \frac{1}{Z_\phi}\left(\frac{\dot{m}_\sigma^2}{k^2} - \eta_\sigma(p^2+\mu_\sigma)\right). \tag{9.9}$$

The triangle diagrams that contribute to the flow of h_σ^2 are zero for one fermion flavour. We have

$$\partial_t \left(\quad \right)_{\text{Yuk}} = \quad + \quad = 0\,, \qquad \partial_t \left(\quad \right)_{\text{Yuk}} = \quad + \quad = 0\,. \tag{9.10}$$

Hence, the flow of the Yukawa coupling is completely governed by the anomalous dimensions. For Litim's cutoff evaluated at $p = 0$ we obtain flow equations for the Yukawa system without gravity

$$\dot{\mu}_\sigma = (\eta_\sigma - 2)\mu_\sigma + \frac{h_\sigma^2\,(5-\eta_\psi)}{20\pi^2}\,, \tag{9.11a}$$

$$\dot{h}_\sigma^2 = (\eta_\sigma + 2\eta_\psi)h_\sigma^2\,, \tag{9.11b}$$

$$\eta_\sigma = -\frac{(\eta_\psi - 4)\,h_\sigma^2}{16\pi^2}\,, \tag{9.11c}$$

$$\eta_\psi = -\frac{(\eta_\phi - 5)\,h_\sigma^2}{40\pi^2\,(1+\mu_\sigma)^2}\,, \tag{9.11d}$$

which agrees with [66]. Before analyzing this system of flow equations in more detail, we consider the relation of this system to the NJL-model discussed in the previous section. Using equation (9.3) we derive a flow equation for the 4-Fermi coupling λ_σ. It reads

$$\dot{\lambda}_\sigma = 2\lambda_\sigma + k^2\partial_t\left(\frac{h_\sigma^2}{m_\sigma^2}\right) = \frac{\dot{h}_\sigma^2}{\mu_\sigma} - \frac{h_\sigma^2}{\mu_\sigma^2}\frac{\dot{m}_\sigma^2}{k^2}\,, \tag{9.12}$$

$$= 2\lambda_\sigma + (\eta_\sigma + 2\eta_\psi)\lambda_\sigma - \frac{\lambda_\sigma}{\mu_\sigma}\left(\eta_\sigma\mu_\sigma + \frac{h_\sigma^2\,(5-\eta_\psi)}{20\pi^2}\right)\,, \tag{9.13}$$

$$= 2(1+\eta_\psi)\lambda_\sigma - \lambda_\sigma^2\frac{(5-\eta_\psi)}{20\pi^2}\,. \tag{9.14}$$

This result differs from the beta function for λ_σ we derived from the four fermion diagram given in (8.9a). As is discussed in [66], we recover the flow (9.14) for the 4-Fermi case by a suitable projection of the 4-Fermi flow with γ-matrices. We account the deviation of (9.14) from (8.9a) for the absence of the Fierz ambiguity in the bosonized description of the theory.

Now we discuss the flow of our Yukawa model without gravity. Figure 9.2 depicts a stream plot of the system of flow equations given by (9.11). The Yukawa model without gravity admits only a Gaussian fixed point. It has one UV-irrelevant and a marginal direction. For Gaussian fixed points, the linear stability is determined completely by the canonical scaling, i.e., the mass dimensions of the couplings μ_σ and h_σ^2. The critical exponents for the Gaussian fixed point are given in Table 9.1. In the marginal eigendirection the fixed point is weakly repulsive. This indicates a logarithmical running of the coupling towards a Landau pole driven by the anomalous dimensions of the theory. In Figure 9.2 the slow running is reflected by the green arrow close to fixed point.

9.2 Yukawa-Gravity System

The introduction of gravity gives rise to a variety of different diagrams that contribute to the flow of h_σ. Furthermore, in great difference to what we had in the 4-Fermi case, the Yukawa system is not decoupled from the rest of the gravity-fermion system. Instead it couples back via the anomalous dimensions of the fermion and the graviton. The system of flow equations is given by

$$\partial_t\,(\;\longrightarrow\;)^{-1}_{\text{Grav-Yuk}} = \partial_t\,(\;\longrightarrow\;)_{\text{Yuk}} + \partial_t\,(\;\longrightarrow\;)_{\text{Grav}}\,, \tag{9.15a}$$

$$\partial_t\,(\;\text{- - - - - -}\;)^{-1}_{\text{Grav-Yuk}} = \partial_t\,(\;\text{- - - - - -}\;)_{\text{Yuk}} + \partial_t\,(\;\text{- - - - - -}\;)_{\text{Grav}}\,, \tag{9.15b}$$

$$\partial_t\left(\text{- -}\right)_{\text{Grav-Yuk}} = \frac{1}{2} + + - \tag{9.15c}$$

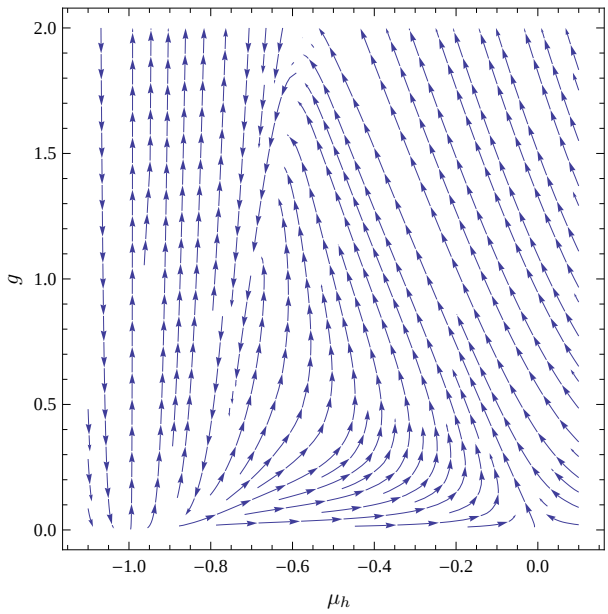

Figure 9.3: Phase diagram of a simplified gravity-matter system with $N_f = 1$ and $N_s = 2$. The system without Yukawa interaction exhibits two fixed points, one of which is the Gaussian one.

The only contributions to the system we have to calculate constitute the flow of h_σ^2. For Litim's cutoff at $p = 0$, we have

$$\dot{h}_\sigma^2 = (\eta_\sigma + 2\eta_\psi)h_\sigma^2 + \frac{g h_\sigma^2}{560\,(1+\mu_h)^2\,(1+\mu_\sigma)^2\,\pi}\Big(-47\eta_h\left(3 + 22\mu_\sigma + 19\mu_\sigma^2\right) , \\ + 4\eta_\psi\,(1+\mu_h)\left(61 + 94\mu_\sigma + 33\mu_\sigma^2\right) - 4\left(273 + 94(-21 + 2\eta_\sigma)\mu_\sigma - 1071\mu_\sigma^2 \right. \\ \left. +\mu_h\left(371 + 2(-301 + 94\eta_\sigma)\mu_\sigma + 203\mu_\sigma^2\right)\right)\Big) . \quad (9.16)$$

9.2.1 Gravity-Matter system

In this section, we specify the gravity-matter system we employ for the analysis of the gravity-Yukawa. We employ the the simplified gravity-matter system discussed in section 7.2.2 for $N_f = 2$, $N_s = 1$, $\mu_\sigma \neq 0$. Thus, we identify λ_3 and the graviton mass μ_h by

$$\lambda_3 = -\frac{1}{2}\mu_h . . \quad (7.1)$$

The three-dimensional parameter space of the simplified gravity-matter system with $\mu_\sigma \neq 0$ is given by

$$(g, \mu_h, \mu_\sigma) .$$

FP-Number	g^*	μ_σ^*	$\theta_{1,2}$
1	0	0	$\{-2, 2\}$
2	0.66	-0.73	$\{-21 \pm 49i\}$

Table 9.2: Fixed points for the gravity-matter system with $N_f = 1$ and $N_s = 0$ for $m_\sigma = 0$. Fixed point 2 is UV-attractive whereas the Gaussian fixed point has one UV-unstable direction.

For $\mu_\sigma = 0$ the phase diagram for (g, μ_h) is depicted in Figure 9.3. The phase diagram suggests two fixed points for the system. They are given in Table 9.2. The UV-behavior is controlled by the UV-attractive non-Gaussian fixed point.

9.2.2 Merging the two Systems

After having studied the Yukawa and the gravity-matter systems separately, we now investigate the interplay of both systems. To this end, we sum up the flow contribution both systems according to (9.15) and include the Yukawa-coupling. The set of flowing parameters extends to four. We have

$$(g, h_\sigma^2, \mu_h, \mu_\sigma).$$

The fixed point values for the gravity-Yukawa system are given in Table 9.3. Clearly, the combined system admits again, a Gaussian fixed point (FP 1). Also we have the non-Gaussian fixed that we conjectured in equation (9.5) (FP 2). A third non-Gaussian fixed point with non-vanishing Yukawa-coupling $h_\sigma^{2,*} \neq 0$ is also observed (FP 3). Interestingly, for FP 2 the non-interacting matter-gravity subsystem has approached its non-Gaussian fixed point, whereas the Yukawa subsystem is at its Gaussian fixed point. The residual gravity interactions at FP 2 turn h_σ^2 into a perturbatively relevant coupling. Thus, h_σ^2 does not run into a Landau pole in the UV. The Yukawa-gravity theory admits a sensible UV limit which is not true for Yukawa system without gravity.

FP	$g*$	$h_\sigma^{2,*}$	μ_h^*	μ_σ^*	$\theta_{1,2,3}$
1	0	0	0	0	$\{2, 0, -2, -2\}$
2	0.66	0	-0.73	0	$\{-21 \pm 49i, -4.1, -2.6\}$
3	0.63	4.18	-0.72	0.22	$\{-21 \pm 47i, -1.1, 1.5\}$

Table 9.3: Fixed points and critical exponents of the gravity-Yukawa system. The Gaussian fixed points persist after unification and result in an overall Gaussian fixed point. Furthermore, two other fixed points (FP 2 and FP 3) with vanishing and non-vanishing Yukawa-coupling $h_\sigma^{2,*}$ are found.

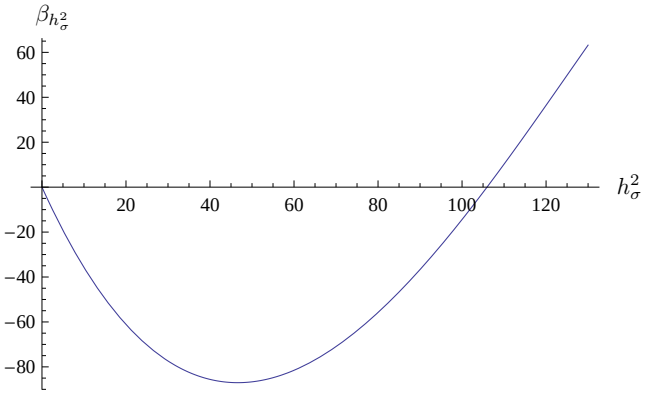

Figure 9.4: The β-function for the Yukawa coupling in the vicinity of FP2. One can see, that there exists a UV-stable fixed point for $h_\sigma^2 = 0$. Thus the initially marginal coupling becomes relevant in the UV due to gravity interactions.

Figure 9.4 depicts the β-function for h_σ^2 as function of h_σ^2 in the vicinity of FP2. The negative slope around $h_\sigma^2 = 0$ reflects the UV-stability of the fixed point. This is opposed to what we found for $\beta_{h_\sigma^2}$ in the pure Yukawa (see Figure 9.1). The third and last fixed point, FP3, has non-vanishing Yukawa coupling and is UV unstable. Furthermore, it has a non-vanishing scalar mass. Apparently, the Yukawa interaction at FP 3 slightly perturbs the fixed point values of the gravity-matter subsystem.

9.3 Conclusions and Outlook

In our simple model of a gravity-Yukawa system the initially marginal Yukawa coupling becomes relevant due to gravitational interactions. For the complete system, we found a fully attractive UV fixed point. Thereby, the running of the Yukawa coupling towards a Landau pole is prevented by the interaction with gravity. Thus, the interaction of matter systems with asymptotically safe quantum gravity can have a curing effect on the UV behavior of marginal couplings. If this mechanism generalises to more than one fermion flavour it could be a great asset to the Standard Model. There it would allows a well defined UV limit for the Yukawa interactions.

An interesting further study could concern the relation between the flow of h_σ^2 and that of λ_σ in the 4-Fermi system. Since both are connected by a Hubbard-Stratonovich transformation in flat space, h_σ^2 is interpreted as modeling a momentum dependent Yukawa coupling. As discussed in the beginning of this chapter two couplings are related by equation (9.12). A very interesting question could be how the avoidance of chiral symmetry breaking at the Planck scale discussed in chapter 8 expresses itself in the gravity-Yukawa system.

10 Discussion and Conclusions

In this work, we studied the asymptotic safety scenario of quantum gravity and its consistency under the inclusion of matter. In the first part I, we introduced the methods which we used for our investigation.

In the second part II, we first considered the locality in momentum space of the graviton n-point functions. We showed that the flow of the graviton 3-point function approaches a constant for large momenta. Thus, the ratio of the flow for the 3-point functions and the 3-points function itself quickly approaches to zero for large momenta. This property is absent in many other quantum field theories. Therefore, we account it for diffeomorphism invariance of the formulation. We argue that locality is mandatory for quantum gravity. When 'flowing up' towards the UV, non-local theories obtain a spurious dependence on the path integral regularization [39] at high energies which we regard as unphysical. Locality in momentum space for the graviton 2-point function was shown in [27].

In the latter of Part II we verified the non-Gaussian fixed point for the pure gravity system. Subsequently, we used the non-Gaussian fixed point of the pure gravity system as a starting point for the analysis of the gravity-matter system. Thus, we successively introduced an increasing number of fermion and scalar fields and observed the impact of the matter perturbations of the non-Gaussian fixed point. We found that the pure-gravity non-Gaussian fixed point persists under the inclusion of arbitrary numbers of fermions and scalars. Furthermore, in all considered truncation stages the behaviour of the fixed point under the inclusion of matter was consistent. Thus, fermions are in favor of the non-Gaussian fixed point. Furthermore, the inclusion of fermion fields lowers the fixed point values of the dimensionless Newton coupling g and the dimensionless graviton mass μ_h. The fixed point value of the 'third cosmological constant' λ_3 is increased with increasing fermion number. We interpret this behaviour as gravitational shielding of fermions in the UV.

Scalar fields have the opposite effect on the non-Gaussian fixed point of the pure gravity setup. Thus, they are in disfavor of the non-Gaussian fixed point within the effective one-loop approximation. However, the system non-Gaussian fixed point persists under the inclusion of an arbitrary number of scalar fields. The successive increase of the number of scalars leads to an increase of the fixed point values for g and μ. The coupling λ_3 is lowered at the fixed point with increasing number of scalars. Hence, scalars were found to enhance gravity in the UV. The results we found for the impact of non-interacting matter on the non-Gaussian fixed point are different from other investigations [20, 21]. On an effective one-loop basis, the matter contributions in [20, 21, 60, 61] have the opposite signs to what we found.

Although all of these sources used different truncations and approximation schemes, the sign difference on the one- loop level is alarming and should be studied further.

We investigated all systems with and without the dynamical treatment of λ_3. We found that including λ_3 improves the behaviour of the considered systems. Thus, it lowers the anomalous dimensions in the pure gravity system. Furthermore, it decreases the critical exponents of the non-Gaussian fixed point in all systems considerably. This is in agreement with the findings in [17, 21, 64], where the inclusions of higher order operators lead to convergence of the critical exponents.

On the technical level, it was found that the approximation of momentum dependencies of the 2-point functions and the graviton 3-point functions by means of the derivatives at $p = 0$ is not justified. Instead, an improved momentum projection scheme was employed in section 7.3.2 which reflects the actual momentum dependence of the flow more accurately.

In Part III we investigated the implications of the asymptotic safety scenario on interacting matter systems. We interpreted these as toy models for the unification of the Standard Model of Particle physics and asymptotically safe quantum gravity. In chapter 8 we considered induced 4-fermion interactions that are generated by graviton fluctuation. We showed, that the induced correlations for our system cannot break chiral symmetry at the Planck scale. We were able to show this for our truncation on general, regulator independent grounds for an arbitrary number of fermion flavours. This result suggests, that there is a natural mechanism which prevents fermions from gaining mass at the Planck scale. These findings are in agreement with those in [22] for a specific regulator. We see this result as further evidence for the compatibility of the Standard Model of Particle Physics and asymptotically safe quantum gravity. The result that chiral symmetry is not broken by gravity at the Planck scale is in agreement with the observation of light fermions in the universe and, thus, with the Standard Model of Particle Physics [22].

In chapter 9 we considered a Yukawa theory in the presence of asymptotically safe quantum gravity. We investigated the influence of the interacting UV fixed point of quantum gravity on the flow of the Yukawa interaction. Without gravity, the Yukawa coupling is marginal and approaches a Landau pole according to a perturbative treatment [29, 71–73]. The introduction of gravitational interactions in the UV was found to make the Yukawa coupling perturbatively relevant. We interpret this as a curing effect of the UV behaviour of asymptotically safe quantum gravity on the Yukawa system. It suggests that a Landau poles in systems of this type are avoided through the interaction with gravity. This is seen as further evidence for the consistency of asymptotically safe quantum gravity with the Standard Model of Particle Physics.

This work provides further evidence for the asymptotic safety scenario of quantum gravity. We were able to confirm the finding of a non-Gaussian fixed point of the renormalisation group flow. Furthermore, the inclusion of non-interacting and interacting matter was consistent with the asymptotic safety scenario. We found evidence for consistence of the Standard Model of Particle Physics with asymptotically safe quantum gravity for two toy models of 4-Fermi and Yukawa interactions.

Part IV

Appendix

A Notation and Conventions

Multi-Indices

Within this work, in particular in the first chapters we will employ a multi-index notation which we adopt from [34]. The multi-indices $\boldsymbol{\mathcal{A}}$ include all external and internal indices of the general superfield Φ. A superfield is a vector consisting of all fluctuating quantum fields and is given by

$$\Phi_{\boldsymbol{a}} = (h_{\mu\nu}(x_1), \bar{c}_\rho(x_2), c_\sigma(x_3), \bar{\psi}^a_A(x_4), \psi^b_B(x_5), \phi^c(x_6))\,, \tag{A.1}$$

where $\mu, \nu, \rho, \sigma \in \{1, \ldots, 4\}$ are spacetime indices, $a, b \in \{1, \ldots, N_f\}$ are fermion flavour indices, $A, B \in \{1, \ldots, 4\}$ are spinor indices and $c \in \{1, \ldots, N_s\}$ is a colour index. In general, $\mathbf{a_i}$ is given by

$$\mathbf{a_i} = (\text{flavour index}, \text{colour index}, \text{spacetime indices}, \text{spinor index}, \text{coordinate}) \tag{A.2}$$

The coordinates can be given by a spacetime or a momentum vector $\boldsymbol{x}$ or $\boldsymbol{p}$, respectively. As an example, we consider the spinor field $\bar{\psi}$. For $\bar{\psi}$ in position space we have

$$\bar{\psi}_{\mathbf{a}} = \bar{\psi}^a_A(\mathbf{x}) \tag{A.3}$$

Hence, in case of $\bar{\psi}$, $\mathbf{a}$ is given by

$$\mathbf{a} = (a, A, \mathbf{x}) \tag{A.4}$$

The raising and lowering of multi-indices is performed with help of the ultra-local metric $\boldsymbol{\gamma}$ which should not be confused with the γ-matrices important for the formulation of covariant spinors. The metric $\boldsymbol{\gamma}$ is diagonal in field space for scalar fields as h or ϕ. However, for spinor fields it is antisymmetric. Hence, for the pair of fermion fields $\phi_{\boldsymbol{\mathcal{A}}} = (\bar{\psi}^m_A(x), \psi^n_B(x))_{\mathcal{A}}$, the field-space part of $\boldsymbol{\gamma}$ is given by

$$(\gamma^{\mathcal{A}\mathcal{B}}) = \begin{pmatrix} 0 & 1 \\ -1 & 0 \end{pmatrix} \tag{A.5}$$

Furthermore, $\boldsymbol{\gamma}$ is diagonal in all other indices and a δ-function in position or momentum space, accounting for ultra-locality. Therefore, the non-trivial behavior of $\boldsymbol{\gamma}$ is present in field space. Raising and lowering of indices in field space is defined via

$$\varphi^{\mathcal{A}} = \gamma^{\mathcal{A}\mathcal{B}}\varphi_{\mathcal{B}} \tag{A.6}$$

$$\varphi_{\mathcal{A}} = \varphi^{\mathcal{B}}\gamma_{\mathcal{B}\mathcal{A}} \tag{A.7}$$

We denote field variations by

$$\frac{\delta \mathcal{F}[\phi]}{\delta \phi^{\mathbf{a}}} = \mathcal{F}[\phi]_{\mathbf{a}|}. \tag{A.8}$$

Spacetime Indices

In this work, we will mainly calculate in flat background with euclidean signature of the metric. For that, we assume that there exists a well defined analytic continuation of the (mostly-plus) Minkowski metric $\tilde{\eta}_{\mu\nu}$ to the computationally favored 4-dimensional Euclidean metric $\eta_{\mu\nu}$

$$(\tilde{\eta}_{\mu\nu}) = \mathrm{diag}(-1,1,1,1) \longrightarrow (\delta_{\mu\nu}) = (\eta_{\mu\nu}) \tag{A.9}$$

In general, it is unclear whether the analytic continuation is possible without picking up poles or discontinuities in the complex plane. Within this work however, we will just assume the continuation exists.

We define the symmetrization of spacetime indices for a general tensor M as

$$M_{\mu\ldots(\nu\rho)\ldots\sigma} = \frac{1}{2}\left(M_{\mu\ldots\nu\rho\ldots\sigma} + M_{\mu\ldots\rho\nu\ldots\sigma}\right) \tag{A.10}$$

Fourier Transform

The Fourier we use to transform to transform between momentum and position coordinates for a general function f is given by

$$\tilde{f}(\mathbf{p}) = \int f(\mathbf{x}) e^{-i\mathbf{x}\cdot\mathbf{p}} \frac{d^4x}{(2\pi)^4} \tag{A.11}$$

$$f(\mathbf{x}) = \int \tilde{f}(\mathbf{p}) e^{i\mathbf{x}\cdot\mathbf{p}} d^4p \tag{A.12}$$

Hence, the δ-function can be written in terms of the Fourier-integral

$$\delta(\mathbf{x}-\mathbf{y}) = \frac{1}{(2\pi)^4} \int e^{\pm i\mathbf{p}\cdot(\mathbf{x}-\mathbf{y})} d^4x \tag{A.13}$$

A.1 Variation of the Classical Action

The curvature tensor is given in terms of the Levi-Civita-connection by

$$R^{\sigma}{}_{\mu\nu\rho} = \Gamma^{\sigma}_{\mu\rho,\nu} - \Gamma^{\sigma}_{\mu\nu,\rho} + 2\Gamma^{\tau}_{\mu(\nu}\Gamma^{\sigma}_{\rho)\tau}\,. \tag{A.14}$$

The connection in terms of the metric reads

$$\Gamma^{\sigma}_{\mu\nu} = \frac{1}{2} g^{\sigma\tau}\left(2g_{\tau(\mu,\nu)} - g_{\mu\nu,\tau}\right)\,. \tag{A.15}$$

We write the n^{th}-variation of the connection in terms $\delta g_{\mu\nu} = h_{\mu\nu}$ as

$$\delta^n \Gamma^{\nu}_{\mu\lambda} = (-1)^{n-1} \frac{n!}{2} h^{(n-1)\mu\sigma} (2\bar{D}_{(\mu} h_{\lambda)\sigma} - \bar{D}_{\sigma} h_{\lambda\mu}) \tag{A.16}$$

With these relations we can formulate the variation of the curvature scalar. We arrive at the Ricci tensor $R_{\mu\nu}$ by contacting two indices of the curvature tensor according to

$$R^{\sigma}{}_{\mu\sigma\rho} = R_{\mu\rho} \,. \tag{A.17}$$

Contraction the Ricci tensor we arrive at

$$g^{\mu\nu} R_{\mu\mu} = R^{\mu}{}_{\mu} = R \,. \tag{A.18}$$

We derive variations of the square root of the determinant of the metric as follows. We write

$$\sqrt{g} = e^{\frac{1}{2} \operatorname{Tr} \ln g_{\mu\nu}} \,. \tag{A.19}$$

Having this, we apply Fàa di Bruno's formula for the derivation of the variations.

The derivation of the variations of the γ-matrices, the spin metric $\mathfrak{h}$ and the spin connection Γ_{μ} we derived by Kevin Falls and Andreas Rodigast. The detailed derivation can be found in [57]. The calculations of the vertices were done with help of TARDIS, a computer prgram for the derivation of FRG equations from the classical action. TARDIS was written by Andreas Rodigast.

A.2 Gauge Dependencies

Graviton Green's Functions for general gauges

$\alpha = 0$, $\beta = -1$

$$(\Gamma_k^{(hh)} + R_k) = \begin{pmatrix} \frac{1}{32\pi}\left(m_h^2 + p^2(r+1)\right) & 0 & 0 & 0 \\ 0 & \frac{\alpha m_h^2 + p^2(r+1)}{32\pi\alpha} & 0 & 0 \\ 0 & 0 & -\frac{\alpha m_h^2 + p^2(r+1)(4\alpha-3)}{64\pi\alpha} & -\frac{\sqrt{3}\left(\alpha m_h^2 + p^2(r+1)\right)}{64\pi\alpha} \\ 0 & 0 & -\frac{\sqrt{3}\left(\alpha m_h^2 + p^2(r+1)\right)}{64\pi\alpha} & \frac{\alpha m_h^2 + p^2(r+1)}{64\pi\alpha} \end{pmatrix} \tag{A.20}$$

$$(\Gamma_k^{(hh)}+R_k)^{-1}\circ\dot{R}_k^h\circ(\Gamma_k^{(hh)}+R_k)^{-1}=$$
$$\begin{pmatrix}\frac{32\pi p^2\dot{R}}{\left(m_h^2+p^2(r+1)\right)^2} & 0 & 0 & 0\\ 0 & \frac{32\pi p^2\dot{R}\alpha}{\left(\alpha m_h^2+p^2(r+1)\right)^2} & 0 & 0\\ 0 & 0 & -\frac{16\pi p^2\dot{R}}{\left(m_h^2+p^2(r+1)\right)^2} & -\frac{16\pi\sqrt{3}p^2\dot{R}}{\left(m_h^2+p^2(r+1)\right)^2}\\ 0 & 0 & -\frac{16\pi\sqrt{3}p^2\dot{R}}{\left(m_h^2+p^2(r+1)\right)^2} & \frac{16\pi p^2\dot{R}\left(\alpha(4-3\alpha)m_h^4+2p^2(r+1)\alpha m_h^2+p^4(r+1)^2(4\alpha-3)\right)}{\left(m_h^2+p^2(r+1)\right)^2\left(\alpha m_h^2+p^2(r+1)\right)^2}\end{pmatrix} \tag{A.21}$$

General α and β

$$(\Gamma_k^{(hh)}+R^h)=$$
$$\begin{pmatrix}\frac{m_h^2+p^2(r+1)}{32\pi} & 0 & 0 & 0\\ 0 & \frac{\alpha m_h^2+p^2(r+1)}{32\pi\alpha} & 0 & 0\\ 0 & 0 & -\frac{4\alpha m_h^2+p^2(r+1)\left(16\alpha-3(\beta-1)^2\right)}{256\pi\alpha} & \frac{\sqrt{3}\left(p^2(r+1)(\beta+3)(\beta-1)-4m_h^2\alpha\right)}{256\pi\alpha}\\ 0 & 0 & \frac{\sqrt{3}\left(p^2(r+1)(\beta+3)(\beta-1)-4m_h^2\alpha\right)}{256\pi\alpha} & \frac{4\alpha m_h^2+p^2(r+1)(\beta+3)^2}{256\pi\alpha}\end{pmatrix} \tag{A.22}$$

$$(\Gamma_k^{(hh)}+R^h)^{-1}=\begin{pmatrix}\frac{32\pi}{m_h^2+p^2(r+1)} & 0 & 0 & 0\\ 0 & \frac{32\pi\alpha}{\alpha m_h^2+p^2(r+1)} & 0 & 0\\ 0 & 0 & m_w & m_{sw}\\ 0 & 0 & m_{ws} & m_s\end{pmatrix} \tag{A.23}$$

with

$$m_w=-\frac{16\pi\left(4\alpha m_h^2+p^2(r+1)(\beta+3)^2\right)}{4\alpha m_h^4+2p^2(r+1)\left(-\beta^2+2\alpha+3\right)m_h^2+p^4(r+1)^2(\beta+3)^2} \tag{A.24}$$

$$m_s=\frac{16\pi\left(4\alpha m_h^2+p^2(r+1)\left(16\alpha-3(\beta-1)^2\right)\right)}{4\alpha m_h^4+2p^2(r+1)\left(-\beta^2+2\alpha+3\right)m_h^2+p^4(r+1)^2(\beta+3)^2} \tag{A.25}$$

$$m_{sw}=\frac{16\sqrt{3}\pi\left(p^2(r+1)\left(\beta^2+2\beta-3\right)-4m_h^2\alpha\right)}{4\alpha m_h^4+2p^2(r+1)\left(-\beta^2+2\alpha+3\right)m_h^2+p^4(r+1)^2(\beta+3)^2} \tag{A.26}$$

$$m_{ws}=m_{sw} \tag{A.27}$$

$$(\Gamma_k^{(hh)} + R_k)^{-1} \circ \dot{R}_k^h \circ (\Gamma_k^{(hh)} + R_k)^{-1} = \begin{pmatrix} \frac{32\pi p^2 \dot{R}}{\left(m_h^2 + p^2(r+1)\right)^2} & 0 & 0 & 0 \\ 0 & \frac{32\pi p^2 \dot{R}\alpha}{\left(\alpha m_h^2 + p^2(r+1)\right)^2} & 0 & 0 \\ 0 & 0 & n_s & n_{sw} \\ 0 & 0 & n_{ws} & n_w \end{pmatrix} \tag{A.28}$$

with

$$n_w = -\frac{16\pi p^2 \dot{R}}{\det \boldsymbol{n}} \left(4\alpha m_h^4 \left((\beta-3)^2 - 12\alpha\right) + 8\alpha(\beta+3)^2 m_h^2 p^2 (r+1) + (\beta+3)^2 p^4 (r+1)^2 \left(16\alpha - 3(\beta-1)^2\right)\right) \tag{A.29}$$

$$n_s = \frac{16\pi p^2 \dot{R}}{\det \boldsymbol{n}} \left(4\alpha m_h^4 \left(4\alpha - 3(\beta+1)^2\right) + 8\alpha(\beta+3)^2 m_h^2 p^2 (r+1) + (\beta+3)^4 p^4 (r+1)^2\right) \tag{A.30}$$

$$n_{sw} = -\frac{16\sqrt{3}\pi p^2 \dot{R}}{\det \boldsymbol{n}} \left(-4\alpha m_h^4 \left(4\alpha - \beta^2 + 2\beta + 3\right) - 8\alpha(\beta+3)^2 m_h^2 p^2 (r+1) + (\beta-1)(\beta+3)^3 p^4 (r+1)^2\right) \tag{A.31}$$

$$\det \boldsymbol{n} = \left(4m_h^4 \alpha + 2m_h^2 p^2 (r+1)\left(2\alpha - \beta^2 + 3\right) + p^4 (r+1)^2 (\beta+3)^2\right)^2 \tag{A.32}$$

Anomalous dimensions

It is an interesting question in which way the flow depends on the graviton gauge choice. As an example of the gauge dependence of the calculated quantities we take a look at the matter anomalous dimension as a function of the gauge parameter β. Recapitulate that for most of the present work, we made the gauge choice

$$\alpha = 0 \tag{A.33}$$

$$\beta = 1 \tag{A.34}$$

For $\alpha = 0$ both gauge fixing parameters are at a fixed point [74] for any β. Therefore, we can choose β at will and still do not have worry about flowing gauge parameters. In terms of an arbitrary β, the anomalous dimensions of the matter fields ψ and ϕ

are given by:

$$\begin{aligned}\eta_\psi =&\frac{1}{32\pi\left(\mu_h+1\right)^2\left((\beta+3)^2-2\left(\beta^2-3\right)\mu_h\right)^2}\Big((\eta_h-6)g\Big((\beta+3)^2(5\beta(\beta+10)+81)\\&+(2\beta(\beta(5\beta(3\beta-2)-112)+18)+354)\mu_h^2-8(\beta+3)^2\left(5\beta^2-14\right)\mu_h\Big)\Big)\\&-\frac{(\beta-3)g\left(3\left((7\eta_f-34)\mu_f+\eta_f-6\right)-\beta(\eta_f-6)\left(\mu_f-1\right)\right)}{40\pi\left(\mu_f+1\right)^2\left(2\left(\beta^2-3\right)\mu_h-(\beta+3)^2\right)}\\&-\frac{3(\beta+3)^2g\left(\eta_h\left(112\mu_f-3(\beta-13)(\beta+3)\right)-7\left(160\mu_f-3(\beta-13)(\beta+3)\right)\right)}{560\pi\left(\mu_f+1\right)\left((\beta+3)^2-2\left(\beta^2-3\right)\mu_h\right)^2}\end{aligned} \tag{A.35}$$

$$\begin{aligned}\eta_s =&-\frac{12(\beta+3)^2g\mu_s^2}{\pi\left(\mu_s+1\right)^2\left((\beta+3)^2-2\left(\beta^2-3\right)\mu_h\right)^2}-\\&\frac{(\beta+3)^2g\left((\beta+1)^2(\eta_h-8)+32(\eta_h-6)\mu_s\right)}{16\pi\left(\mu_s+1\right)\left((\beta+3)^2-2\left(\beta^2-3\right)\mu_h\right)^2}+\\&\frac{g\left((\beta+1)^2(\eta_s-8)-32\beta(\eta_s-6)\mu_s\right)}{16\pi\left(\mu_s+1\right)^2\left(2\left(\beta^2-3\right)\mu_h-(\beta+3)^2\right)}\end{aligned} \tag{A.36}$$

In particular, let us take a look at the scalar anomalous dimension η_ϕ for massless scalars, i.e. $\mu_\phi = 0$

$$\eta_\phi\Big|_{\mu_s=0} = \frac{(\beta+1)^2g\left((\eta_s-8)\left(2\left(\beta^2-3\right)\mu_h-(\beta+3)^2\right)-(\beta+3)^2(\eta_h-8)\right)}{16\pi\left((\beta+3)^2-2\left(\beta^2-3\right)\mu_h\right)^2} \tag{A.37}$$

We note, that the scalar anomalous dimension vanishes in the case $\beta = 1$

$$\eta_\phi\Big|_{\beta=1,\mu_s=0} = 0, \tag{A.38}$$

which precisely the gauge we are using (cf. (A.33)). The choice $\beta = -3$ also offers a simplifaction since it make two out of three term in equation (A.37) vanish. This is a choice of gauge for which the graviton propagator is diagonal in the projection basis and has only two non-vanishing components:

$$\eta_\phi\Big|_{\beta=-3,\mu_s=0} = \frac{(\eta_s-8)g}{48\pi\mu_h}, \tag{A.39}$$

One can notice from equation (A.37) that there no choice of gauge is able to change the sign of the anomalus dimension. Thus, the sign of the anomalous dimension at least in this case and for a De-Donder-type gauge is gauge independent. The fermion anomalous dimension η_ψ cannot be set to zero that easily. However, (A.35) becomes particularly simple for $\beta = 3$. In this case η_ψ reads

$$\eta_\psi\Big|_{\beta=3} = \frac{25(\eta_h-6)g}{96\pi\left(\mu_h+1\right)^2}+\frac{g\left(3(\eta_f-6)\left(\mu_f-1\right)+3\left((7\eta_f-34)\mu_f+\eta_f-6\right)\right)}{80\pi\left(\mu_f+1\right)^2\mu_h} \tag{A.40}$$

For massless fermions, equation (A.40) even takes the simple form

$$\eta_\psi\Big|_{\beta=3,\mu_f=0} = \frac{25(\eta_h-6)g}{96\pi\left(\mu_h+1\right)^2} \tag{A.41}$$

Hence, tuning the parameter β can have computational advantages like the vanishing of some of the anomalous dimensions. However, the variation obey certain restrictions such as fixed signs. A detailed optimisation could lead to a significaNT simplification of the flow.

A.3 Distributive Corrections

In order to extract momentum dependent quantities from the diagrams, we have to take second derivatives of Heaviside-Theta function. This is sometimes problematic since it involves products of distributions. For the treatment of the contracted diagrams Mathematica is used, which is not capable of solving this problem.Hence, we want to find the non-analytical correction due to the second derivative of the fermion propagator by using pen and paper. Our analysis is done for a Litim-type shape-function for scalars (gravitons and ghosts) and fermions:

$$r_{\mathrm{s}}(p) = \left(\frac{1}{p}-1\right)\theta(1-p^2) \tag{A.42a}$$

$$r_{\mathrm{f}}(p) = \left(\frac{1}{p}-1\right)\theta(1-p^2) \tag{A.42b}$$

The corresponding propagators read:

$$G_{\mathrm{f}}(p) = \frac{1}{-i\not{p} - i(\frac{\not{p}}{p}-\not{p})\theta(1-p^2)+m_f} \tag{A.43a}$$

$$G_{\mathrm{s}}(p) = \frac{1}{p^2+(1-p^2)\theta(1-p^2)+m_s^2} \tag{A.43b}$$

We rewrite the Green's functions by splitting the into the parts, where the respective θ-function is constant. The equations (A.43) can be conveniently be rewritten as

$$G_i(p) = f_i(p)\theta(1-p^2) + g_i(p)\theta(p^2-1) \tag{A.44}$$

with $i \in \{\mathrm{s},\mathrm{f}\}$. The functions f_i and g_i are given by:

$$f_{\mathrm{s}}(p) = \frac{1}{1+m^2} \qquad f_{\mathrm{f}}(p) = \frac{\left(i\frac{\not{p}}{p}+m\mathbb{1}\right)}{1+m^2} \tag{A.45}$$

$$g_{\mathrm{s}}(p) = \frac{1}{p^2+m^2} \qquad g_{\mathrm{f}}(p) = \frac{i\not{p}+m\mathbb{1}}{p^2+m^2} \tag{A.46}$$

Since the Green's functions are continuous, we have

$$f_i(p=1) = g_i(p=1) \tag{A.47}$$

For our analysis, we are interested in propagators with $p = p + q$. For convenience we introduce the notation $\boldsymbol{pq} = \boldsymbol{p} + \boldsymbol{q}$. Hence, we write

$$G_i(pq) = f_i(pq)\theta(1-pq^2) + g_i(pq)\underbrace{\theta(pq^2-1)}_{1-\theta(1-pq^2)} \tag{A.48}$$

$$= (f_i(pq) - g_i(pq))\theta(1-pq^2) - f_2(pq) \tag{A.49}$$

Since we are only interested in those parts of $\partial_p G$ and $\partial_p^2 G$, which are proportional to δ, we get rid of the second term in (A.49). Now, we take the first derivative of the remainder $G_{i,\delta}$ with respect to p

$$\partial_p G_{i,\delta}(pq) = \underbrace{-(f_i(pq) - g_i(pq))\delta(1-pq^2)2(p+qx)}_{=0}$$

$$+ \frac{p+qx}{pq}(f_i'(pq) - g_i'(pq))\theta(1-pq^2) \tag{A.50}$$

$$\partial_p G_{i,\delta}(pq) = \frac{p+qx}{pq}(f_i'(pq) - g_i'(pq))\theta(1-pq^2) \tag{A.51}$$

The first term in (A.50) is zero, because of (A.47). Thus, the first derivative will not have a contribution to the non-analytic part, since there is no δ-function involved. By taking another derivative of (A.51) and keeping only the term proportional to the δ-function, we get:

$$\partial_p^2 G_{i,\delta}(pq) = \qquad = -2(p+qx)\frac{p+qx}{pq}(f_i'(pq) - g_i'(pq))\delta(1-pq^2) \tag{A.52}$$

What appears in the diagrams is the product of (A.52) with the θ-function from $\dot{R}$, i.e., $\frac{1}{2}\theta(1-q^2)\partial_p^2 G_{i,\delta}(pq)$ evaluated at $p = 0$. This product can be calculated by regularising the δ and θ functions by a small parameter ε and then taking the limit $p \to 0$. This leads us to

$$\frac{1}{2}\theta_\varepsilon(1-q^2)\partial_p^2 G_{i,\delta}^\varepsilon(q) = -qx^2(f_i'(q) - g_i'(q))\theta_\varepsilon(1-q^2)\delta_\varepsilon(1-q^2) \tag{A.53}$$

Now we can take the limit $\varepsilon \to 0$:

$$\frac{1}{2}\theta(1-q^2)\partial_p^2 G_{i,\delta}(q) = -\frac{1}{2}qx^2(f_i'(q) - g_i'(q))\delta(1-q^2) \tag{A.54}$$

$$= -\frac{1}{4}x^2(f_i'(1) - g_i'(1))\delta(1-q) \tag{A.55}$$

By plugging in the derivatives

$$\partial_p f_{\mathrm{s}}(p=1) = 0 \qquad \partial_p f_{\mathrm{f}}(p=1) = \frac{i(\not{1}_{\not{p}} - \not{p})}{1+m^2} \tag{A.56}$$

$$\partial_p g_{\mathrm{s}}(p=1) = -\frac{2}{(1+m^2)^2} \qquad \partial_p g_{\mathrm{f}}(p=1) = \frac{i\not{1}_{\not{p}}}{1+m^2} - \frac{2(i\not{p} + m\mathbb{1})}{(1+m^2)^2} \tag{A.57}$$

Now, we bring everything together and write down the δ-contributions to the diagrams coming from the Green's functions $G_{i,\delta}$.

$$\frac{1}{2}\theta(1-q^2)\partial_p^2 G_{\mathrm{s},\delta}(q) = -\frac{x^2}{4(1+m^2)^2}\left((1-m^2)i\not{q}+2m\mathbb{1}\right)\delta(1-q) \tag{A.58a}$$

$$\frac{1}{2}\theta(1-q^2)\partial_p^2 G_{\mathrm{f},\delta}(q) = -\frac{x^2}{2(1+m^2)^2}\delta(1-q) \tag{A.58b}$$

The expressions (A.58) are used as additive diagrams with the respective Green's functions with momentum $\boldsymbol{p}+\boldsymbol{q}$ replaced by (A.58). It was verified that the resulting complete analytic results are equal to numerical result obtained with regularized θ-functions.

A.4 Fixed Points N_f Fermions with 4-Fermi Coupling

$$\lambda^*_{+,1} = -\frac{-\sqrt{2A\mathfrak{g}_N(2N-1)+Q_N^2}+Q_N}{4A(2N-1)} \tag{A.59a}$$

$$\lambda^*_{-,1} = -\lambda_{+,1} \tag{A.59b}$$

$$\lambda^*_{+,2} = -\frac{\sqrt{2A\mathfrak{g}_N(2N-1)+Q_N^2}+Q_N}{2A(2N-1)} \tag{A.59c}$$

$$\lambda^*_{-,2} = -\lambda_{+,2} \tag{A.59d}$$

$$\lambda^*_{+,3} = \frac{\sqrt{2A\mathfrak{g}_N(N-1)\left(2N^2+5N+9\right)+(N+3)^2Q_N^2}+(N+3)Q_N}{2A\left(2N^2+5N+9\right)} \tag{A.59e}$$

$$\lambda^*_{-,3} = \frac{-(N+3)\sqrt{2A\mathfrak{g}_N(N-1)\left(2N^2+5N+9\right)+(N+3)^2Q_N^2}+Q_N(3N^2+4N+9)}{2A(N-1)\left(2N^2+5N+9\right)} \tag{A.59f}$$

$$\lambda^*_{+,4} = \frac{-\sqrt{2A\mathfrak{g}_N(N-1)\left(2N^2+5N+9\right)+(N+3)^2Q_N^2}+(N+3)Q_N}{2A\left(2N^2+5N+9\right)} \tag{A.59g}$$

$$\lambda^*_{-,4} = \frac{(N+3)\sqrt{2A\mathfrak{g}_N(N-1)\left(2N^2+5N+9\right)+(N+3)^2Q_N^2}+Q_N(3N^2+4N+9)}{2A(N-1)\left(2N^2+5N+9\right)} \tag{A.59h}$$

where $Q = 1+\eta_\psi+\mathfrak{f}_N$. The first fixed point $\mathrm{FP}_1 = (\lambda^*_{+,1}, \lambda^*_{-,1})$ is again, the mean-to-be Gaussian fixed point for $g = 0$. Since the annihilation of fixed points takes place,

if the arguments in the square roots become imaginary, we now have two conditions for chiral symmetry breaking. These are given by:

$$2A\mathfrak{g}_N(2N-1)+Q^2<0 \tag{A.60a}$$

$$2A\mathfrak{g}_N(N-1)\left(2N^2+5N+9\right)+(N+3)^2Q^2<0 \tag{A.60b}$$

A.5 Gravity-Yukawa Diagrams

In the simplest approximation, we evaluate the flow at external momentum equal to zero, $p=0$, using Litim's regulator:

$$\eta_\psi = \frac{1}{8}\frac{\partial^2}{\partial p^2}\bigg|_{p=0}\dot{\Gamma}^{\bar{\psi}\psi} = \frac{h_\sigma^2\,(5-\eta_\phi)}{40\pi^2\,(1+\mu_\sigma)^2} \tag{A.61}$$

$$\frac{\dot{m}_\sigma^2}{k^2}-\eta_\sigma\mu_\sigma = \dot{\Gamma}^{\phi_i\phi_i}\bigg|_{p=0} = \frac{h_\sigma^2\,(5-\eta_\psi)}{20\pi^2} \tag{A.62}$$

$$\eta_\sigma = \frac{-1}{2}\frac{\partial^2}{\partial p^2}\bigg|_{p=0}\Gamma^{\phi_i\phi_i} = \frac{h_\sigma^2\,(4-\eta_\psi)}{16\pi^2} \tag{A.63}$$

As a first step, we investigate the behavior of the Yukawa-Gravity system for vanishing momenta for the tensor structure $\mathbb{1}\otimes\mathbb{1}-\gamma_5\otimes\gamma_5$.

$$\begin{aligned}\dot{\mu}_\sigma =&(\eta_\sigma-2)\mu_\sigma+\frac{h_\sigma^2\,(5-\eta_\psi)}{20\pi^2}+\\&+\frac{g\mu_\sigma}{2\pi}\left(\frac{(6-\eta_h)}{(1+\mu_h)^2\,(1+\mu_\sigma)}-\frac{(6-\eta_\phi)\,\mu_\sigma}{(1+\mu_h)\,(1+\mu_\sigma)^2}\right)\end{aligned} \tag{A.64a}$$

$$\begin{aligned}\dot{\mu}_h =&(\eta_h-2)\mu_h+\text{gravity part}\\&+\frac{g}{6\pi}\left(\frac{(\eta_\phi-6)\,\mu_\sigma}{(\mu_\sigma+1)^2}-\frac{\eta_\phi-10}{10\,(\mu_\sigma+1)^3}+(\eta_\psi-6)-\frac{3(\eta_\psi-7)}{16}\right)\end{aligned} \tag{A.64b}$$

$$\eta_\sigma = -\frac{(\eta_\psi-3)\,h_\sigma^2}{16\pi^2}+\frac{g}{2\pi}\left(\frac{(\eta_h-6)\,\mu_\sigma}{(1+\mu_h)^2\,(1+\mu_\sigma)}+\frac{(\eta_\phi-6)\,\mu_\sigma}{(1+\mu_h)\,(1+\mu_\sigma)^2}\right) \tag{A.64c}$$

$$\begin{aligned}\eta_\psi =&-\frac{(\eta_\phi-5)\,h_\sigma^2}{40\pi^2\,(1+\mu_\sigma)^2}+\\&+\frac{g}{4\pi}\left(-\frac{9\,(\eta_h-7)}{20\,(1+\mu_h)^2}+\frac{9\,(\eta_h-6)}{8\,(1+\mu_h)^2}-\frac{\eta_\psi-6}{5\,(1+\mu_h)}\right)\end{aligned} \tag{A.64d}$$

$$\eta_h = \text{gravity part}+\frac{g}{2\pi}\frac{(7-\eta_\psi)}{48} \tag{A.64e}$$

A.6 Gauge dependencies

The anomalous dimensions

It is an interesting question in which way the flow depends on the graviton gauge choice. As an example of the gauge dependence of the calculated quantities we take

a look at the matter anomalous dimension as a function of the gauge parameter β. Recapitulate that for most of the present work, we made the gauge choice

$$\alpha = 0 \tag{A.65}$$

$$\beta = -1 \tag{A.66}$$

For $\alpha = 0$ both gauge fixing parameters are at a fixed point [74] for any β. Therefore, we can choose β at will and still do not have worry about flowing gauge parameters. In terms of an arbitrary β, the anomalous dimensions of the matter fields ψ and ϕ are given by:

$$\begin{aligned}\eta_\psi =& \frac{1}{32\pi\left(\mu_h+1\right)^2\left((\beta+3)^2-2\left(\beta^2-3\right)\mu_h\right)^2}\Big((\eta_h-6)g\Big((\beta+3)^2(5\beta(\beta+10)+81)\\ &+(2\beta(\beta(5\beta(3\beta-2)-112)+18)+354)\mu_h^2-8(\beta+3)^2\left(5\beta^2-14\right)\mu_h\Big)\Big)\\ &-\frac{(\beta-3)g\left(3\left((7\eta_f-34)\mu_f+\eta_f-6\right)-\beta(\eta_f-6)\left(\mu_f-1\right)\right)}{40\pi\left(\mu_f+1\right)^2\left(2\left(\beta^2-3\right)\mu_h-(\beta+3)^2\right)}\\ &-\frac{3(\beta+3)^2g\left(\eta_h\left(112\mu_f-3(\beta-13)(\beta+3)\right)-7\left(160\mu_f-3(\beta-13)(\beta+3)\right)\right)}{560\pi\left(\mu_f+1\right)\left((\beta+3)^2-2\left(\beta^2-3\right)\mu_h\right)^2}\end{aligned} \tag{A.67}$$

$$\begin{aligned}\eta_s =& -\frac{12(\beta+3)^2g\mu_s^2}{\pi\left(\mu_s+1\right)^2\left((\beta+3)^2-2\left(\beta^2-3\right)\mu_h\right)^2}-\\ &\frac{(\beta+3)^2g\left((\beta+1)^2(\eta_h-8)+32(\eta_h-6)\mu_s\right)}{16\pi\left(\mu_s+1\right)\left((\beta+3)^2-2\left(\beta^2-3\right)\mu_h\right)^2}+\\ &\frac{g\left((\beta+1)^2(\eta_s-8)-32\beta(\eta_s-6)\mu_s\right)}{16\pi\left(\mu_s+1\right)^2\left(2\left(\beta^2-3\right)\mu_h-(\beta+3)^2\right)}\end{aligned} \tag{A.68}$$

In particular, let us take a look at the scalar anomalous dimension η_ϕ for massless scalars, i.e. $\mu_\phi = 0$

$$\eta_\phi\Big|_{\mu_s=0} = \frac{(\beta+1)^2g\left((\eta_s-8)\left(2\left(\beta^2-3\right)\mu_h-(\beta+3)^2\right)-(\beta+3)^2(\eta_h-8)\right)}{16\pi\left((\beta+3)^2-2\left(\beta^2-3\right)\mu_h\right)^2} \tag{A.69}$$

We note, that the scalar anomalous dimension vanishes in the case $\beta = -1$

$$\eta_\phi\Big|_{\beta=-1,\mu_s=0} = 0, \tag{A.70}$$

which precisely the gauge we are using (cf. (A.65)). The choice $\beta = -3$ also offers a simplifaction since it make two out of three term in equation (A.69) vanish. This is a choice of gauge for which the graviton propagator is diagonal in the projection basis and has only two non-vanishing components:

$$\eta_\phi\Big|_{\beta=-3,\mu_s=0} = \frac{(\eta_s-8)g}{48\pi\mu_h}, \tag{A.71}$$

One can notice from equation (A.69) that there no choice of gauge is able to change the sign of the anomalus dimension. Thus, the sign of the anomalous dimension at least in this case and for a De-Donder-type gauge is gauge independent. The fermion anomalous dimension η_ψ cannot be set to zero that easily. However, (A.67) becomes particularly simple for $\beta = 3$. In this case η_ψ reads

$$\eta_\psi\Big|_{\beta=3} = \frac{25(\eta_h - 6)g}{96\pi\left(\mu_h + 1\right)^2} + \frac{g\left(3(\eta_f - 6)\left(\mu_f - 1\right) + 3\left((7\eta_f - 34)\mu_f + \eta_f - 6\right)\right)}{80\pi\left(\mu_f + 1\right)^2\mu_h} \tag{A.72}$$

For massless fermions, equation (A.72) even takes the simple form

$$\eta_\psi\Big|_{\beta=3,\mu_f=0} = \frac{25(\eta_h - 6)g}{96\pi\left(\mu_h + 1\right)^2} \tag{A.73}$$

Hence, tuning the parameter β can have computational advantages like the vanishing of some of the anomalous dimensions. However, the variation obey certain restrictions such as fixed signs. A detailed optimisation could lead to a significaNT simplification of the flow.

B Bibliography

[1] G. 't Hooft and M. Veltman, "One loop divergencies in the theory of gravitation," *Annales Poincare Phys.Theor.* **A20** (1974) 69–94.

[2] **BICEP2** Collaboration, P. Ade *et al.*, "Detection of B-Mode Polarization at Degree Angular Scales by BICEP2," *Phys.Rev.Lett.* **112** no. 24, (2014) 241101, arXiv:1403.3985 [astro-ph.CO].

[3] S. Weinberg, "ULTRAVIOLET DIVERGENCES IN QUANTUM THEORIES OF GRAVITATION," *General Relativity: An Einstein centenary survey, Eds. Hawking, S.W., Israel, W; Cambridge University Press* (1979) 790–831.

[4] D. J. Gross and F. Wilczek, "Ultraviolet Behavior of Non-Abelian Gauge Theories," *Physical Review Letters* **30** (June, 1973) 1343–1346.

[5] H. D. Politzer, "Reliable Perturbative Results for Strong Interactions?," *Phys.Rev.Lett.* **30** (1973) 1346–1349.

[6] S. M. Christensen and M. J. Duff, "QUANTUM GRAVITY IN TWO + epsilon DIMENSIONS," *Phys. Lett.* **B79** (1978) 213.

[7] R. Gastmans, R. Kallosh, and C. Truffin, "Quantum Gravity Near Two-Dimensions," *Nucl. Phys.* **B133** (1978) 417.

[8] K. G. Wilson, "Renormalization group and critical phenomena. 1. Renormalization group and the Kadanoff scaling picture," *Phys.Rev.* **B4** (1971) 3174–3183.

[9] J. Polchinski, "Renormalization and Effective Lagrangians," *Nucl.Phys.* **B231** (1984) 269–295.

[10] C. Wetterich, "Exact evolution equation for the effective potential," *Phys.Lett.* **B301** (1993) 90–94.

[11] T. R. Morris, "The Exact renormalization group and approximate solutions," *Int. J. Mod. Phys.* **A9** (1994) 2411–2450, arXiv:hep-ph/9308265.

[12] M. Reuter, "Nonperturbative Evolution Equation for Quantum Gravity," *Phys. Rev.* **D57** (1998) 971–985, arXiv:hep-th/9605030.

[13] W. Souma, "Nontrivial ultraviolet fixed point in quantum gravity," *Prog.Theor.Phys.* **102** (1999) 181–195, arXiv:hep-th/9907027 [hep-th].

[14] M. Reuter and F. Saueressig, "Renormalization group flow of quantum gravity in the Einstein-Hilbert truncation," *Phys.Rev.* **D65** (2002) 065016, arXiv:hep-th/0110054 [hep-th].

[15] A. Codello, R. Percacci, and C. Rahmede, "Ultraviolet properties of f(R)-gravity," *Int. J. Mod. Phys.* **A23** (2008) 143–150, arXiv:0705.1769 [hep-th].

[16] D. Benedetti, P. F. Machado, and F. Saueressig, "Asymptotic safety in higher-derivative gravity," *Mod. Phys. Lett.* **A24** (2009) 2233–2241, arXiv:0901.2984 [hep-th].

[17] K. Falls, D. Litim, K. Nikolakopoulos, and C. Rahmede, "A bootstrap towards asymptotic safety," arXiv:1301.4191 [hep-th].

[18] D. Dou and R. Percacci, "The running gravitational couplings," *Class.Quant.Grav.* **15** (1998) 3449–3468, arXiv:hep-th/9707239 [hep-th].

[19] A. Codello, R. Percacci, and C. Rahmede, "Investigating the Ultraviolet Properties of Gravity with a Wilsonian Renormalization Group Equation," *Annals Phys.* **324** (2009) 414–469, arXiv:0805.2909 [hep-th].

[20] P. Donà, A. Eichhorn, and R. Percacci, "Matter matters in asymptotically safe quantum gravity," *Phys.Rev.* **D89** (2014) 084035, arXiv:1311.2898 [hep-th].

[21] Schröder, Jan, *Aspects of Quantum Gravity and Matter*. PhD thesis, University of Sussex, 2015.

[22] A. Eichhorn and H. Gies, "Light fermions in quantum gravity," *New J.Phys.* **13** (2011) 125012, arXiv:1104.5366 [hep-th].

[23] A. Eichhorn, "Quantum-gravity-induced matter self-interactions in the asymptotic-safety scenario," *Phys.Rev.* **D86** (2012) 105021, arXiv:1204.0965 [gr-qc].

[24] N. Christiansen, "Towards Ultraviolet Stability in Quantum Gravity," Master's thesis, Heidelberg University, 2011.

[25] N. Christiansen, D. F. Litim, J. M. Pawlowski, and A. Rodigast, "Fixed points and infrared completion of quantum gravity," *Phys.Lett.* **B728** (2014) 114–117, arXiv:1209.4038 [hep-th].

[26] B. Knorr, "Towards Global Completeness in Asymptotically Safe Gravity," Master's thesis, Heidelberg University, 2013.

[27] N. Christiansen, B. Knorr, J. M. Pawlowski, and A. Rodigast, "Global Flows in Quantum Gravity," arXiv:1403.1232 [hep-th].

[28] N. Christiansen, B. Knorr, J. Meibohm, J. M. Pawlowski, M. Reichert, and A. Rodigast, "Local Quantum Gravity," arXiv:1403.1232 [hep-th].

[29] V. D. Barger, M. Berger, and P. Ohmann, "Supersymmetric grand unified theories: Two loop evolution of gauge and Yukawa couplings," *Phys.Rev.* **D47** (1993) 1093–1113, arXiv:hep-ph/9209232 [hep-ph].

[30] U. Harst and M. Reuter, "QED coupled to QEG," *JHEP* **1105** (2011) 119, arXiv:1101.6007 [hep-th].

[31] M. E. Peskin and D. V. Schroeder, *An Introduction to quantum field theory*. Addison-Wesley, Reading, 1995.

[32] H. Gies, "Introduction to the functional RG and applications to gauge theories," *Lect.Notes Phys.* **852** (2012) 287–348, arXiv:hep-ph/0611146 [hep-ph].

[33] J. Berges, N. Tetradis, and C. Wetterich, "Non-perturbative renormalization flow in quantum field theory and statistical physics," *Phys. Rept.* **363** (2002) 223–386, arXiv:hep-ph/0005122.

[34] J. M. Pawlowski, "Aspects of the functional renormalisation group," *Annals Phys.* **322** (2007) 2831–2915, arXiv:hep-th/0512261 [hep-th].

[35] S. Weinberg, *The Quantum theory of fields. Vol. 2: Modern applications*. Cambridge University Press, Cambridge, 1996. Cambridge, UK: Univ. Pr. (1996) 489 p.

[36] N. Bogoliubov and O. a. Parasiuk, "On the Multiplication of the causal function in the quantum theory of fields," *Acta Math.* **97** (1957) 227–266.

[37] K. Hepp, "Proof of the Bogolyubov-Parasiuk theorem on renormalization," *Commun.Math.Phys.* **2** (1966) 301–326.

[38] W. Zimmermann, "Convergence of Bogolyubov's method of renormalization in momentum space," *Commun.Math.Phys.* **15** (1969) 208–234.

[39] E. Manrique and M. Reuter, "Bare Action and Regularized Functional Integral of Asymptotically Safe Quantum Gravity," *Phys. Rev.* **D79** (2009) 025008, arXiv:0811.3888 [hep-th].

[40] S. Weinberg, "What is quantum field theory, and what did we think it is?," arXiv:hep-th/9702027 [hep-th].

[41] R. Percacci, "Asymptotic Safety," arXiv:0709.3851 [hep-th]. to appear in 'Approaches to Quantum Gravity: Towards a New Understanding of Space, Time and Matter' ed. D. Oriti, Cambridge University Press.

[42] M. Reuter and F. Saueressig, "Quantum Einstein Gravity," arXiv:1202.2274 [hep-th].

[43] D. Litim and A. Satz, "Limit cycles and quantum gravity," arXiv:1205.4218 [hep-th].

[44] J. Braun, H. Gies, and D. D. Scherer, "Asymptotic safety: a simple example," *Phys.Rev.* **D83** (2011) 085012, arXiv:1011.1456 [hep-th].

[45] J. Kovacs, S. Nagy, and K. Sailer, "Asymptotic safety in the sine-Gordon model," *Phys.Rev.* **D91** no. 4, (2015) 045029, arXiv:1408.2680 [hep-th].

[46] G. 't Hooft and M. Veltman, "One loop divergencies in the theory of gravitation," *Annales Poincare Phys.Theor.* **A20** (1974) 69–94.

[47] D. F. Litim, "Optimized renormalization group flows," *Phys.Rev.* **D64** (2001) 105007, arXiv:hep-th/0103195 [hep-th].

[48] L. Abbott, "The Background Field Method Beyond One Loop," *Nucl.Phys.* **B185** (1981) 189.

[49] F. Freire, D. F. Litim, and J. M. Pawlowski, "Gauge invariance and background field formalism in the exact renormalization group," *Phys.Lett.* **B495** (2000) 256–262, arXiv:hep-th/0009110 [hep-th].

[50] E. Manrique and M. Reuter, "Bimetric Truncations for Quantum Einstein Gravity and Asymptotic Safety," *Annals Phys.* **325** (2010) 785–815, arXiv:0907.2617 [gr-qc].

[51] U. Harst and M. Reuter, "The 'Tetrad only' theory space: Nonperturbative renormalization flow and Asymptotic Safety," *JHEP* **1205** (2012) 005, arXiv:1203.2158 [hep-th].

[52] P. Dona and R. Percacci, "Functional renormalization with fermions and tetrads," *Phys.Rev.* **D87** no. 4, (2013) 045002, arXiv:1209.3649 [hep-th].

[53] H. A. Weldon, "Fermions without vierbeins in curved space-time," *Phys.Rev.* **D63** (2001) 104010, arXiv:gr-qc/0009086 [gr-qc].

[54] H. Gies and S. Lippoldt, "Fermions in gravity with local spin-base invariance," *Phys.Rev.* **D89** (2014) 064040, arXiv:1310.2509 [hep-th].

[55] S. Lippoldt, "Spin-base invariance of Fermions in arbitrary dimensions," arXiv:1502.05607 [hep-th].

[56] H. Gies and S. Lippoldt, "Global surpluses of spin-base invariant fermions," arXiv:1502.00918 [hep-th].

[57] M. Reichert, "Asymptotically Safe Local Quantum Gravity with Matter," Master's thesis, Heidelberg University, 2015.

[58] D. F. Litim and J. M. Pawlowski, "Flow equations for Yang-Mills theories in general axial gauges," *Phys.Lett.* **B435** (1998) 181–188, arXiv:hep-th/9802064 [hep-th].

[59] K. Stelle, "Renormalization of Higher Derivative Quantum Gravity," *Phys.Rev.* **D16** (1977) 953–969.

[60] F. Larsen and F. Wilczek, "Renormalization of black hole entropy and of the gravitational coupling constant," *Nucl.Phys.* **B458** (1996) 249–266, arXiv:hep-th/9506066 [hep-th].

[61] X. Calmet, "Renormalization of Newton's Constant and Particle Physics," arXiv:1002.0473 [hep-ph].

[62] J. M. Pawlowski, "On Wilsonian flows in gauge theories," *Acta Phys.Slov.* **52** (2002) 475.

[63] D. F. Litim and J. M. Pawlowski, "Renormalization group flows for gauge theories in axial gauges," *JHEP* **0209** (2002) 049, arXiv:hep-th/0203005 [hep-th].

[64] K. Falls, D. F. Litim, K. Nikolakopoulos, and C. Rahmede, "Further evidence for asymptotic safety of quantum gravity," arXiv:1410.4815 [hep-th].

[65] A. Eichhorn, H. Gies, and M. M. Scherer, "Asymptotically free scalar curvature-ghost coupling in Quantum Einstein Gravity," *Phys. Rev.* **D80** (2009) 104003, arXiv:0907.1828 [hep-th].

[66] J. Braun, "Fermion Interactions and Universal Behavior in Strongly Interacting Theories," *J.Phys.* **G39** (2012) 033001, arXiv:1108.4449 [hep-ph].

[67] J. Zinn-justin, *Quantum Field Theory and Critical Phenomena*. 1996.

[68] H. Gies, J. Jaeckel, and C. Wetterich, "Towards a renormalizable standard model without fundamental Higgs scalar," *Phys. Rev.* **D69** (2004) 105008, arXiv:hep-ph/0312034.

[69] R. L. Stratonovich, "On a Method of Calculating Quantum Distribution Functions," *Soviet Physics Doklady* **2** (July, 1957) 416.

[70] J. Hubbard, "Calculation of Partition Functions," *Phys. Rev. Lett.* **3** (Jul, 1959) 77–78. http://link.aps.org/doi/10.1103/PhysRevLett.3.77.

[71] H. Gies and J. Jaeckel, "Renormalization flow of QED," *Phys.Rev.Lett.* **93** (2004) 110405, arXiv:hep-ph/0405183 [hep-ph].

[72] D. F. Litim and F. Sannino, "Asymptotic safety guaranteed," *JHEP* **1412** (2014) 178, arXiv:1406.2337 [hep-th].

[73] D. F. Litim, M. Mojaza, and F. Sannino, "Vacuum stability of asymptotically safe gauge-Yukawa theories," arXiv:1501.03061 [hep-th].

[74] D. F. Litim and J. M. Pawlowski, "On general axial gauges for QCD," *Nucl.Phys.Proc.Suppl.* **74** (1999) 329–332, arXiv:hep-th/9809023 [hep-th].

Erklärung:

Ich versichere, dass ich diese Arbeit selbstständig verfasst habe und keine anderen als die angegebenen Quellen und Hilfsmittel benutzt habe.

Heidelberg, den (Datum) .....

Acknowledgements

I thank Jan Martin Pawlowski for the supervision of this Master's thesis and for interesting discussions. Furthermore, I thank Jürgen Berges for agreeing to be the second corrector. I am grateful for my family's continuous support. In particular, I thank my girlfriend Sophia who is always there for me. I thank Manuel Reichert, Nicolai Christiansen, Andreas Rodigast, Kevin Falls and Tobias Henz for interesting discussions and for a great teamwork. Also, I am thankful to Tina Herbst, Tobias Henz, Nicolai Christiansen and Igor Böttcher for helpful suggestions.